ERCB/AGS Earth Sciences Report 2008-01

ERCB

A Study of Peridotitic Garnet Xenocryst Compositions from Selected Ultramafic Bodies in the Northern Alberta Kimberlite Province: Implications for Mantle Stratigraphy and Garnet Classification

Energy Resources Conservation Board

AGS

ERCB/AGS Earth Sciences Report 2008-01

A Study of Peridotitic Garnet Xenocryst Compositions from Selected Ultramafic Bodies in the Northern Alberta Kimberlite Province: Implications for Mantle Stratigraphy and Garnet Classification

D.R. Eccles[1] and A. Simonetti[2]

[1] Energy Resources Conservation Board/
Alberta Geological Survey
[2] Department of Earth & Atmospheric Science,
University of Alberta

March 2008

ISBN 978-0-7785-6945-9

Eccles, D.R. and Simonetti, A. (2008): A study of peridotitic garnet xenocryst compositions from selected ultramafic bodies in the northern Alberta kimberlite province: implications for mantle stratigraphy and garnet classification; Energy Resources Conservation Board, ERCB/AGS Earth Sciences Report 2008-01, 47 p.

Author address:
A. Simonetti
Department of Earth & Atmospheric Sciences
University of Alberta
Edmonton, Alberta T6G 2E3
E-mail: antonio.simonetti @ualberta.ca

Published March 2008 by:
Energy Resources Conservation Board
Alberta Geological Survey
4th Floor, Twin Atria Building
4999 – 98th Avenue
Edmonton, Alberta
T6B 2X3
Canada

Tel: (780) 422-1927
Fax: (780) 422-1918
E-mail: EUB.AGS-Infosales@gov.ab.ca
Website: www.ags.gov.ab.ca

Contents

Table

Figures

Appendices

Acknowledgments

We thank Ian Graham of Kennecott Exploration Inc., and Tom McCandless and Chris Hood of Stornoway Diamond Corporation for donating the garnet xenocrysts used in this study. Their willingness to participate is a great example of how government-industry collaboration can continue to improve the geology of Alberta.

With respect to the Mountain Lake xenocrysts, Overburden Drilling Management Limited of Nepean, Ontario provided timely and efficient processing of bulk samples for indicator-minerals. Don Resultay, Stefanie Schmidberger and Sergei Matveev of the University of Alberta are thanked for their parts in probe mount preparation and electron microprobe analytical work.

Finally, Steven Creighton of the University of Alberta and Melissa Kirkley of Diamondex Resources Ltd. are thanked for peer-review comments that improved the overall manuscript.

Abstract

Electron microprobe (EMPA) major-element analyses of peridotitic garnet xenocrysts from the northern Alberta kimberlite province typically have well-defined lherzolitic paragenesis with geochemical affinities that are uncharacteristic of garnet in diamondiferous kimberlite. Yet approximately 67% of the Buffalo Head Hills kimberlite field bodies contain diamonds with at least three kimberlite occurrences having estimated diamond contents of between 13 and 55 carats per hundred tonnes. This conundrum is important because the major element composition of periodotitic garnet has been used extensively to establish criteria for target evaluation in diamond exploration. A comprehensive set of garnet xenocrysts from the three separate ultramafic rock fields in northern Alberta were analyzed by LA-ICP-MS. These trace element data provide information additional to EMPA data that quantify parameters indicative of diamond potential and provide new information on the chemical nature of the lower crust-subcontinental lithosphere beneath northern Alberta.

This report shows that distinct compositional changes in garnet xenocryst Ti, REE, Y and Zr provide a means of separating garnets into distinct geochemical groups that disclose evidence for varying degrees of depletion or re-enrichment of the protolith. Based on garnet compositions—and using T_{Ni} as a proxy of depth—at least five lithological transitions are inferred for the lower crustal-sublithospheric mantle underlying northern Alberta. From low to high-T, these regions include the following: fertile lherzolite, chromite–clinopyroxene–garnet equilibrium trend garnet and wehrlite (<870ºC), low-T lherzolite (870ºC to 950ºC), melt metasomatized wehrlite (950º–1000ºC), depleted lherzolite and melt metasomatized lherzolite (1000º–1130ºC), and moderately fertile lherzolite and high-Ti melt metasomatized lherzolite (>1130ºC).

These compositional groups can serve as a proxy for future evaluation of garnet compositions in Alberta because they also distinguish inter- and intra-field mantle variations. In terms of diamond prospects in northern Alberta, one transitional mantle layer associated with the Buffalo Head Hills field includes a predominance of 1000º to 1130ºC, low-Ti, Y and Zr-depleted lherzolite that implies a diamond window in the mantle underlying the Buffalo Head Hills of between 160 km and 180 km. In contrast, both the Mountain Lake and Birch Mountain areas seem to be characterized by either a hot, less depleted asthenospheric-type mantle, or by mantle regions characterized by relatively cool geotherms.

These findings have significant implication for the documentation and evaluation of known occurrences of kimberlite and in the evaluation of surficial kimberlite-indictor mineral surveys critical to target selection in Alberta and other areas of the western North America.

1 Introduction

Kimberlite is a volcanic rock derived deep within the Earth. The consensus reached on kimberlites is that they are formed deep within the mantle (at a depth between 150 and 450 km) from enriched exotic mantle compositions, and erupt rapidly and violently, often with considerable carbon dioxide and other volatile components. This depth of melting and generation makes kimberlites prone to hosting diamond, which forms in the Earth's mantle at depths exceeding 120 km under extremely high pressure and temperature (40 kbar and 900° C). In their rapid ascent to the Earth's surface, kimberlitic melts entrain xenoliths (fragments) or xenocrysts (minerals) derived from mantle peridotite, Archean and Proterozoic lower crustal material, and overlying Phanerozoic rock formations. When xenoliths are disaggregated during or post-eruption, resistant mantle xenocrysts, such as garnet, chromite, ilmenite and chrome diopside, can serve as a proxy for the original mantle rock in which they were derived. Therefore, kimberlites and their entrained xenoliths and xenocrysts provide a unique opportunity to view the nature of these otherwise inaccessible geologic environments, such as the lithospheric upper mantle and lower crust.

A northeast propagating trend of three ultramafic rock fields has been discovered in northern Alberta: from southwest to northeast, these include the Mountain Lake ultramafic cluster, and the Buffalo Head Hills and Birch Mountains kimberlite fields (Figure 1). The Buffalo Head Hills kimberlite field is known to carry representative mantle xenoliths, whereas the Mountain Lake cluster and Birch Mountains field are either essentially devoid of fresh mantle xenoliths or they are too altered for investigation. Garnet xenocrysts, however, are common in all northern Alberta ultramafic bodies.

In situ quantitative analysis by laser ablation inductively coupled plasma mass spectrometry (LA-ICP-MS) has rapidly developed into one of the most powerful analytical techniques, capable of producing high precision determination of trace elements at sub-ppm detection limits. Hence, the goal of this study is to provide a comprehensive set of trace element data from garnet xenocryst suites derived from ultramafic magmatism across northern Alberta. These trace element patterns record a diverse range of geochemical behaviour controlled by pressure, temperature and composition of their host rock-type that enable interpretations about the chemical nature of a cross-section of lower crustal-sublithospheric mantle (SLM) beneath northern Alberta.

2 General Geology and Previous Northern Alberta Mantle Investigations

Geological units of northern Alberta range in age from Archean to Recent and are exposed as broad northwesterly trending belts, decreasing in age to the southwest (Hamilton et al., 1999). Precambrian rocks are exposed in the northeast and form the basement for a wedge of Phanerozoic strata that reach a maximum thickness of approximately 6000 m in front of the Cordilleran fold-and-thrust belt to the southwest. Phanerozoic strata have been deposited in the Western Canada Sedimentary Basin (WCSB) in two fundamentally different tectonosedimentary environments: (a) Late Proterozoic to Middle Jurassic passive continental margin and (b) Middle Jurassic to Oligocene foreland basin. Ultramafic intrusions have penetrated through approximately 2300 m, 1600 m and 500 m of Phanerozoic sedimentary rock in the Mountain Lake, Buffalo Head Hills and Birch Mountains areas, respectively.

Basement rocks have been assigned to more or less distinct continental slivers accreted to the composite Churchill province during the assembly of western Laurentia (~2.0–1.8 Ga; e.g., Hoffman, 1988; Ross et al., 1994). Alternatively, accretion may have involved a uniform continental fragment—separated from and welded back to the Churchill province (Burwash et al., 2000). Pană (2003) suggested the northern Alberta basement may have an Archean inheritance, based on Sm-Nd model ages greater than U-Pb crystallization ages and the observation that most of the WCSB in northern Alberta is underlain

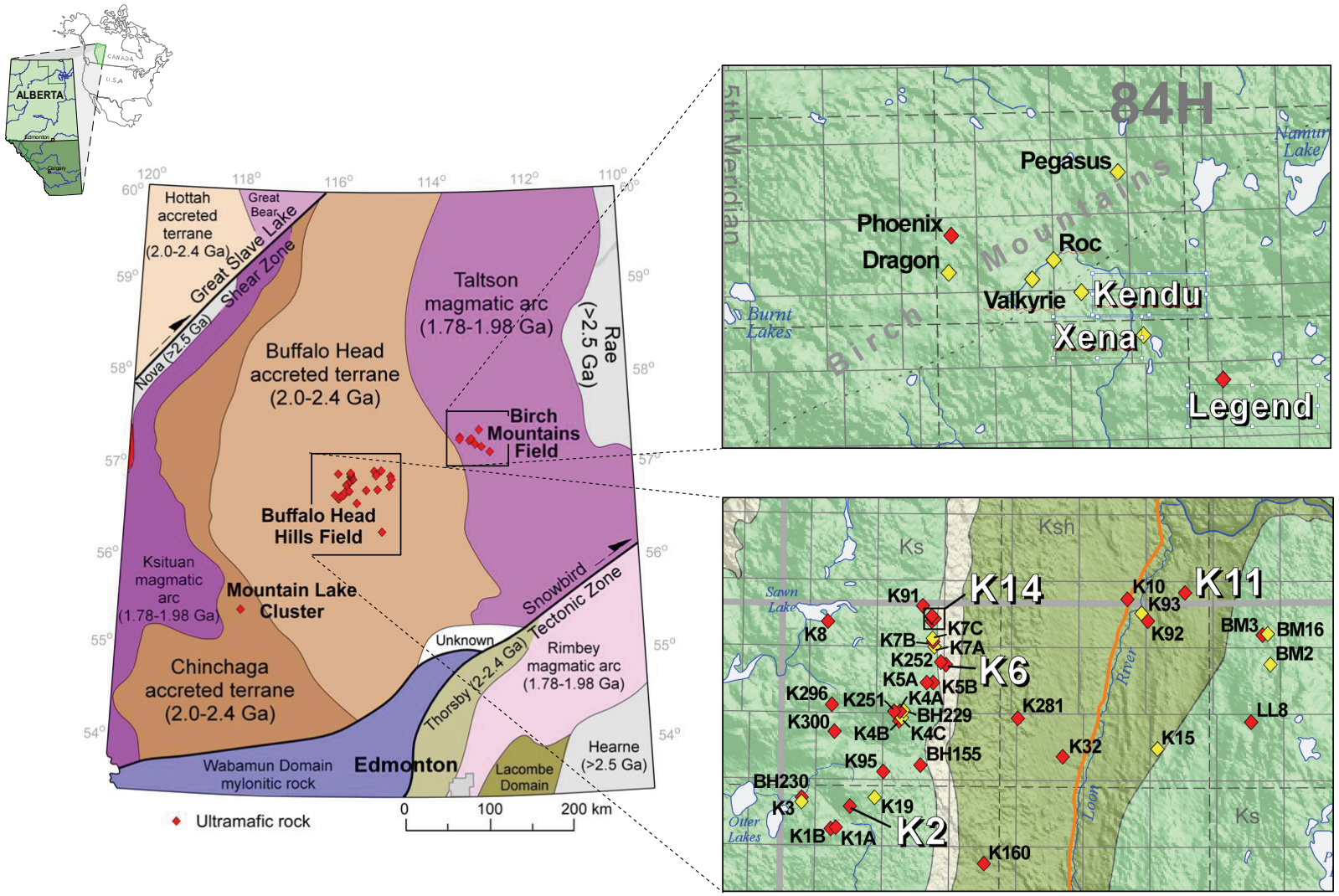

Figure 1. Ultramafic rock occurrences in the northern Alberta kimberlite province on the inferred basement domain map of Ross et al. (1994). Inset maps show the detailed location of individual ultramafic bodies in the Buffalo Head Hills and Birch Mountains kimberlite fields. On the inset maps, ultramafic bodies, from which garnet xenocrysts were used in this study, are in larger white shadowed font. Red and yellow diamond location markers depict diamondiferous and barren kimberlites, respectively. Mountain Lake is reportedly subeconomic.

by granulite terranes intruded during Hudsonian tectonomagmatic batholitic complexes. Basement subdivisions beneath the WCSB in northern Alberta have been inferred (due to lack of outcrop exposure and core samples) from potential field data, particularly aeromagnetic and geochronological data. They show that Alberta is underlain by Proterozoic rocks with Mountain Lake, Buffalo Head Hills and Birch Mountains ultramafic rocks situated within the ~2.17–2.08 Ga Chinchaga and ~2.32–1.99 Ga Buffalo Head accreted terranes, and ~1.98–1.94 Ga Taltson Magmatic Zone, respectively (Figure 1; Ross et al., 1991; Thériault and Ross, 1991; Ross et al., 1994).

Radiogenic (Rb-Sr phlogopite and U-Pb perovskite) and palynological age determinations on ultramafic rocks in the northern Alberta kimberlite province range between ~88 Ma and ~60 Ma (Leckie et al., 1997; Carlson et al., 1999; Heaman et al., 2003; Skelton et al., 2003; Eccles et al., in press). Based on petrography, whole-rock and mineral separate geochemistry, and radiogenic isotopes, Eccles et al. (2004) and Eccles (2004) suggested primitive (Buffalo Head Hills) to evolved (Birch Mountains) magmatic signatures can be distinguished from the Mountain Lake hybrid ultramafic body. In addition, they described intra-field variations in rock classification. Thus, garnet xenocrysts analyzed in this study comprise a combination of kimberlite, hybrid and non-kimberlite sources. Garnet xenocrysts from diamondiferous Buffalo Head Hills bodies (K6, K11 and K14) were sampled by kimberlite. The Buffalo Head Hills K2 body may belong to a cluster of weakly diamondiferous/barren hybrid ultramafic rocks in the southwestern part of the Buffalo Head Hills field that are significantly younger (~60 Ma) than the ~88–81 Ma diamondiferous kimberlites (Eccles et al., in press). In contrast to the kimberlite-dominant Buffalo Head Hills field, garnet xenocrysts collected for this study from the Mountain Lake, and Birch Mountains Kendu and Xena bodies were sampled by magma with non-kimberlite affinities (e.g., ultrabasic, olivine alkali basalt/basanite; Eccles, 2004; Eccles et al., 2004).

Previous mantle xenolith and diamond inclusion studies are limited to the Buffalo Head Hills. Aulbach et al. (2004) reported that mantle xenoliths from the K6, K11 and K14 Buffalo Head Hills kimberlites include spinel lherzolite, garnet-spinel lherzolite, garnet harzburgite, sheared garnet lherzolite and pyroxenite. Garnet xenocrysts from their study defined a model conductive paleogeotherm corresponding to a heat flow of 38–39 mW/m^2. These authors also concluded that

- pyroxenite and garnet spinel lherzolite are restricted to the shallow mantle;
- fertile garnet lherzolites are concentrated at shallow depths (<140 km) and prevail at depths <110 km;
- depleted peridotites are concentrated between 120 to 160 km with Ca-saturated garnet harzburgite concentrated in a layer between 140 to 160 km depth at 1000º to 1200ºC;
- melt-metasomatized lherzolites, similar to sheared-lherzolites, are concentrated between 140 to 180 km and prevail at depths of >170 km; and
- the sheared garnet lherzolite lies on an inflection of the calculated geotherm and may constrain the depth of the lithosphere-asthenosphere boundary (LAB) to approximately 180 km depth.

Diamond inclusion studies by Davies et al. (2004) and Banas et al. (2006) have recovered garnet, olivine, clinopyroxene, ferropericlase, spinel, and rutile that span the peridotitic, eclogitic, eclogitic/websteritic and websteritic parageneses. Of the 16 garnet inclusions recovered, 11 have low-Cr eclogitic, three are lherzolitic and individual grains include P-type majoritic and wehrlitic sources. Lherzolitic garnet-clinopyroxene pairs give equilibration temperatures of 1100º to 1200ºC ± 50ºC on a 40 mW/m^2 geotherm (Davies et al., 2004).

3 Methodology

Garnet xenocrysts were collected from selected bodies within all three areas of ultramafic magmatism in northern Alberta, including the Mountain Lake cluster: south body, Buffalo Head Hills field: K2, K6, K11 and K14 bodies, and Birch Mountains: Kendu, Legend and Xena bodies (Table 1).

Table 1. A summary of the ultramafic bodies and garnet xenocrysts selected for this study. Diamond contents from Creighton and Eccles (2002), Skelton et al. (2003) and Eccles et al. (2008).

Ultamafic body	Area/field	Rock type	Location (NAD82)			DMS (cpht) *	Weight (kg)	Microdiamond testing**		Number of analysis	
			Easting	Northing	Zone			Macros (>0.5 mm)	Micros (<0.5 mm)	EMP***	ICP-MS****
Mountain Lake	Mountain Lake	Non-archetypal kimberlite	454697	6145542	11		44.8	0	0	30	26
K2	Buffalo Head Hills	Non-archetypal kimberlite	571486	6288052	11		1603.9	0	3	40	28
K6	Buffalo Head Hills	Kimberlite	585184	6308955	11		23761.9	14+	81+	12	6
K11	Buffalo Head Hills	Kimberlite	619596	6320345	11	4.4				26	15
K14	Buffalo Head Hills	Kimberlite	582822	6315364	11	11.7				42	21
Kendu	Birch Mountains	Non-archetypal kimberlite	368503	6353633	12		170.0	0	0	15	19
Legend	Birch Mountains	Kimberlite	386142	6340825	12		406.5	0	4	16	17
Xena	Birch Mountains	Non-archetypal kimberlite	376792	6347526	12		130.7	0	0	5	8

* Dense media separation mini-bulk sample results (carats per hundred tonnes)

** Diamond >0.1 mm are reported as number of stones

*** Electron microprobe major element analysis

**** Inductively coupled plasma mass spectrometry trace element analysis

Quantitative chemical analyses of major elements were obtained on mineral grain separates using a JEOL8900 electron microprobe (EMPA) at the University of Alberta. The silicate grains were analyzed using an accelerating voltage of 20 kV, beam diameter of 1 μm to 10 μm and beam current of 20 nA. Peak and background counting times were 30 seconds. Standards were natural minerals from the Smithsonian microbeam set of standards (Jarosewich, 2002) and regularly analyzed to ensure the calibration remained valid throughout the probing session.

In situ trace element analyses of individual garnet grains were obtained using an ELAN6000 quadruple ICP-MS coupled to a UP213 nm laser ablation system at the University of Alberta. Complete details for this technique are available in Schmidberger et al. (2007) and summarized as follows. For trace element determinations, the NIST SRM 612 glass standard and garnet grains were ablated using a 160 μm spot size, 5 Hz repetition rate and energy density of approximately 13 J/cm^2. Ablation runs were conducted in a mixed He/Ar atmosphere (ratio of 0.5:0.1 L/min), and mixed with Ar (1.03 L/min- coolant gas) prior to entering the torch assembly. The laser ablation cell was flushed with a higher flow rate of He (up to 0.9 L/min) for approximately 1 min in between laser ablation runs to ensure adequate particle washout. A typical analysis consisted of an approximately 25-second background measurement followed by ablation for approximately 40 seconds. The NIST SRM 612 glass standard was used as the external calibration standard and CaO concentration, measured using EPMA as the internal standard. Data reduction and concentration determinations were obtained using the GLITTER® (XP version, Macquarie University) laser ablation software. Schmidberger et al. (2007) report relative standard deviations (2σ) for most elements measured in the garnet grains that range from 3% to 15% with detection limits for most trace elements varying between 0.01 ppm and 0.05 ppm.

Temperatures of last equilibration were calculated using the Ni-in-garnet geothermometer of Canil (1999), where

$$T_{Ni}\ (^{o}C) = 8772 / (2.53 - \ln D_{Ni}^{gt/ol})$$

We use this geothermometer because it is based on experiments at natural abundances versus the empirical calibration of conventional thermobarometry of Ryan et al. (1996). We assume garnet is in equilibrium with mantle olivine having an average Ni concentration of 2900 ppm (Ryan et al., 1996). Canil (1999) reported that the range of possible Ni in olivine results in an uncertainty of ±30ºC in T_{Ni} and an uncertainty in experimental calibration of ±70ºC (2σ; Canil, 1999).

4 Results

Electron microprobe major element data are listed in Appendix 1. A total of 217 in situ LA-ICP-MS trace element analyses were completed on 111 garnet xenocrysts, including the following: 50 analyses from the Mountain Lake cluster, 67 analyses from the Birch Mountains field, and 100 analyses from the Buffalo Head Hills field. We present a 'filtered' subset of these data in Appendix 2, which total 140 analyses after removal of garnet data with low Cr_2O_3 (<2.0 wt. %; i.e., eclogitic), low totals (<98 wt. %) and/or unrealistic temperatures (e.g., <650ºC or >1500ºC). As a verification of data validity, Figure 2a shows that with the exception of a few grains (mainly those from Mountain Lake), there is a good correlation (R = 0.89) between the EMPA and LA-ICP-MS analyses for Ti in garnet cores. A comparison of the Ni-in-garnet temperatures (Canil, 1999) to those obtained by the Mn-in-garnet thermometer (Grütter et al., 1999) is illustrated in Figure 2b to have moderate to good correlation (R = 0.83) with the 1:1 correlation line showing that T_{Mn} is increasingly offset to higher temperatures with increasing T.

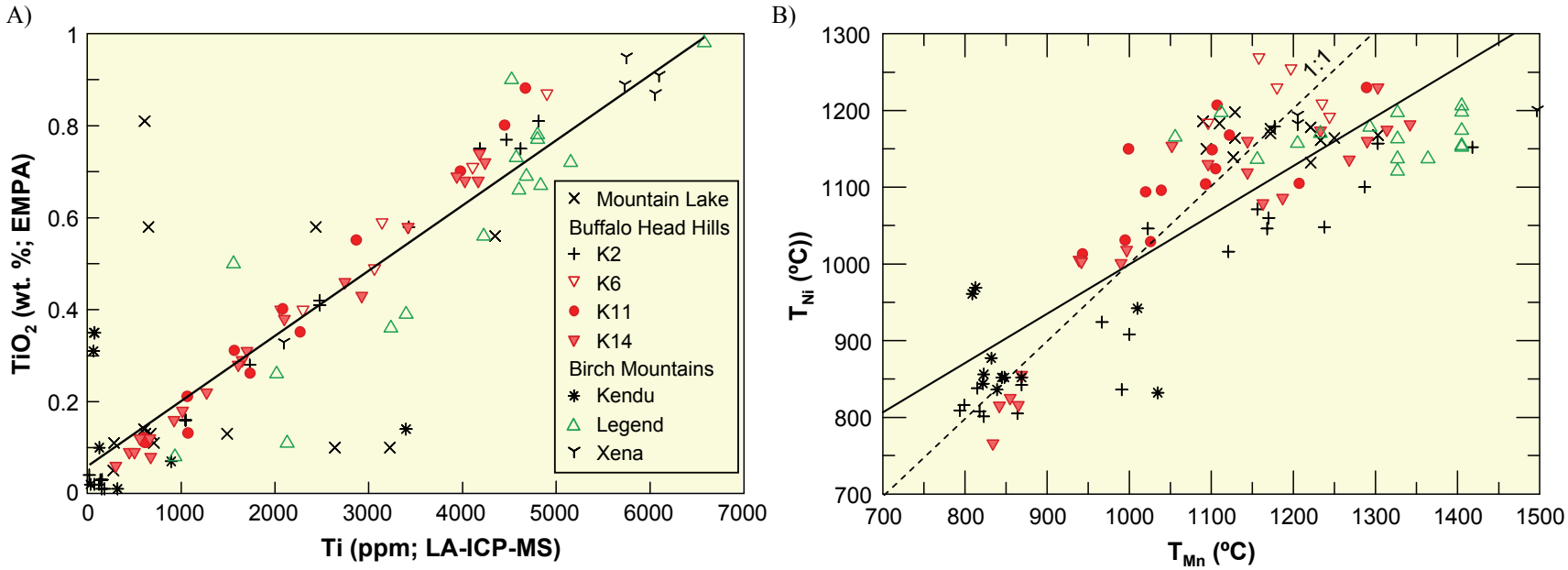

Figure 2. Comparisons of EMPA versus LA-ICP-MS analyses using Ti, and of single garnet thermometric techniques using identical garnet cores. Ni-in-garnet temperatures are calculated using the methods of Canil (1999). Mn-in-garnet temperatures are calculated using the methods of Grütter et al. (1999). Trend lines are represented by solid lines. The T_{Ni} versus T_{Mn} 1:1 line is represented by a dashed line.

4.1 Temperature-Pressure Estimates

Because the exact age of the mantle underlying Alberta on the western edge of Laurentia is unknown and likely younger than the Archean mantle of the Slave Province, NWT, or other diamond-producing regions of the world, we must immediately address the concern that lower concentrations of Ni in olivine-associated younger mantle could provide unrealistic (higher) garnet T_{Ni} temperature estimates. By varying the Ni concentrations in olivine using arbitrary values of 2000 to 3500 ppm Ni, the Canil (1999) calculations only produced changes in T_{Ni} garnet of approximately 100ºC—not enough to have a significant impact on the major conclusions of this study.

The range in T_{Ni} recorded by garnet from all ultramafic bodies sampled in this study is between 766ºC and 1269ºC (Figure 3). The T_{Ni} histograms show garnet xenocrysts analyzed in this study show distinct thermal distributions. Garnet from Mountain Lake is restricted to the 1150º–1200ºC range. The Buffalo Head Hills has two thermal distributions, one at 825º–850ºC and a broad T_{Ni} range from 1025º to 1275ºC. Birch Mountains has three T_{Ni} distributions at 850º–900ºC, 950º–1025ºC and 1125º–1275ºC. Kendu garnet is restricted to a low-T_{Ni} distribution of between 850º to 1025ºC. Widely distributed garnet T_{Ni} is evident in K2 and K14. High-T_{Ni} garnets (>1100ºC) are associated with wide range of bodies (Mountain Lake, K6, K11, K14, Legend and Xena), but are exclusively the only garnet T_{Ni} recorded in Mountain Lake, K6 and Xena.

The T_{Ni} values for each garnet can be projected to a known xenolith-derived paleogeotherm to give some estimate of the depth range sampled by the garnet suite. Based on xenolith-studies, Aulbach et al. (2004) obtained a geotherm of 38–39 mW/m^2 for mantle beneath the Buffalo Head Hills field. Depth estimates obtained by projecting T_{Ni} to this paleogeotherm infer that the Buffalo Head Hills ultramafics sampled garnet over an interval of approximately 100 to 230 km (median approximately 160 km). Depth estimates from the Mountain Lake and Birch Mountains garnet suites cannot be made with any certainty since each of these regions have poor kimberlite representation and lack a reliable regional, xenolith-based paleogeotherm. We suspect, however, that higher Precambrian surface heat flow in these regions (e.g., Bachu and Burwash, 1994) most likely reflects a higher geothermal gradient.

4.2 Geochemical Garnet Groupings: Overview of Analytical Results

Garnet geochemical results are illustrated using a variety of bivariate diagrams, where Figures 4–11 represent data from the Mountain Lake, K2, K6, K11, K14, Kendu, Legend, and Xena ultramafic bodies, respectively. With the exception of K6, Legend, and Xena, the ultramafic bodies exhibit two or three distinct trace element distribution patterns, some of which can be observed in several bodies. Therefore, we subdivide the trace element data into compositionally similar groups based on chemical relationships between chondrite-normalized rare earth elements (REE_N) patterns, CaO-Cr_2O_3, Zr-Y, and T_{Ni}. The data are presented in this fashion to avoid repetition, to determine inter- and intra-body garnet xenocryst compositional trends, and to serve as a comparative model for future evaluations of garnet compositions in Alberta. Garnet-type classification nomenclature (e.g., depleted lherzolite) has been included for each compositional group to provide clarity throughout this report. The garnet group analytical results are described below in order of low to high degrees of re-enrichment. Our interpretations are provided later in the discussion section of this report.

4.2.1 Geochemical Group A: Depleted Lherzolite (red-filled diamonds on figures)

The Group A garnet type is only observed in Buffalo Head Hills garnet xenocrysts, including moderate-T_{Ni} garnet from the K11 and K14 bodies, and a single garnet from K6 (Figures 6, 7 and 8). Geochemically,

A) Mountain Lake

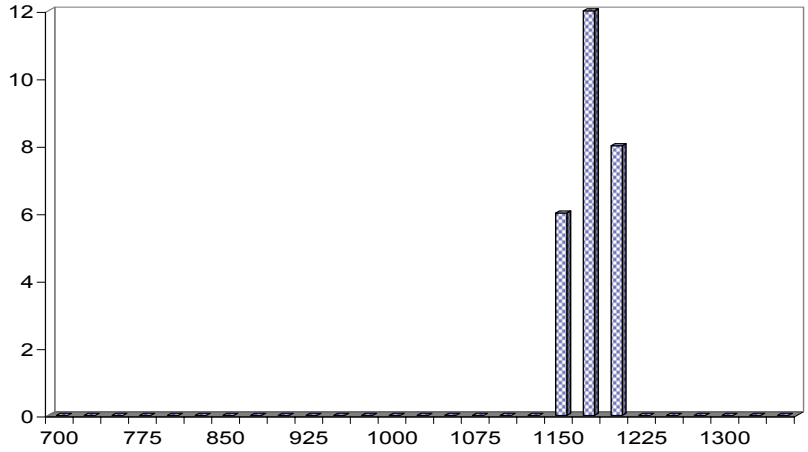

B) Buffalo Head Hills

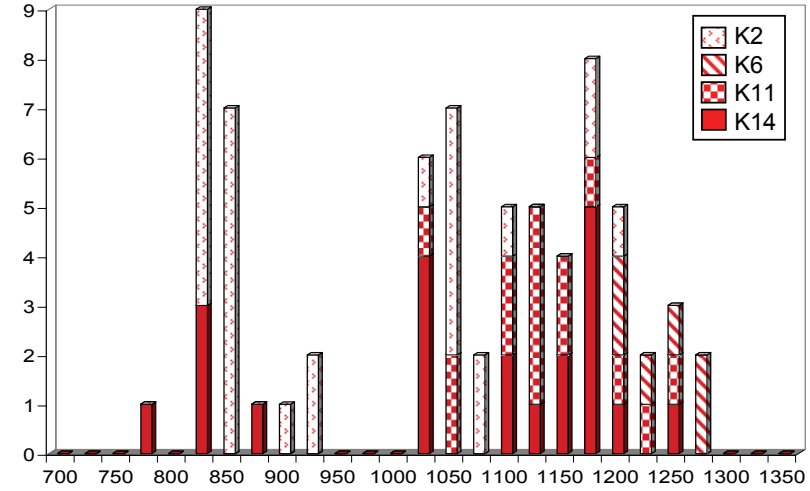

C) Birch Mountains

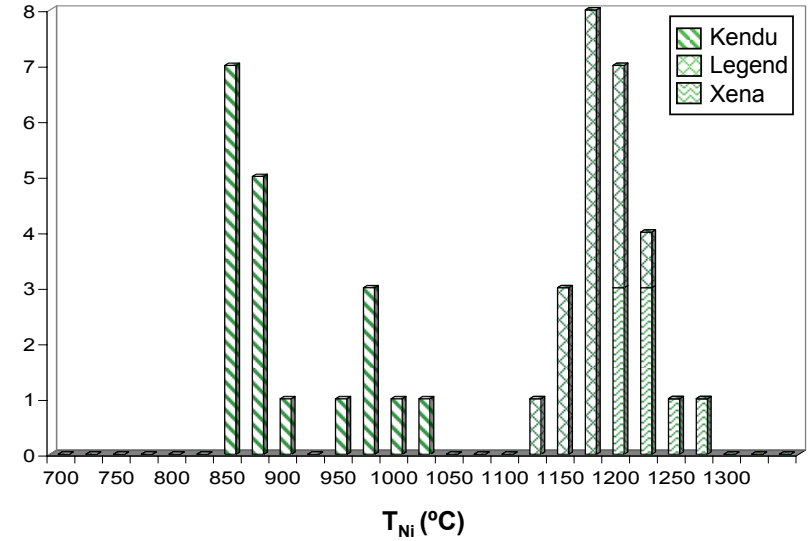

Figure 3. Distribution of T_{Ni} for garnet xenocrysts from selected ultramafic bodies in the northern Alberta kimberlite province. T_{Ni} is calculated using the garnet Ni thermometer of Canil (1999).

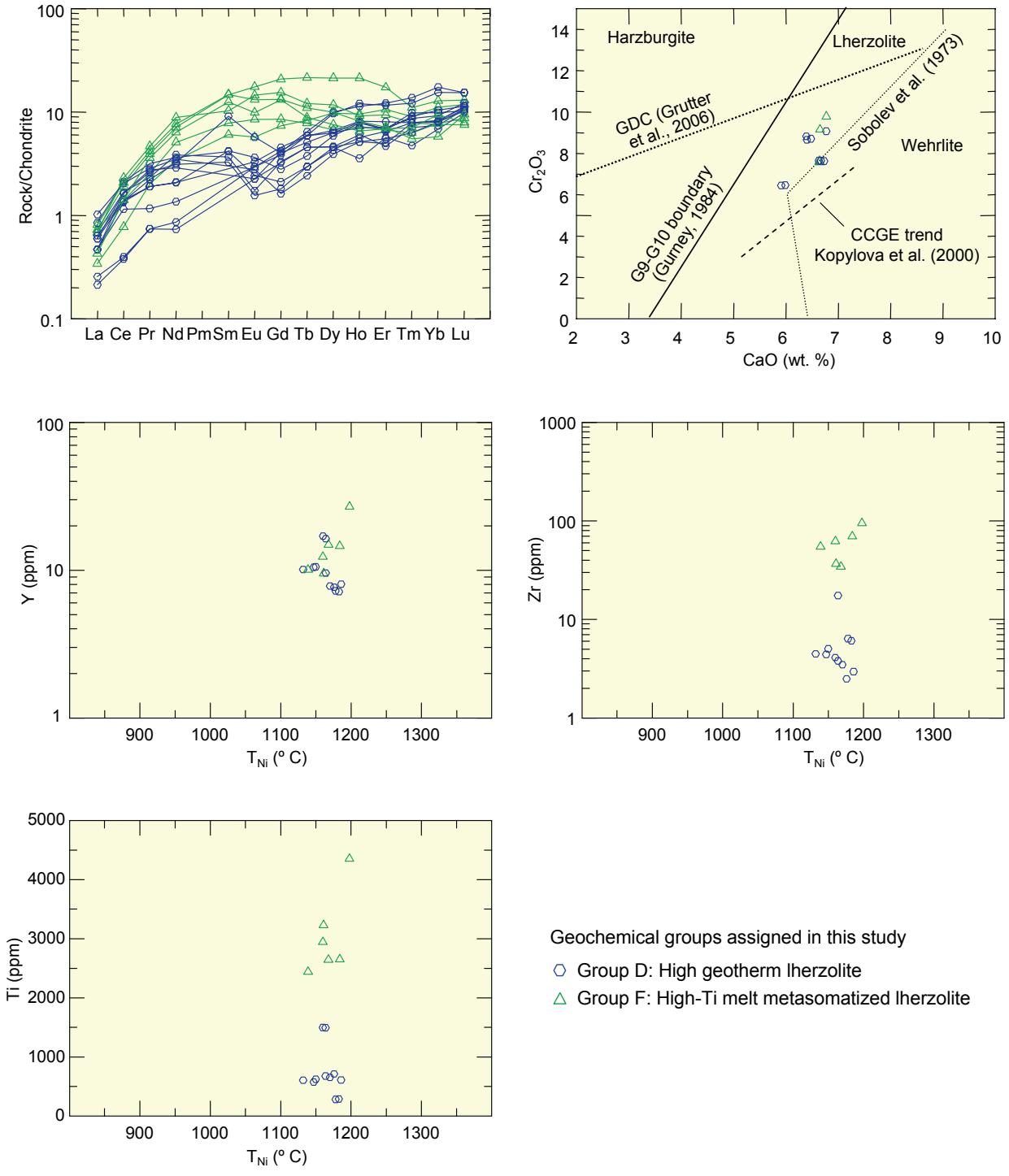

Figure 4. Normalized rare earth element diagram and selected bivariate geochemical plots for selected garnet xenocryst cores from Mountain Lake. Chondrite values from McDonough and Sun (1995).

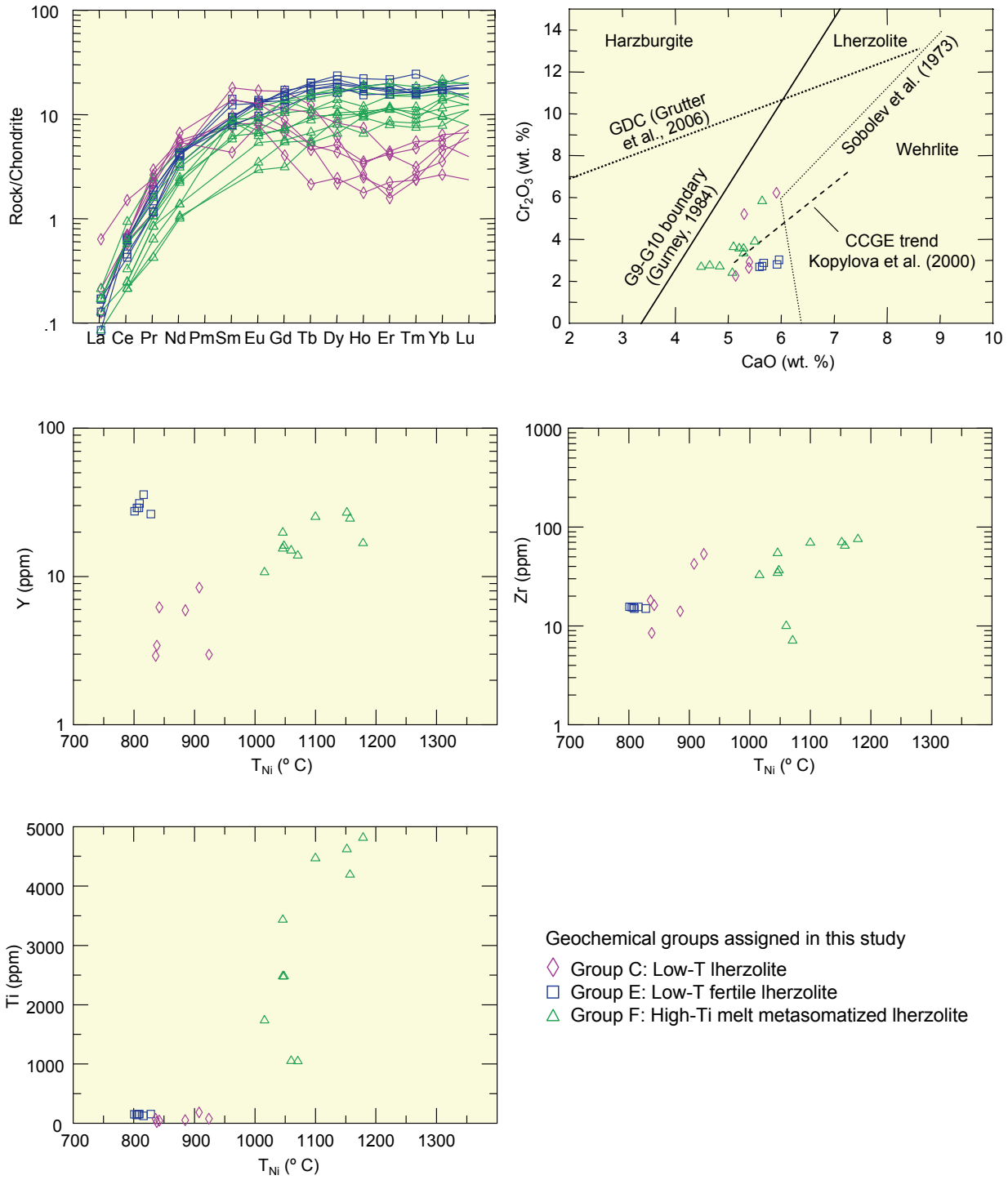

Figure 5. Normalized rare earth element diagram and selected bivariate geochemical plots for selected garnet xenocryst cores from K2, Buffalo Head Hills. Chondrite values from McDonough and Sun (1995).

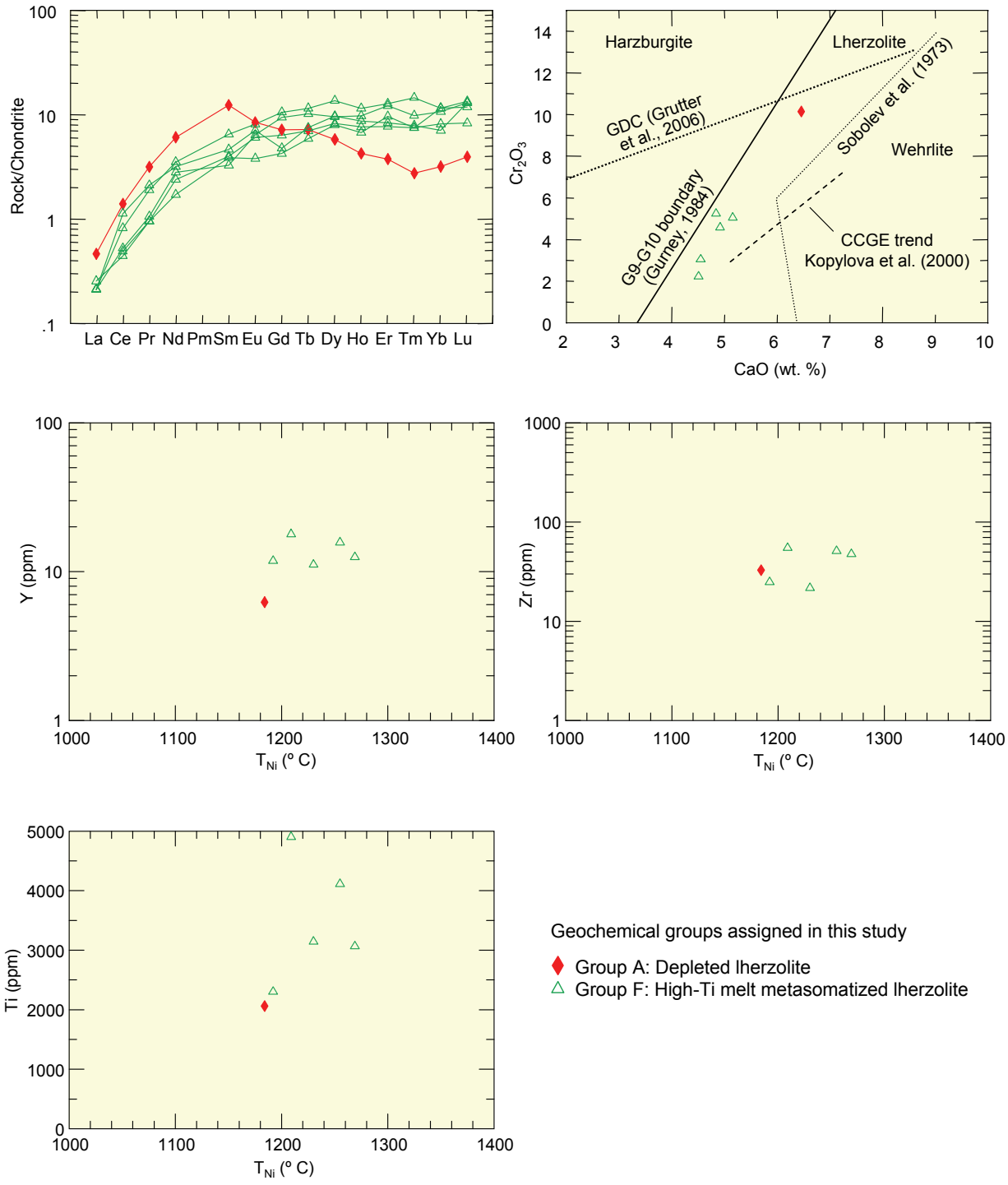

Figure 6. Normalized rare earth element diagram and selected bivariate geochemical plots for selected garnet xenocryst cores from K6, Buffalo Head Hills. Chondrite values from McDonough and Sun (1995).

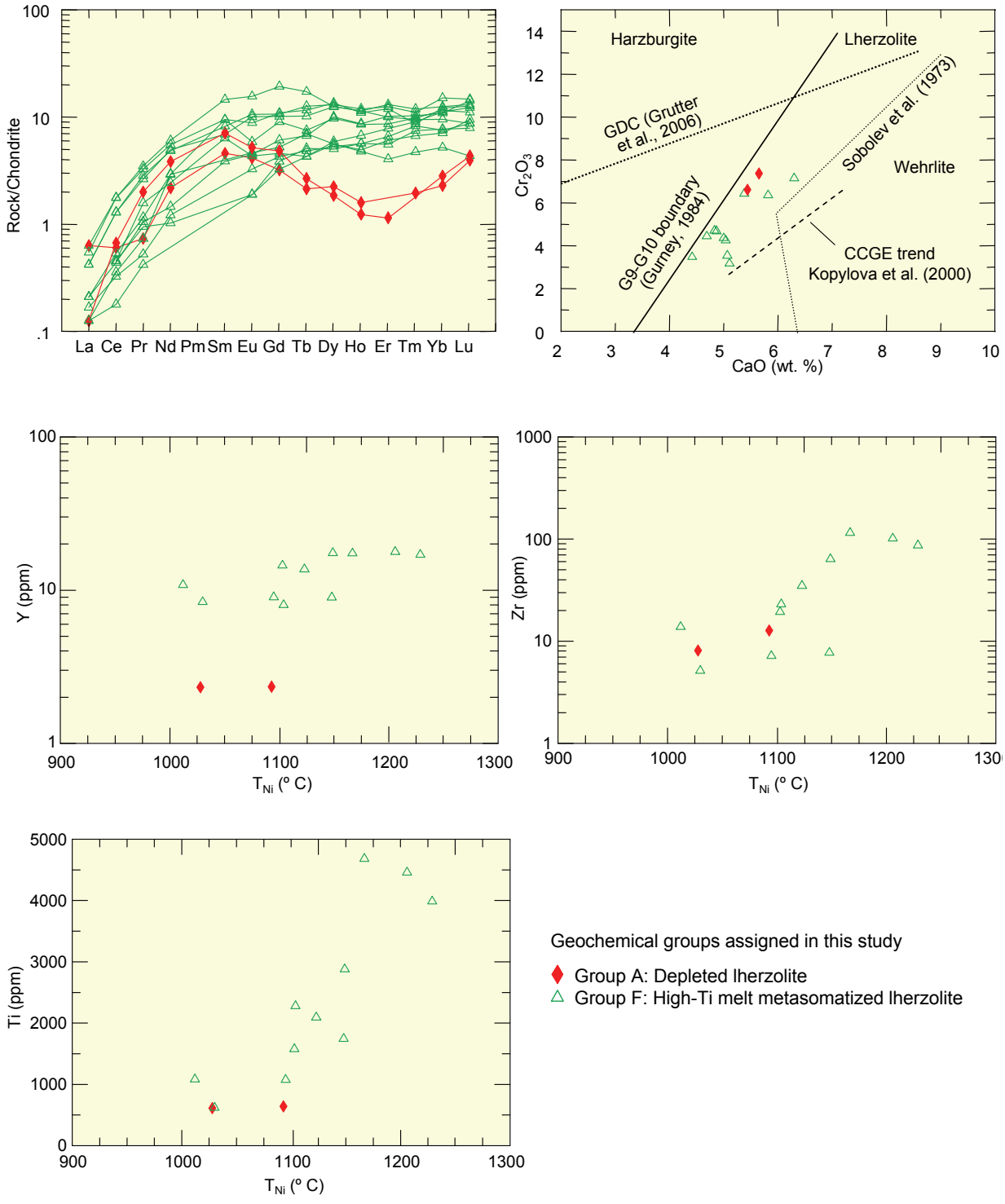

Figure 7. Normalized rare earth element diagram and selected bivariate geochemical plots for selected garnet xenocryst cores from K11, Buffalo Head Hills. Chondrite values from McDonough and Sun (1995).

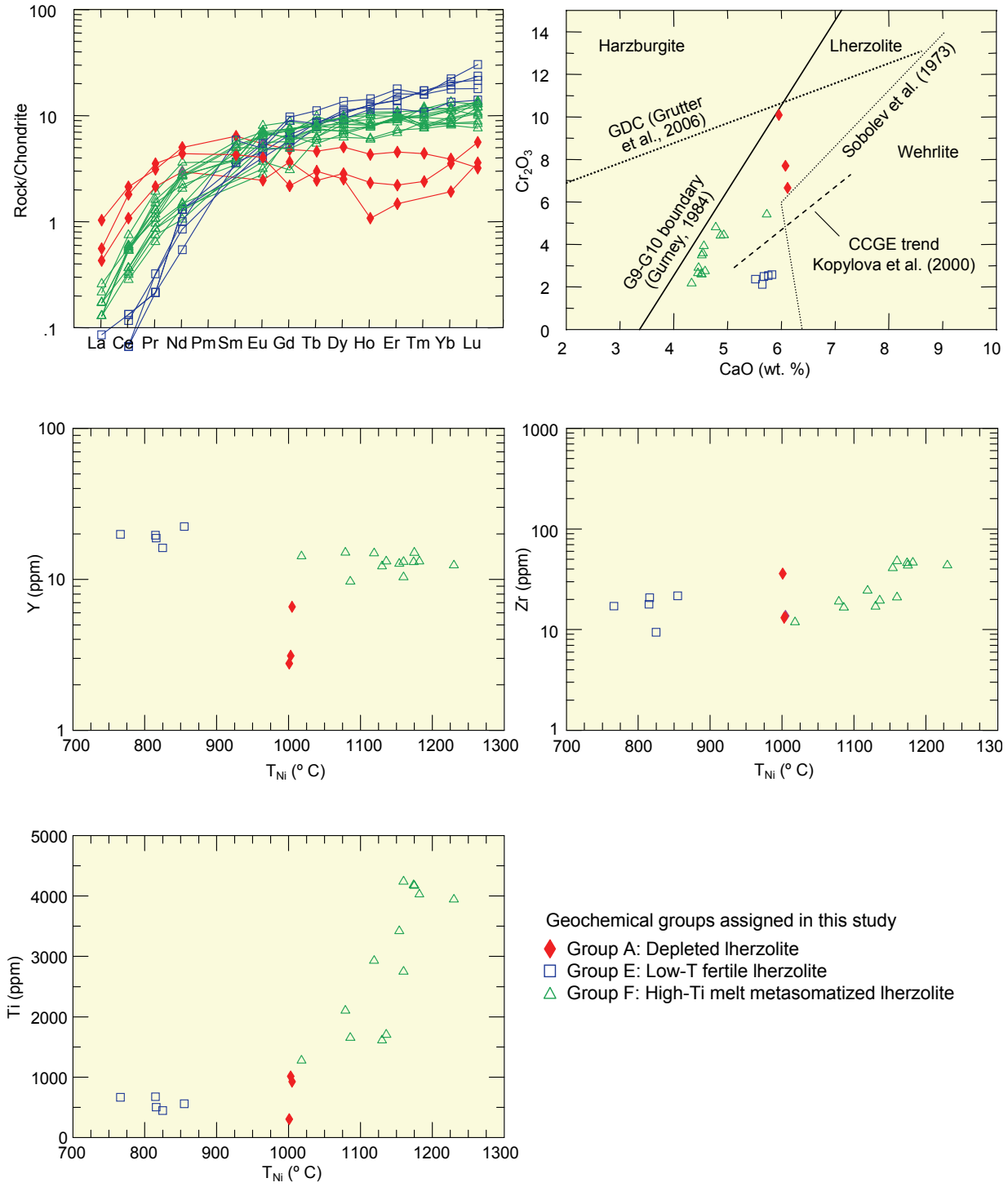

Figure 8. Normalized rare earth element diagram and selected bivariate geochemical plots for selected garnet xenocryst cores from K14, Buffalo Head Hills. Chondrite values from McDonough and Sun (1995).

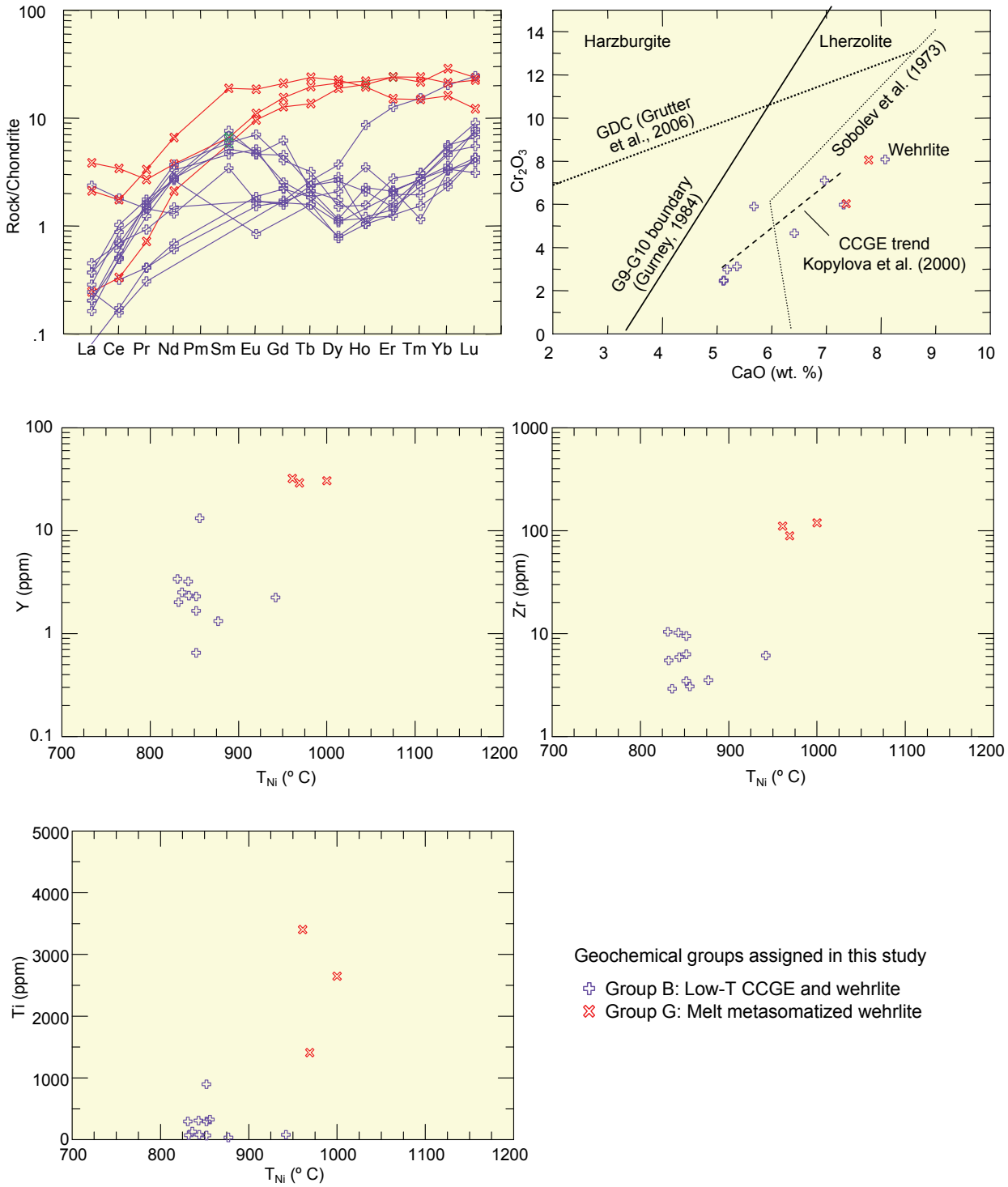

Figure 9. Normalized rare earth element diagram and selected bivariate geochemical plots for selected garnet xenocryst cores from Kendu, Birch Mountains. Chondrite values from McDonough and Sun (1995).

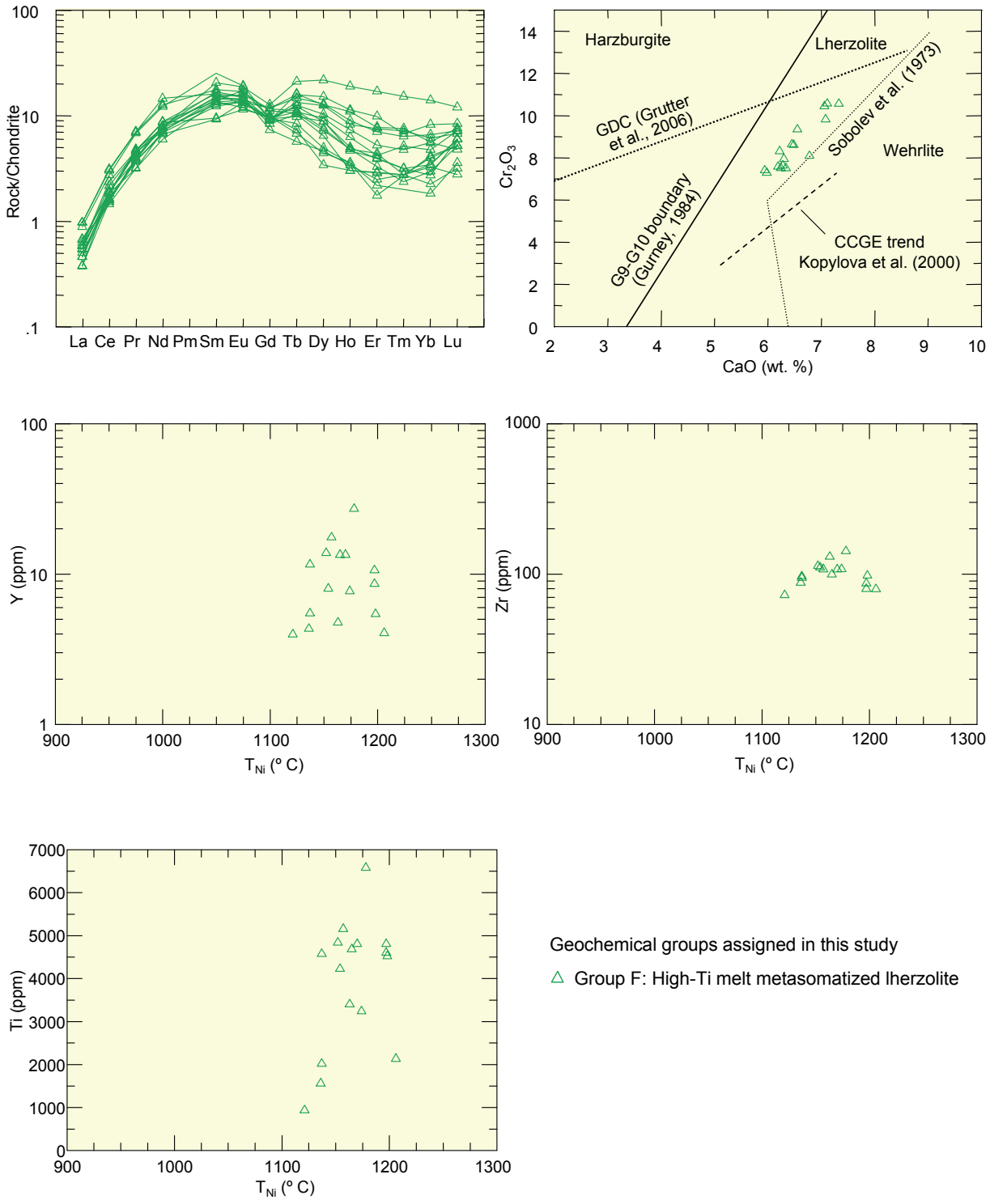

Figure 10. Normalized rare earth element diagram and selected bivariate geochemical plots for selected garnet xenocryst cores from Legend, Birch Mountains. Chondrite values from McDonough and Sun (1995).

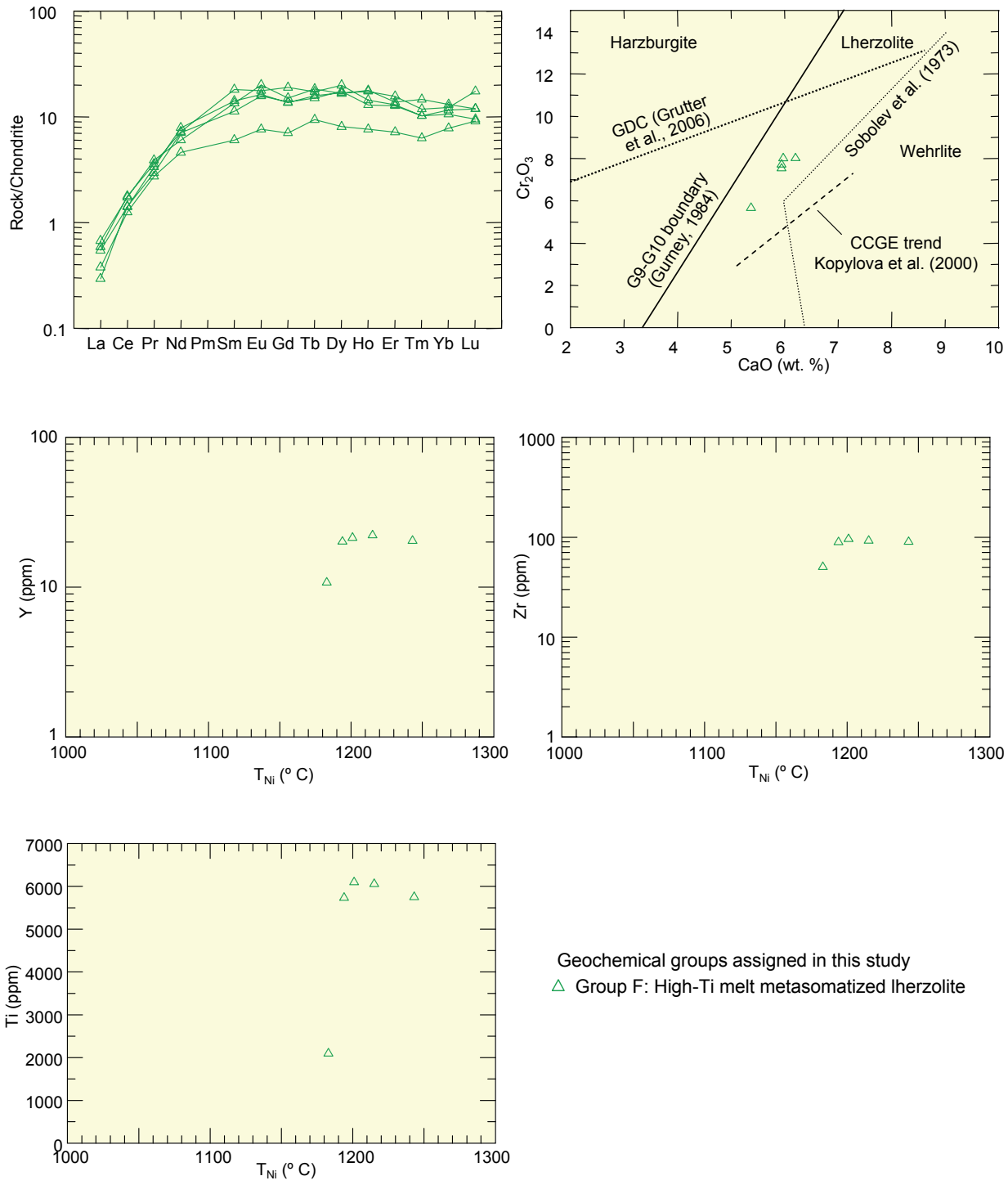

Figure 11. Normalized rare earth element diagram and selected bivariate geochemical plots for selected garnet xenocryst cores from Xena, Birch Mountains. Chondrite values from McDonough and Sun (1995).

the grains have similar profiles to Group C low-T depleted lherzolite, but can be differentiated by their higher-T_{Ni}, elevated Cr_2O_3 and lower Y. Group A garnet are characterized by

- an objective way of assigning shape to REE patterns is by using the $(Nd/Y)_N$ ratio, which is <1 and >1 for normal and sinuous patterns, respectively (Pearson et al., 1998). The Group A garnet have relatively flat to sinuous REE patterns with Nd_N/Y_N ratio of between 1.1 and 2.4;
- a lherzolite classification on the CaO-Cr_2O_3 plot with CaO and Cr_2O_3 values of between 5.4 wt. % to 6.1 wt. % and between 6.6 wt. % to 10.1 wt. %, respectively;
- depleted median Ti (640 ppm), Zr (13.1 ppm) and Y (2.8 ppm) relative to the other groups; and
- moderate T_{Ni} of between 1002ºC and 1005ºC relative to the other garnet groups, with the exception of single higher-T_{Ni} garnet from K6 (1184ºC).

4.2.2 Geochemical Group B: Low-T CCGE and Wehrlite (purple crosses on figures)

These low temperature (T_{Ni} of 831º–942ºC) garnets are only observed to occur within the Kendu body (Figure 9). The garnets are unique in that they

- are the only garnets in this dataset to follow the chromite–clinopyroxene–garnet equilibrium (CCGE) trend of Kopylova et al. (2000) in CaO-Cr_2O_3 space; the trend is reportedly found only in spinel–garnet peridotite xenoliths and attributed to equilibration of garnet with spinel by the exchange $Mg_2Al_3 \leftrightarrow Ca_2Cr_3$. Wehrlitic garnets are also evident on the CaO-Cr_2O_3 diagram (Figure 9);
- have the lowest total REE_N abundance and highest degree of sinuosity (median Nd_N/Y_N ratios of 2.4) in this dataset; and
- have low Y (0.7–13.2 ppm) and Zr (2.9–10.4 ppm), and depleted Ti (median of 129 ppm) relative to the other groups.

4.2.3 Geochemical Group C: Low-T Lherzolite (purple diamonds on figures)

The Group C profile is only observed in garnet xenocrysts from the Buffalo Head Hills K2 body (Figure 5). Geochemically, the grains are characterized by

- REE_N patterns with a high degree of sinuosity (median Nd_N/Y_N ratio of 1.4). REE pattern hinges occur at Sm_N, Ho_N and Er_N;
- a lherzolite classification on the CaO-Cr_2O_3 plot with variable CaO (5.2–5.9 wt. %) and Cr_2O_3 (2.3–6.2 wt. %);
- similar compositions as the Group E low-T fertile lherzolitic garnet in CaO-Cr_2O_3 space, Zr and Ti, with the exception of Y, which has a lower median value of 4.7 ppm; and
- low T_{Ni} of between 836º and 924ºC (median 864ºC) relative to the other groups.

4.2.4 Geochemical Group D: Moderately Fertile Lherzolite (dark blue circles on figures)

These high-T_{Ni} (1132º to 1186ºC) garnets are associated only with the Mountain Lake bodies (Figure 4). They are similar in composition to Group F high-Ti melt metasomatized lherzolitic garnet, but can be

distinguished from Group F and other groups by

- low Zr composition (<17.4 ppm with median at 4.4 ppm) with variable Ti (Figure 4);
- steep REE_N profiles, some with distinct negative Eu_N anomalies; and
- high-Cr_2O_3 (6.5–9.1 wt. %) in comparison to most garnets from the other groups.

4.2.5 Geochemical Group E: Low-T Fertile Lherzolite (blue squares on figures)

Group E garnet was observed in low-T_{Ni} xenocrysts from the K2 and K14 bodies (Figures 5 and 8). There are several striking compositional differences between this group and others investigated in this study including

- high-Y values of between 16.2 ppm and 35.7 ppm (median 26.4 ppm) with contrasting depleted (0.01–0.1 wt. %) TiO_2;
- normal increasing REE_N abundances from La_N to Lu_N, and the lowest degree of sinuosity in this dataset with an $(Nd/Y)_N$ median of 0.08;
- a CaO-Cr_2O_3 value directly below that of the CCGE trend of Kopylova et al. (2000) with high CaO (5.5–6.0 wt. %) and low Cr_2O_3 (2.1–3.0 wt. %); and
- the lowest median T_{Ni} in this dataset of 815ºC.

4.2.6 Geochemical Group F: High-Ti Melt Metasomatized Lherzolite (green triangles on figures)

Garnets designated as Group F constitute the most prolific geochemical signature in this study—about half of the xenocrysts belong to this group. With the exception of the Kendu body, Group F garnet is present in all ultramafic bodies studied in this report (Figures 4–8, 10 and 11). Group F dominates the K6 garnet suite and defines the only garnet type observed in the Legend and Xena bodies. For K6 and Xena, this might be related to the fewer number of grains available for study. Group F garnet compositions are characterized by

- normalized rare earth element (REE_N) patterns with a sharp positive-trending slope between La and Sm, flattening of the $MREE_N$ followed by slightly positive $HREE_N$. Group F garnets have a moderate degree of sinuosity in comparison to other garnet groups and can be described as normal with a median $(Nd/Y)_N$ of 0.5 for Mountain Lake, K2, Legend, Xena. In addition, Group F has the highest total REE_N abundance in this dataset;
- a lherzolitic classification on the CaO-Cr_2O_3 plot with variable CaO (4.3–7.3 wt. %) and Cr_2O_3 (2.2–10.5 wt. %). Group F includes garnet with the highest Cr_2O_3 compositions (up to 10.5 wt. %) from the Legend body (Figure 10);
- the highest concentrations of Ti (maximum of 6,579 ppm and median of 3,424 ppm) and high-Zr (median of 63 ppm) relative to the other groups. Despite elevated Ti abundances, these garnets also have high Mg (up to 161 345 ppm) and Cr (up to 78 948 ppm). The high-Cr_2O_3 grains (>9 wt. %) correlate well with high-Ti and –Zr; and
- moderate to high T_{Ni} of between 1016º and 1269ºC (median 1167ºC) relative to the other groups.

4.2.7 Geochemical Group G: Melt Metasomatized Wehrlite (red ' X's on figures)

These moderate temperature (T_{Ni} of 961º–1000ºC) garnet xenocrysts belong solely to the Kendu body and can easily be recognized by

- their composition within the field of wehrlite in CaO-Cr_2O_3 space (Figure 9);
- the highest median values of Y (31 ppm) and Zr (111 ppm) in this dataset; and
- their unique REE_N signatures containing the highest overall abundance of REE_N in this dataset, with distinctly enriched La_N-Ce_N in comparison to all other garnet $LREE_N$.

5 Implications for Mantle Stratigraphy Across Northern Alberta

The abundances of trace elements such as Ti, Zr, Y and REE in mantle garnets are dependent on the degree of depletion or re-enrichment of the protolith, and, thus, believed to constrain lithological transitions in the mantle (e.g., the "Y-edge" as an indicator of T at the inferred base of the lithosphere; Griffin and Ryan, 1995). By plotting these elements against T_{Ni}, a proxy for depth, or against each other, compositional changes in garnet xenocryst cores can provide evidence for the protolith and metasomatic history of the SLM and lower crust underlying northern Alberta. Discrimination diagrams Ti vs. T_{Ni}, Y vs. T_{Ni}, Zr vs. T_{Ni}, Y vs. Zr and Nd/Y_N vs. Sc/Y_N are presented in Figures 12 to 16, respectively.

Generally, the garnet-xenocryst core compositions from the northern Alberta kimberlite province show distinct changes in either garnet Group-type or concentration of Ti, Zr and Y that signify transitional breaks in the mantle underlying northern Alberta. These 'stratigraphic breaks' occur at approximately 755ºC, 870ºC, 950ºC, 1000ºC and 1130ºC (Figures 12–14). In addition, the trace element data provide evidence for various mantle processes in northern Alberta including depletion and re-enrichment of peridotitic garnet (Figures 15 and 16). Because it is practical to have both intra- and inter-field mantle condition variations in northern Alberta, the following discussion focuses on the characteristics of garnet compositions of each individual field.

5.1 Chinchaga Terrane (Mountain Lake)

Garnet xenocryst cores from Mountain Lake are restricted to high-T_{Ni} >1130ºC domains (Figures 12–14). As previously shown (Figure 4), two garnet types are evident: Group F high-Ti melt metasomatized lherzolite and Group D moderately fertile lherzolite. Thus, the high-T garnet-types sampled by Mountain Lake volcanism reflect entrainment of either two different protoliths or a single protolith that has undergone localized processes. Figures 15 and 16 help to clarify nomenclature assigned to the garnet groups assigned in this study. The Group F garnet has Zr/Y ratios that correspond with high-T melt metasomatism and low-Sc/Y_N suggestive of re-enriched garnet.

In contrast, the Group D garnets trend towards a regime characterized by a high geothermal gradient (Figure 15). Figure 16 shows that Group D garnet is less re-enriched (higher Nd/Y_N and Sc/Y_N) than its counterpart Group F garnet also from Mountain Lake. The negative Eu anomaly (Eu/Eu^*_N between 0.45 and 0.89) in some of the Group D garnet is interesting (Figure 4). Plagioclase-facies peridotite is stable beneath the Mohorovicic discontinuity in areas of high geothermal gradient and thinned crust, or in a shallow lithosphere that has been impregnated by melts (Sen and Leeman, 1991; Pearson et al., 2003). Thus, it is possible that the Group D garnet is representative of a shallow level of SLM, an interpretation consistent with Mountain Lake being classified as non-kimberlite, but not with the high-T_{Ni} associated with these garnets.

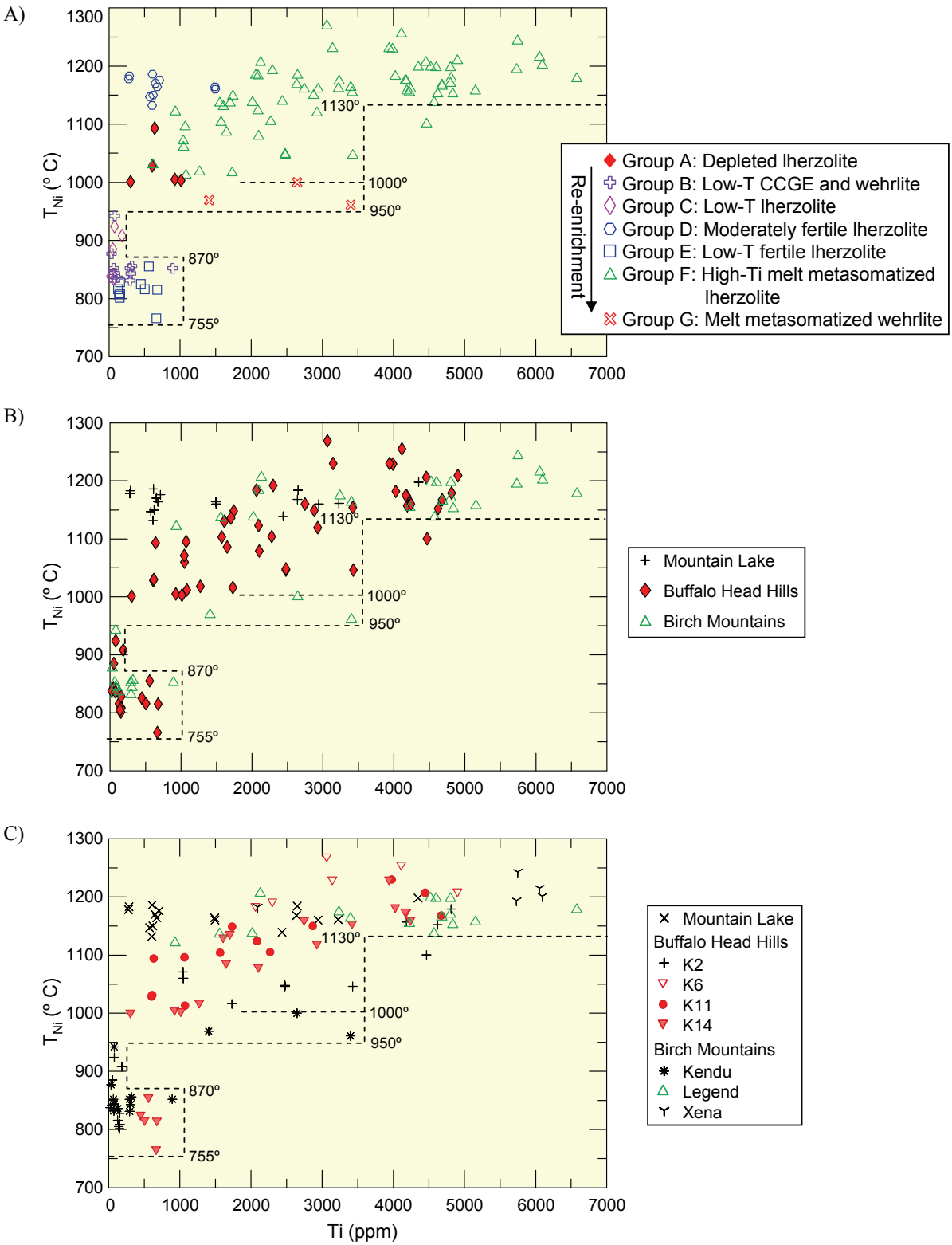

Figure 12. Distribution of T_{Ni} (Canil, 1999) versus Ti for garnets from selected ultramafic bodies of the northern Alberta kimberlite province. The diagrams show garnet xenocryst cores plotted as the following: A) garnet 'groups' as depicted in this study; B) ultramafic fields; and C) individual ultramafic bodies.

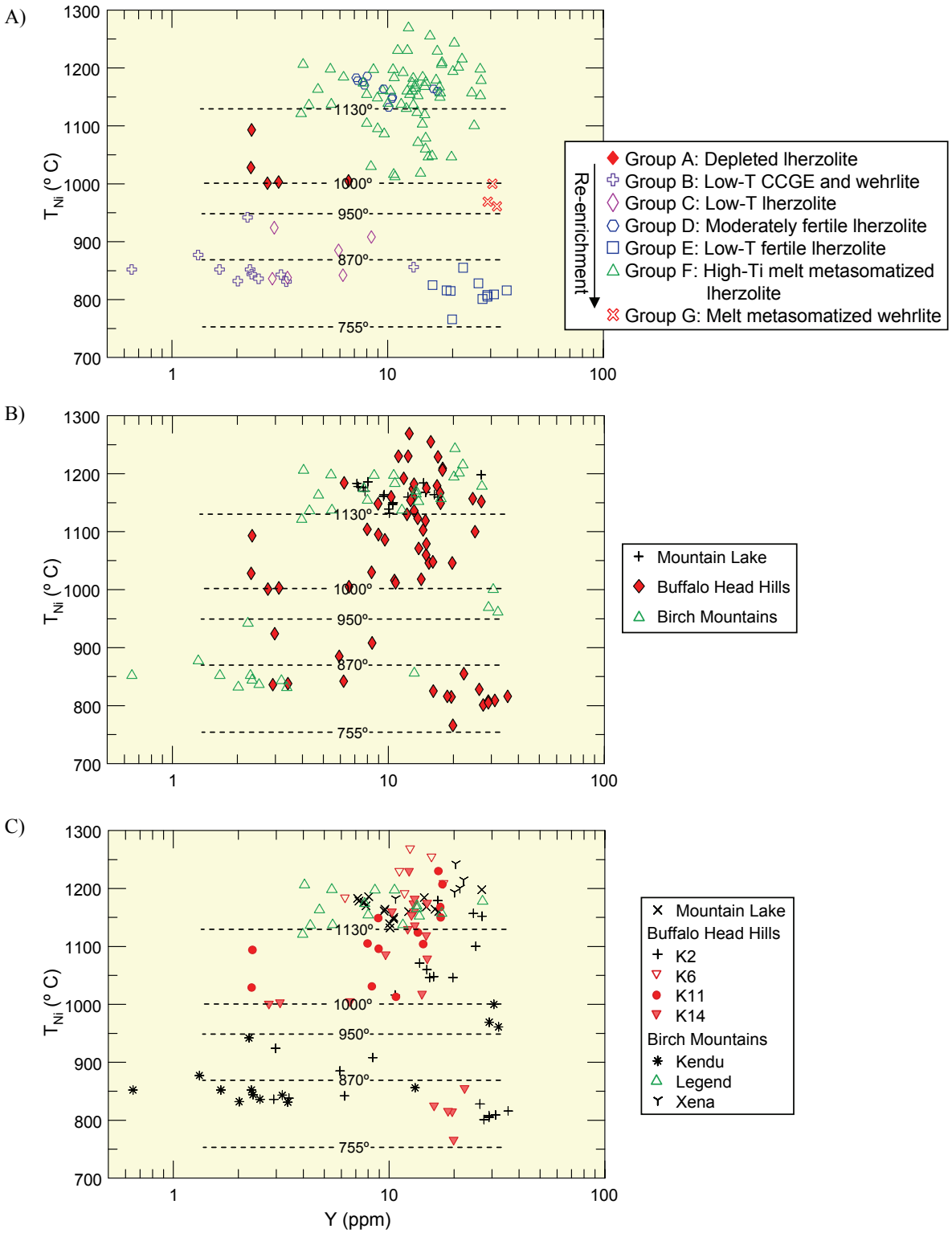

Figure 13. Distribution of TNi (Canil, 1999) versus Y for garnets from selected ultramafic bodies of the northern Alberta kimberlite province. The diagrams show garnet xenocryst cores plotted as the following: A) garnet 'groups' as depicted in this study; B) ultramafic fields; and C) individual ultramafic bodies.

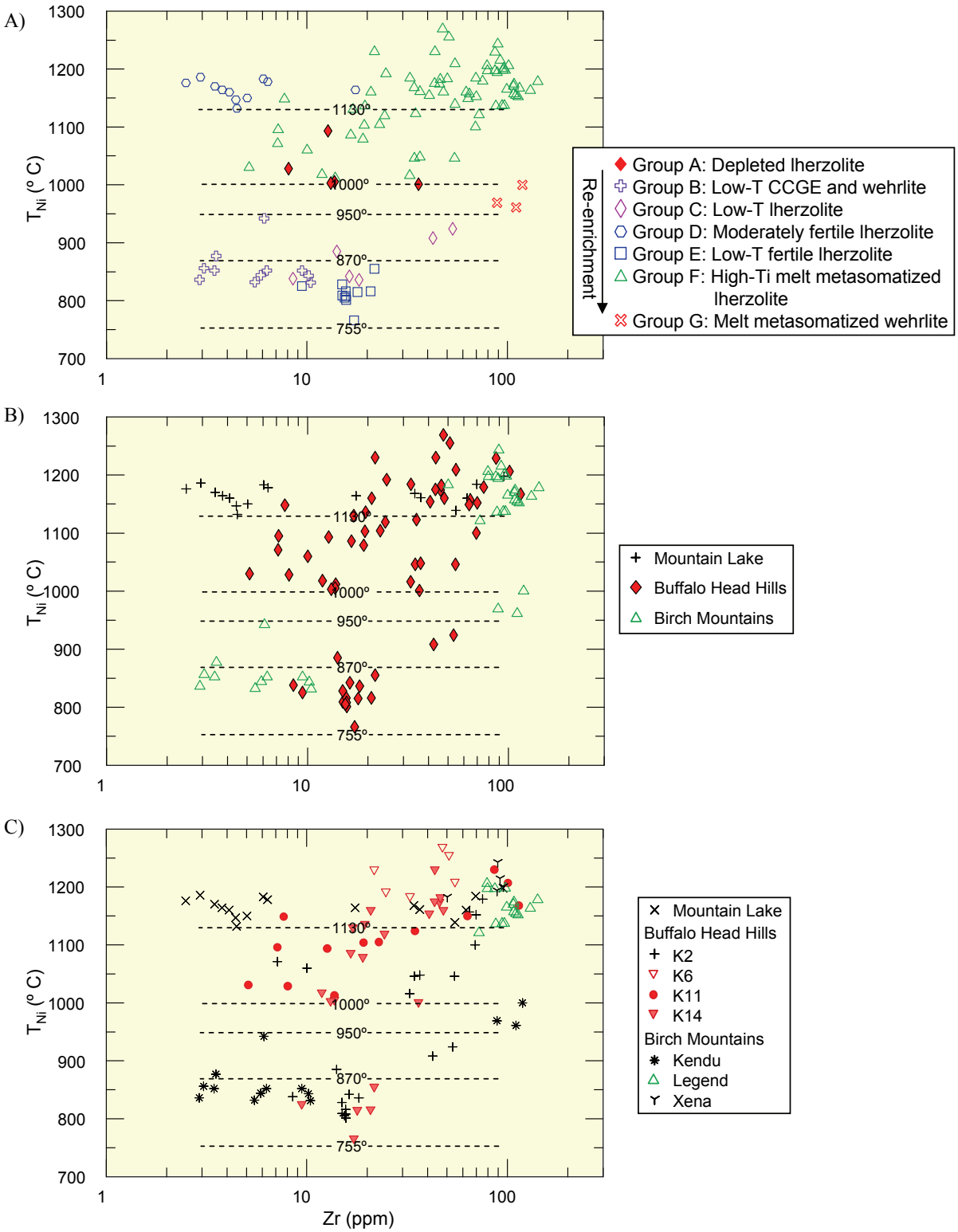

Figure 14. Distribution of TNi (Canil, 1999) versus Zr for garnets from selected ultramafic bodies of the northern Alberta kimberlite province. The diagrams show garnet xenocryst cores plotted as the following: A) garnet 'groups' as depicted in this study; B) ultramafic fields; and C) individual ultramafic bodies.

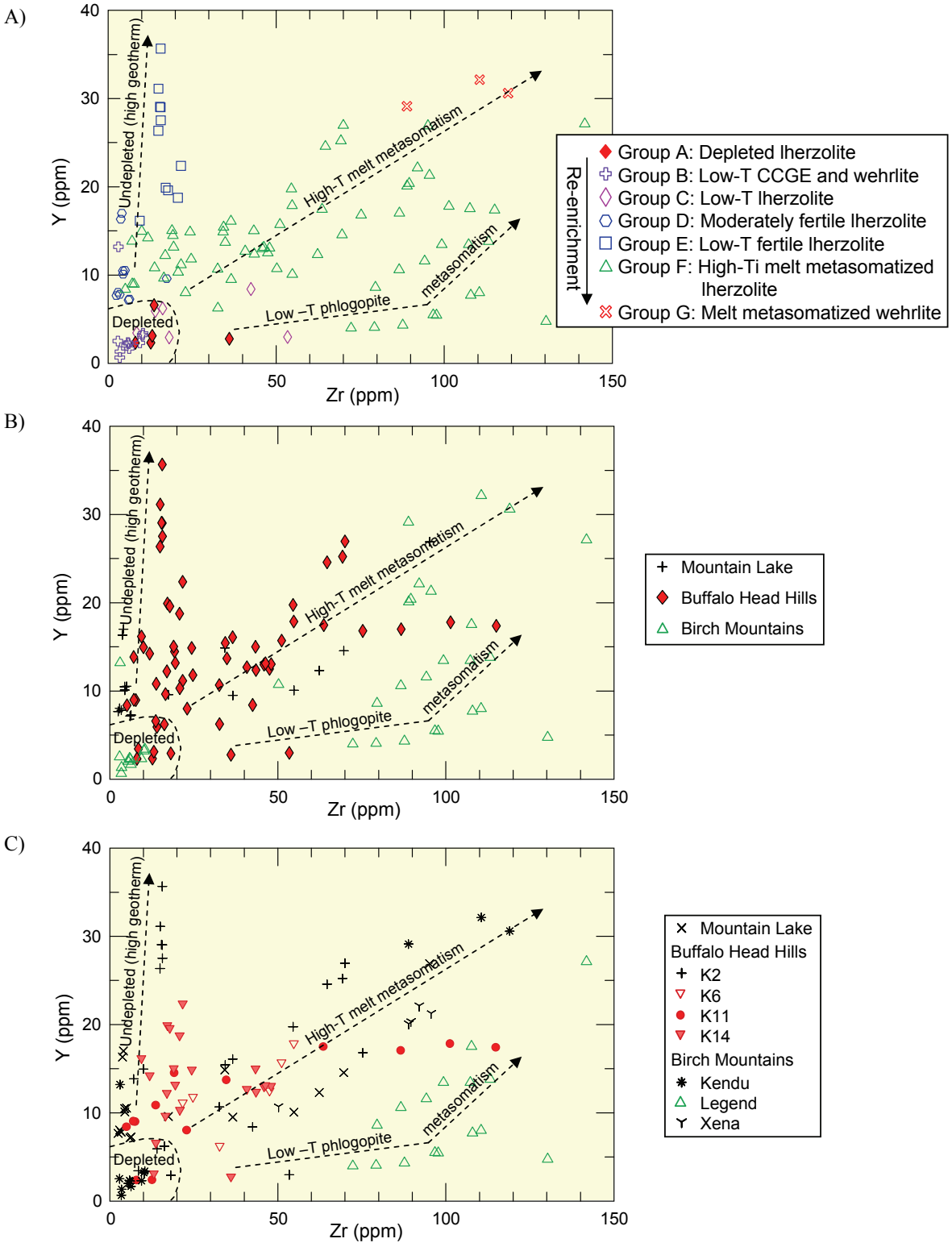

Figure 15. Y versus Zr for garnets from selected ultramafic bodies of the northern Alberta kimberlite province. The diagrams show garnet xenocryst cores plotted as the following: A) garnet 'groups' as depicted in this study; B) ultramafic fields; and C) individual ultramafic bodies. Fields and metasomatic trends from Griffin et al. (1999e).

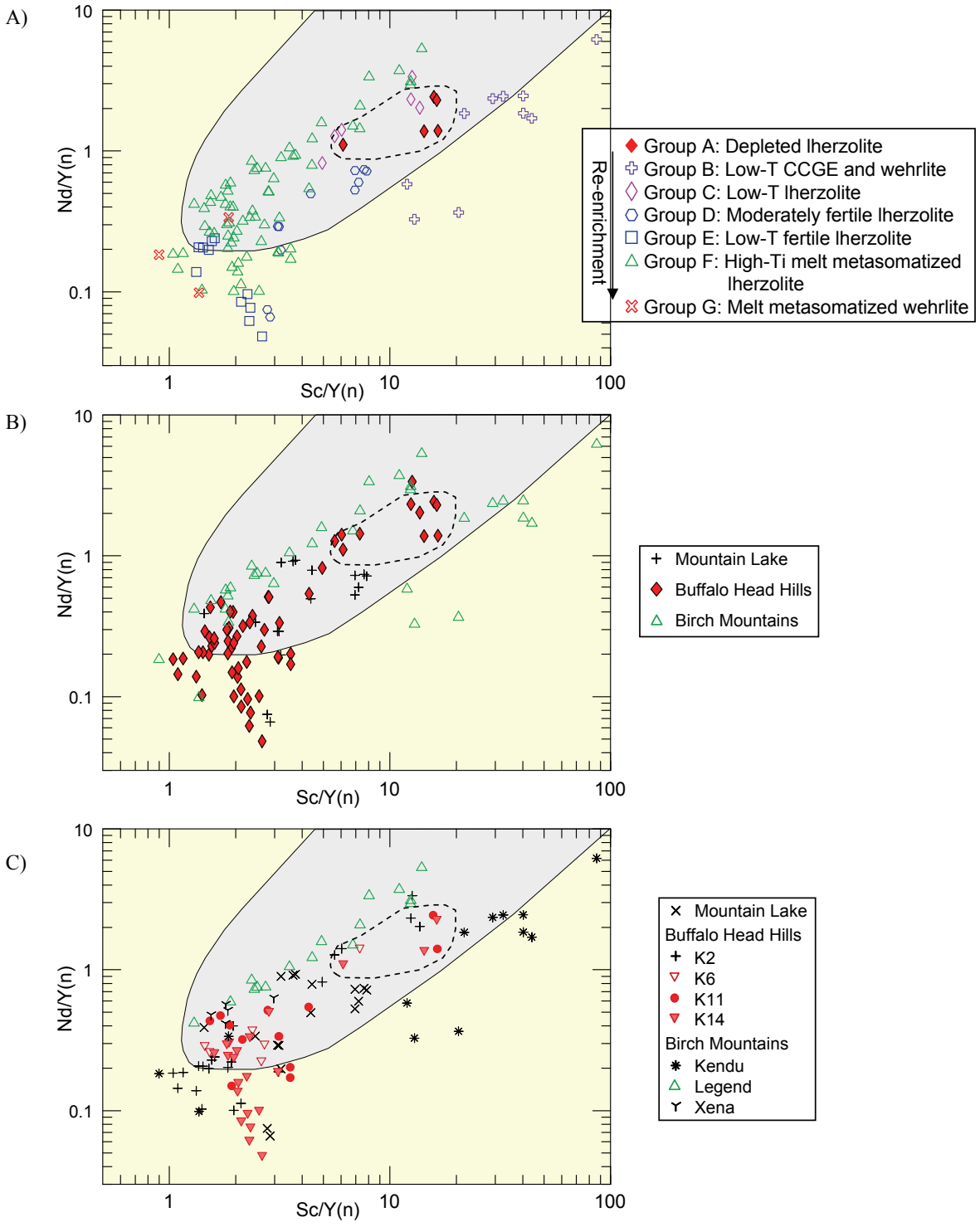

Figure 16. Correlation of the degree of sinuosity of REE pattern $(Nd/Y)_N$ ratio with depletion $(Sc/Y)_N$ for garnets from selected ultramafic bodies of the northern Alberta kimberlite province. The diagrams show garnet xenocryst cores plotted as the following: A) garnet 'groups' as depicted in this study; B) ultramafic fields; and C) individual ultramafic bodies. Shaded field encompasses diamond inclusion garnet from Pearson et al. (1998). The dashed line represents the apparent northern Alberta diamond field based on the location of depleted Group A lherzolite.

A deeper origin is favoured for Mountain Lake peridotite. The co-existence of high-Cr garnet with Cr-spinel at Mountain Lake implies that garnet Cr content can be correlated with depth (Grütter et al., 1999). In addition, Skupinski et al. (2001) reported the presence of rod-like β-ilmenite inclusions in olivine from Mountain Lake, a phenomenon that has been related to exsolution from the ultra-high pressure Ti-bearing polymorph of olivine *wadsleyite* at depths of between 300 and 450 km (metamorphic peridotite from Alpe Arami, Central Alps; Dobrzhinetskaya et al., 1996). Therefore, more suitable explanations for the Eu anomaly observed in the Mountain Lake Group D garnet must invoke a deeper source. Two possibilities include the following: Moore et al. (1991), who concluded that negative Eu anomalies in majoritic garnet result from high-pressure, low volume melts; and Stachel et al. (2000), who concluded that negative Eu patterns involve subducted oceanic lithosphere where enrichment in garnet incompatible trace elements is caused by dehydration and/or melt release from subducted slabs.

5.2 Buffalo Head Terrane (Buffalo Head Hills)

Garnets from the Buffalo Head Hills bodies contain a suite of grains that encompasses a thermal range of between 766º and 1269ºC. Based on the transitional layers illustrated in Figures 12, 13 and 14, garnet from the Buffalo Head Hills bodies are evident within four of the five SLM layers: 755º to 870ºC, 870º to 950ºC, 1000º to 1130ºC and >1130ºC. The K2 and K14 bodies sampled a wide range of garnet types with garnet from four and three of the five SLM layers, respectively (Figure 12). Garnet with T_{Ni} of between 1000º and 1130ºC were only sampled within the Buffalo Head Hills field (K2, K11 and K14) and are not present in either the Mountain Lake or the Birch Mountains bodies. This wide-ranging representation of garnet compositions from the Buffalo Head Hills permits a unique reconstruction of the mantle beneath the Buffalo Head Terrane in north-central Alberta from low- T_{Ni} to high- T_{Ni} as follows.

In the Buffalo Head Hills, garnet with T_{Ni} of <870ºC are dominated by Group E garnet xenocrysts from the K2 and K14 bodies. These garnets have the lowest T_{Ni} and highest Y in this dataset, with an REE pattern characterized by a normal REE pattern with elevated, flat HREE (Figures 5, 8, 12, 13 and 14). In addition, these garnets have high Y/Zr ratios and low-Nd/Y_N and –Sc/Y_N (Figures 15 and 16). Collectively, these thermal and geochemical signatures are suggestive of fertile garnet in a shallow SLM setting.

A cluster of Group C garnet from K2 also defines low-T_{Ni} garnet from Buffalo Head Hills; these garnets are evident in the 870º to 950ºC SLM layer (Figures 12–14). Group C garnet has depleted lherzolite compositions with low-Ti, -Y and -Zr, and sinusoidal REE patterns (Figures 5, 12, 13, 14 and 15). Several authors have poised alternative explanations for the formation of low-T_{Ni} depleted garnets similar to the Group C-type garnet observed here. The sinuous REE patterns could be attributed to interaction with a LREE-enriched metasomatic fluid (Hoal et al., 1994; Shimizu, 1999; Shimizu et al., 1997; Stachel et al., 1998). Phlogopite, carbonatite and/or volatile-rich melt metasomatism would cause enrichment of LREE without, or with only a small concomitant enrichment in HFSE (Yaxley et al., 1998; Griffin et al., 1999a; Carbno and Canil, 2002; Aulbach et al., 2004). Finally, Canil et al. (2003) suggested that low Ti_{Ni} garnet might be related to formation of garnet from residues formed at higher oxygen fugacity (fO_2), perhaps in a convergent margin environment. All of these metasomatic styles are common in shallow lithosphere and, thus, we expect some combination of these explanations has influenced Group C garnet.

In the northern Alberta kimberlite province, garnet within the T_{Ni} of between 1000º and 1130ºC are restricted to the Buffalo Head Hills and include Group F and Group A garnet-types from the diamondiferous K11 and K14 bodies, and Group F garnet from diamond-poor K2. The K11 and K14 Group A garnet defines a narrow T_{Ni} range of between approximately 1000º to 1100ºC and has depleted Ti, Zr, and Y, and a flat REE profile (Figures 7, 8, 12, 13, 14, 15 and 16). The depleted Group A garnet compositions are interesting because similar garnet compositions have been observed in kimberlites from the Archean Slave Province and worldwide Archean crustal provinces (Carbno and Canil, 2002; Griffin et

al., 1999b, 1999c, 1999d; Creighton et al., in press). These results also compare well with the approximate position of the diamond stability field and with peridotitic garnet-clinopyroxene inclusion pairs from Buffalo Head Hills diamonds that yield equilibration temperatures of 1100º to 1200ºC ± 50ºC on a 40 mW/m^2 geotherm (Davies et al., 2004).

In contrast, the 1000º to 1130ºC Group F garnet has abundant Ti, Zr and Y suggestive of melt metasomatism (Figures 12 and 15). The high-Ti and -Zr Group F garnet is chemically similar to those documented in garnet xenocryst studies at Fort à la Corne (Canil et al., 2003). Whether this correlation is indicative of similar mantle within these two prairie kimberlite provinces remains to be proven.

Group F garnet also dominates the T_{Ni} >1130ºC SLM layer sampled by the K2, K11 and K14 bodies. Group F garnet has high Y and Zr content, and low Zr/Y ratios that correspond with high-Ti melt metasomatism (Figure 15). Based on the abrupt chemical changes (e.g., Ti, Y and Zr) at the lower high-T_{Ni} layer boundary (1130ºC), the approximate depth of the lithosphere-asthenosphere boundary (LAB) is at a depth of approximately 180 km. This depth matches the LAB depth prediction of Aulbach et al. (2004) based on their P-T correlation of sheared garnet lherzolite. The 180 km LAB depth also agrees with the results of a recent magnetotelluric study in the Buffalo Head Hills by Türkoğlu et al. (2007), who modelled a decrease in electrical resistivity at a depth of approximately 200 km. We caution, however, that this apparent boundary could also be related to a sheared peridotite formed within a restricted thermal aureole in the mantle surrounding the kimberlite conduit/field, which would eliminate inference of a steady state chemical mantle zonation between asthenosphere and lithosphere (Moore and Lock, 2001).

5.3 Taltson Magmatic Zone (Birch Mountains)

Ultramafic bodies in the Birch Mountains area sampled garnet with three distinct thermal ranges (e.g., Figure 12). The Kendu body sampled garnet from the low-T_{Ni} SLM layer (<870ºC) and was the only body to sample garnets within the 950º to 1000ºC layer. Kendu Group B low-T CCGE and wehrlite garnet with T_{Ni} of <870ºC were only observed in the Kendu body. These low-T_{Ni} garnets have ultradepleted compositions (Figures 12–16) and are similar to CCGE-type compositional arrays recognized in moderately calcic garnets from low-T (700º to 900ºC) spinel-garnet wehrlite xenoliths (Kopylova et al., 2000; Carbno and Canil, 2002; Lehtonen et al., 2004). Grütter et al. (2006) report a linear array within Cr_2O_3-CaO diagram at low garnet Cr_2O_3 content occurs at low-P within mantle regions characterized by relatively ‘cool’ geotherms.

Garnets of the Group G low-T_{Ni} (900º to 1000ºC) SLM layer were only observed in the Kendu body. These garnets have high-REE abundance, -Y and -Zr, all of which indicate garnet re-enrichment via high-T melt metasomatism (Figures 12–16). Figures 15 and 16 show this garnet group appears to have undergone the greatest degree of re-enrichment. Aulbach et al. (2004) suggested that wehrlite better preserves melt metasomatic signatures compared to lherzolite, thus we suggest these high CaO garnets be referred to as melt metasomatized wehrlite.

In contrast to Kendu, the Legend and Xena bodies only sampled Group F garnet from high-T_{Ni} SLM layers (>1130ºC). These garnets have varying Y, high-Y and -Zr, and low Zr/Y ratios that correspond with re-enriched high-T melt metasomatism (Figures 12–16). Some of the $MREE_N$ within this group have slight to moderately negative Gd_N anomalies (e.g., Legend and Xena, Figures 10 and 11), which correlate well with Ti and Zr, suggesting an enrichment process involving metasomatism.

High Y-Zr Group F garnet with high Zr/Y ratios and sinusoidal REE were sampled exclusively by the Legend body (Figure 15 and 16). Griffin et al. (1999c) interpreted garnets with this geochemical profile as representative of mantle having undergone phlogopite metasomatism; however, the high Ti and Zr/

Sm_N in the Legend Group F garnet attest to a more complicated metasomatic history probably involving significant melt metasomatic processes. While the Legend garnets do fall within the diamond inclusion field of Pearson et al. (1998) on Figure 16, minimal diamonds have been recovered from Legend. A recent 10.2 tonne mini-bulk sample from Legend yielded a total of one macro-diamond and three micro-diamonds (Grizzly Diamonds Ltd., 2007). We recommend that this field should be revised with the new northern Alberta diamond-inclusion field based on the Nd/Y_N and Sc/Y_N composition of Group A-depleted lherzolite from the Buffalo Head Hills (Figure 16).

6 Implications for Future Garnet Classification in Northern Alberta

The Cr_2O_3 vs. CaO diagram for peridotitic garnet has been used to distinguish classification boundaries for garnets in harzburgite, lherzolite and wehrlite (Sobolev et al., 1973) and is an important factor to prospectors because 85% of peridotitic garnets included in diamond fall to lower Ca than the G10-G9 boundary (Gurney, 1984). This diagram has been further improved by Grütter et al. (2006), who studied garnet in diamond-bearing peridotite xenoliths with primary Cr-spinel and defined a unique Cr-saturated linear trend—known as the graphite-diamond constraint (GDC)—that transect the harzburgite and lherzolite compositional fields in Cr_2O_3-CaO space.

An enigma that has faced garnet xenocryst studies of the Buffalo Head Hills kimberlite field and exploratory surficial indicator-mineral studies in northern Alberta is that very few garnets from diamondiferous bodies plot within the subcalcic harzburgite G10 or high-Cr lherzolite GDC diamond thresholds based on the aforementioned classical mantle mineral chemistry modeling in Cr_2O_3-CaO space. This contention is extended to EMPA peridotitic garnet xenocryst data in this study (Figure 17). The common, but not proven, perception for this phenomenon is that garnet associated with diamond-bearing bodies in northern Alberta is the result of their occurrence within off-craton, younger Paleoproterozoic accreted terranes. Another explanation based on Buffalo Head Hills diamond-inclusion studies of Davies et al. (2004) and Banas et al. (2006), is that northern Alberta diamond has an eclogitic paragenesis based on 12 of the 16 diamond-inclusion garnets recovered being low-Cr eclogite. While this is valid observation, we note that discussion on peridotitic garnet versus diamond content is warranted as the remaining diamond-inclusion garnets include lherzolitic (3 grains) or wehrlitic (1 grain) paragenesis.

Our observations towards this conundrum are important for future diamond exploration in Alberta. This study has shown that alteration of mantle garnet beneath northern Alberta occurs via infiltration of Ti-rich fluids/melts. Thus, it is possible that Ti- and Ca-rich fluids/melts are responsible for conversion of harzburgite to lherzolite. This hypothesis is similar to Creighton et al. (in press), who concluded a similar modification of garnet compositions in the central Slave craton. This theory has further credibility given that Aulbach et al. (2004) documented the occurrence of a relict Ca-undersaturated Cr_2O_3-rich garnet in a garnet harzburgite xenolith—a chemical signature that is virtually exclusive to Archean SLM.

Based on LA-ICP-MS analyses, trace-element analysis of garnet xenocrysts from northern Alberta ultramafic bodies provides an additional means of separating garnets into distinct geochemical groups in comparison to EMPA analysis. The high precision determination of trace elements (particularly those that are not as mobile as, for example, CaO) can help to determine the degree of re-enrichment critical in the identification of depleted mantle favourable for diamond-bearing kimberlite and non-destructive processes in diamond preservation.

If LA-ICP-MS analysis is not a viable option, then some major element relationships can be considered based on the results presented herein. Hood and McCandless (2004) showed that Cr_2O_3 contents in peridotitic garnet can help distinguish between barren and diamondiferous bodies in the Buffalo Head Hills kimberlite field where kimberlite K252, with 55 carats per hundred tonnes, has a pronounced trend

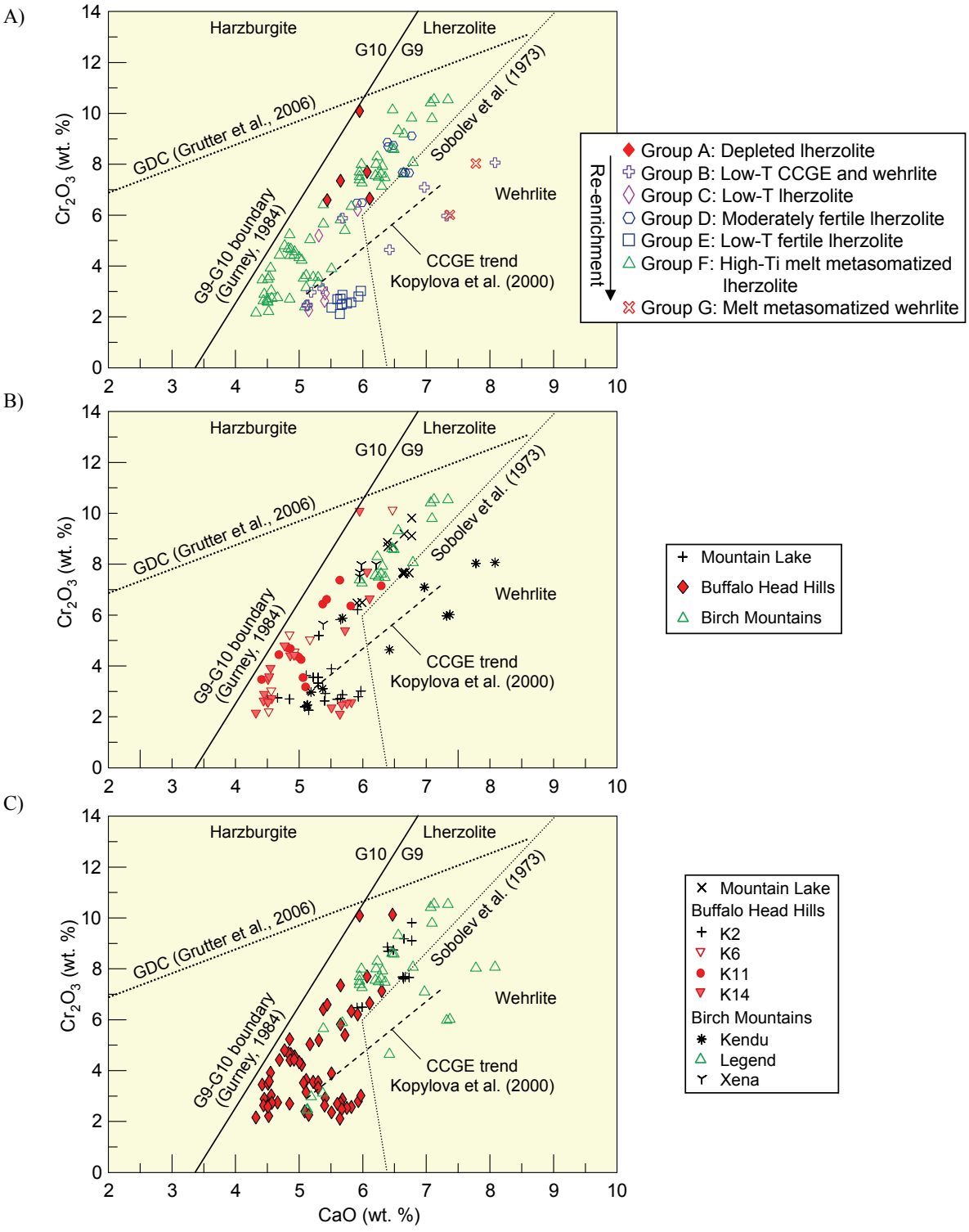

Figure 17. Cr_2O_3 versus CaO diagram for peridotitic garnet from selected ultramafic bodies of the northern Alberta kimberlite province. The diagrams show garnet xenocryst cores plotted as the following: A) garnet 'groups' as depicted in this study; B) ultramafic fields; and C) individual ultramafic bodies. Shaded field encompasses diamond inclusion garnet from Pearson et al. (1998).

of elevated Ca and Cr. We caution that Cr_2O_3, as a proxy for depth (Grütter et al., 1999) can also have significant concentrations in hot, less depleted asthenospheric-type mantle as shown in garnet xenocrysts from the diamond-poor Mountain Lake body. An analogous observation applies to CaO because this study has shown that Ti-rich metasomatic melts/fluids have modified the original garnet composition, possibly from sub-calcic harzburgite to lherzolite. Modeling in Cr_2O_3 vs. CaO space, therefore, might be misleading and we see the need for alternative classification for northern Alberta. For conventional EMPA data, we recommend the comparison between TiO_2 and T_{Mn} be considered. Future EMPA evaluation of peridotitic mantle in northern Alberta may consider the Mn-in-garnet geothermometer and TiO_2 content as indicators of depth and mantle depletion/re-enrichment, respectively. Further scrutiny of garnets satisfying T_{Mn} of between 1000º and 1130ºC (T based on our T_{Ni} results), and low TiO_2 (e.g., <0.2 wt. %), could then factor in Cr_2O_3 with favourable garnet having higher Cr_2O_3 concentrations (e.g., >6 wt. %).

7 Conclusions

Trace element analysis of garnet xenocrysts from northern Alberta ultramafic bodies records a diverse range of geochemical behaviour that enables new interpretations about the chemical nature of lower crustal-SLM beneath northern Alberta.

The range in T_{Ni} recorded by the northern Alberta kimberlite province is between approximately 770º and 1270ºC, and distinct inter- and intra-field thermal distributions occur. Chemical changes in garnet cores define transitional breaks in the mantle underlying northern Alberta. From low- to high-T, these regions include the following: fertile lherzolite, CCGE and wehrlite (<870ºC), low-T lherzolite (870º to 950ºC), melt metasomatized wehrlite (950º to 1000ºC), depleted lherzolite and melt metasomatized lherzolite (1000º to 1130ºC), and moderately fertile lherzolite and high-Ti melt metasomatized lherzolite (>1130ºC). These garnet groups can serve as a comparative model for future evaluations of garnet compositions in Alberta because they help to decipher the degree of depletion or re-enrichment associated with metasomatic events underlying northern Alberta—a contention that has significant implication for the documentation and evaluation of known occurrences of kimberlite in Alberta and surficial kimberlite-indictor mineral studies critical to evaluation of future targets.

The results of this garnet xenocryst trace element study distinguish inter-field mantle variations. Garnets from the Buffalo Head Hills bodies contain a suite of grains that encompasses a thermal range of between 770ºC and 1270ºC. This wide-ranging representation of garnet compositions from the Buffalo Head Hills permits a unique reconstruction of the mantle beneath the Buffalo Head Terrane in north-central Alberta from low T_{Ni} to high T_{Ni}. Of the three ultramafic rock clusters/fields in northern Alberta, depleted lithospheric keel in the Buffalo Head Hills field clearly shows that this region has the best potential to yield diamond-bearing kimberlite. Specifically, the Buffalo Head Hills field is underlain by 1000º to 1130ºC SLM layer with a predominance of depleted peridotite at approximately 160 km depth. We recommend, therefore, that these high-Cr_2O_3, (6.6–10.1 wt. %), low Y (<6.6 ppm) and elevated Nd_N/Y_N (1.1–2.4) depleted lherzolite garnets help to approximate a diamond window in the mantle underlying the Buffalo Head Hills at depths of between 160 km and 180 km, and be considered a proxy for future garnet evaluations in northern Alberta.

In contrast, garnet from the Mountain Lake cluster and Birch Mountains Field exhibit many common features indicative of multiple metasomatic events and extreme low- or high-T of last equilibration. Both the Mountain Lake and Birch Mountain areas seem to be characterized by a geothermal gradient associated with thin lithosphere or a hot, extensively re-enriched asthenospheric-type mantle. Some of the high-Cr garnet from Mountain Lake has depleted Eu anomalies that may indicate a deeply subducted slab source. Low T_{Ni} (<870ºC) garnet from the Birch Mountains Kendu body originated within mantle

regions characterized by relatively cool geotherms. The Legend and Xena bodies only sampled garnet from high T_{Ni} SLM layers (>1130ºC) with high Y and Zr, and low Zr/Y ratios that correspond with re-enriched high-T melt metasomatism. The Legend body also sampled garnet with high Zr/Y ratios and sinusoidal REE_N, attesting to a more complicated metasomatic history that possibly involved significant melt metasomatic processes. These interpretations suggest the Mountain Lake and Birch Mountain regions may either have sampled melt from mantle in a younger region or they may have been extensively modified and affected by younger arc magmatism that possibly occurred on either side of the Buffalo Head Hills accreted terrain.

References

Aulbach, S., Griffin, W.L., O'Reilly, S.Y. and McCandless, T.E. (2004): Genesis and evolution of the lithospheric mantle beneath the Buffalo Head Terrane, Alberta (Canada); Lithos, v. 77, p. 413–451.

Bachu, S. and Burwash, R.A. (1994): Geothermal regime in the Western Canada Sedimentary Basin; *in* Geological Atlas of the Western Canada Sedimentary Basin, G.D. Mossop and I. Shetson (comp.), Canadian Society of Petroleum Geologists and Alberta Research Council, Special Report 4, p. 447–454.

Banas, A., Stachel, T., Muehlenbachs, K. and McCandless, T.E. (2006): Diamonds from the Buffalo Head Hills, Alberta: formation in a non-conventional setting; Lithos, v. 93, p. 199–213.

Burwash, R.A., Kupricka, J. and Wijbrans, J.R. (2000): Metamorphic evolution of the Precambrian basement of Alberta. Canadian Mineralogoist, v. 38, p. 423-434.

Canil, D. (1999): The Ni-in-garnet geothermometer: calibration at natural abundances; Contributions to Mineralogy and Petrology, v. 136, p. 240–246.

Canil, D., Schulze, D.J., Hall, D., Hearn, B.C., Jr. and Milliken, S.M. (2003): Lithospheric roots beneath western Laurentia: the geochemical signal in mantle garnets; Canadian Journal of Earth Science, v. 40, p. 1027–1051.

Carbno, G.B and Canil, D. (2002): Mantle structure beneath the southwest Slave craton, Canada: constraints from garnet geochemistry in the Drybones Bay kimberlite; Journal of Petrology, v. 43. p. 129–142.

Carlson, S.M., Hillier, W.D., Hood, C.T., Pryde, R.P. and Skelton, D.N. (1999): The Buffalo Hills kimberlites: a newly-discovered diamondiferous kimberlite province in north-central Alberta, Canada; *in* Proceedings of the Seventh International Kimberlite Conference, Cape Town, South Africa, J.J. Gurney, J.L. Gurney, M.D. Pascoe and S.H. Richardson (ed.), v. 1, p. 109–116.

Creighton, S.D. and Eccles, D.R. (2002): 2002 Compilation of Alberta ultramafic rock occurrences: location, ground geophysics, drillhole logs and diamond content; Alberta Energy and Utilities Board, EUB/AGS Geo-Note 2002-23, CD.

Creighton, S.D., Stachel, T., McLean, H., Muehlenbachs, K., Simonetti, A., Eichenberg, D. and Luth, R. (in press): Diamondiferous peridotitic microxenoliths from the Diavik Diamond Mine, NT; Contributions to Mineralogy and Petrology.

Davies, R.M., Griffin, W.L., O' Reilly, S.Y. and McCandless, T.E. (2004): Inclusions in diamonds from the K14 and K10 kimberlites, Buffalo Head Hills, Alberta, Canada: diamond growth in a plume?; Lithos, v. 77, p. 99–111.

Dobrzhinetskaya , L., Green II, H.W. and Su Wang (1996): Alpe Arami: a Peridotite massif form depth of more than 300 kilometres; Science, v. 271, p. 1841–1845.

Eccles, D.R. (2004): Petrogenesis of the northern Alberta kimberlite province; M.Sc. thesis, University of Alberta, 131 p.

Eccles, D.R., Heaman, L.M., Luth, R.W. and Creaser, R.A. (2004): Petrogenesis of the Late Cretaceous, northern Alberta kimberlite province; Lithos, v. 77, p. 435–459.

Eccles, D.R., Creaser, R.A., Heaman, L.M. and Ward, J. (in press): Rb-Sr and U-Pb geochronology and setting of the Buffalo Head Hills kimberlite field, Northern Alberta; Canadian Journal of Earth Science.

Griffin, W.L. and Ryan, C.G. (1995): Trace elements in indicator minerals: area selection and target evaluation in diamond exploration; Journal of Geochemical Exploration, v. 53, p. 311–337.

Griffin, W.L., Fisher, N.I., Friedman, J.H., Ryan, C.G. and O'Reilly, S.Y. (1999a): Cr-pyrope garnets in the lithospheric mantle: compositional systematics and relations to tectonic setting; Journal of Petrology, v. 40, p. 679–705.

Griffin, W.L., Doyle, B.J., Ryan, C.G., Pearson, N.J., O'Reilly, S., Davies, R., Kivi, K., van Achterbergh, E. and Natapov, L. (1999b): Layered mantle lithosphere in the Lac de Gras area, Slave craton: composition, structure and origin; Journal of Petrology, v. 40, p. 705–727.

Griffin, W.L., Doyle, B.J., Ryan, C.G., Pearson, N.J., O'Reilly, S., Natapov, L., Kivi, K., Kretschmar, U. and Ward, J. (1999c): Lithosphere structure and mantle terranes: Slave craton, Canada; *in* Proceedings of the Seventh International Kimberlite Conference, Cape Town, South Africa, J.J. Gurney, J.L. Gurney, M.D. Pascoe and S.H. Richardson (ed.), p. 299–306.

Griffin, W.L., Fisher, N.I., Friedman, J., Ryan, C.G. and O'Reilly, S.Y. (1999d): Cr-pyrope garnets in the lithospheric mantle; *in* Compositional Systematics and Relations to Tectonic Setting, Journal of Petrology, v. 40, p 679–704.

Griffin, W.L., Shee, S.R., Ryan, C., Win, R.R. and Wyatt, B.A. (1999e): Harzburgite to lherzolite and back again: metasomatic processes in ultramafic xenoliths from the Wesselton kimberlite, Kimberley, South Africa; Contributions to Mineralogy and Petrology, v. 134, p. 232–250.

Grizzly Diamonds Ltd. (2007): Grizzly diamonds–Legend kimberlite diamond results; news release transmitted by Canadian Corporate News, July 19, 2007 (available online at http://www.grizzlydiamonds.com).

Grütter, H., Apter, D.B. and Kong, J. (1999): Crust-mantle coupling: evidence from mantle-derived xenocrystic garnets; *in* Proceedings of the Seventh International Kimberlite Conference, Cape Town, South Africa, J.J. Gurney, J.L. Gurney, M.D. Pascoe and S.H. Richardson (ed.), p. 307–313.

Grütter, H., Latti, D. and Menzies, A. (2006): Cr-saturation arrays in concentrate garnet compositions from kimberlite and their use in mantle barometry; Journal of Petrology, v. 47(4), p. 801–820.

Gurney, J.J. (1984): A correlation between garnets and diamonds in kimberlite; *in* Kimberlite Occurrence and Origin: a basis for conceptual models in exploration, J.E. Glover and P.G. Harris, (ed.), University of Western Australia Publication 8, p. 143–166.

Hamilton, W.N., Langenberg, W.C., Price, M.C. and Chao, D.K. (1999): Geological map of Alberta; Alberta Energy and Utilities Board, EUB/AGS Map 236, scale 1:1 000 000.

Heaman, L.M., Kjarsgaard, B.A. and Creaser, R.A. (2003): The timing of kimberlite magmatism and implications for diamond exploration: a global perspective; Lithos, v. 71, 153–184.

Hoal, K.E.O., Hoal, B.G., Erlank, A.J. and Shimizu, N. (1994): Metasomatism of the mantle lithosphere recorded by rare earth elements in garnets; Earth and Planetary Science Letters, v. 126, p. 303–313.

Hoffman, P.F. (1988): United plates of America: the birth of a craton; Annual Review of Earth and Planetary Sciences, v. 16, p. 543–604.

Hood, C.T.S. and McCandless, T.E. (2004): Systematic variations in xenocryst mineral composition at the province scale, Buffalo Hills kimberlites, Alberta, Canada; Lithos, v. 77, p. 733–747.

Jarosewich, E. (2002): Smithsonian microbeam standards; Journal of Research of the National Institute of Standards and Technology, v. 107, p. 681–685.

Kopylova, M.G., Price, S.E. and Russell, J.K. (2000): Primitive magma from the Jericho pipe, N.W.T., Canada: constraints on primary kimberlite melt chemistry; Journal of Petrology, v. 41, p. 789–808.

Leckie, D.A., Kjarsgaard, B.A., Peirce, J.W., Grist, A.M., Collins, M., Sweet, A., Stasiuk, L., Tomica, M.A., Eccles, D.R., Dufresne, M.B., Fenton, M.M., Pawlowicz, J.G., Balzer, S.A., McIntyre, D.J. and McNeil, D.H. (1997): Geology of a Late Cretaceous possible kimberlite at Mountain Lake, Alberta—chemistry, petrology, indicator minerals, aeromagnetic signature, age, stratigraphic position and setting; Geological Survey of Canada, Open File Report 3441, 202 p.

Lehtonen, M.L., O'Brien, H.E., Peltonen, P., Johanson, B.S. and Pakkanen, L.K. (2004): Layered mantle at the Karelian craton margin: P-T of mantle xenocrysts and xenoliths from the Kaavi-Kuopio kimberlites, Finland; Lithos, v. 77, p. 593–608.

McDonough, W. F. and Sun, S.S. (1995): The composition of the Earth; Chemical Geology, v. 120, p. 223–253.

Moore, A.E. and Lock, N.P. (2001): The origin of mantle-derived megacrysts and sheared peridotites—evidence from kimberlites in the northern Lesotho Orange Free State (South Africa) and Botswana pipe clusters; South African Journal of Geology, v. 104, p. 23–38.

Moore, R.O., Gurney, J.J., Griffin, W.L. and Shimzu, N. (1991): Ultra-high pressure garnet inclusions in Monastery diamonds: trace element abundance patterns and conditions of origin; European Journal of Mineralogy, v. 3, p. 213–230.

Pană, D.I. (2003): Precambrian basement of the Western Canada Sedimentary Basin in northern Alberta; Alberta Energy and Utilities Board, EUB/AGS Earth Sciences Report 2002-02, 39 p.

Pearson, N.J., Griffin, W.L., Kaminsky, F.V., van Achterbergh, E. and O'Reilly, S.Y. (1998): Trace element discrimination of garnet from diamondiferous kimberlites and lamproites; *in* Seventh International Kimberlite Conference, Cape Town, South Africa, Extended Abstracts, p. 673–675.

Pearson, D.G., Canil, D. and Shirley, S.B. (2003): Mantle samples included in volcanic rocks: xenoliths and diamonds; *in* Treatise on Geochemistry, R.W. Carlson, H.D. Holland and K.K. Turekian (ed.), v. 2, p. 171–275.

Ross, G.M., Broome, J. and Miles, W. (1994): Potential fields and basement structure—Western Canada Sedimentary Basin; *in* Geological Atlas of the Western Canadian Sedimentary Basin, G.D. Mossop and I. Shetson (comp.), Canadian Society of Petroleum Geologists and Alberta Research Council, Special Report 4, p. 41–48.

Ross, G.M., Parrish, R.R., Villeneuve, M.E. and Bowring, S.A. (1991): Geophysics and geochronology of the crystalline basement of the Alberta Basin, Western Canada; Canadian Journal of Earth Sciences, v. 28, p. 512–522.

Ryan, C.G., Griffin, W.L. and Pearson, N.J. (1996): Garnet geotherms: pressure-temperature data from Cr-pyrope garnet xenocrysts in volcanic rocks; Journal of Geophysical Research, v. 101, p. 5611–5625.

Schmidberger, S.S., Simonetti, A., Heaman, L.M., Creaser, R.A. and Whiteford, S. (2007): Lu–Hf, in situ Sr and Pb isotope and trace element systematics for mantle eclogites from the Diavik diamond mine: evidence for Paleoproterozoic subduction beneath the Slave craton, Canada; Earth and Planetary Science Letters, v. 254, p. 55–68.

Sen, G. and Leeman, W.P. (1991): Iron-rich lherzolite xenoliths from Oahu: origin and implications for Hawaiian magma sources; Earth and Planetary Science Letters, v. 102, p. 45–57.

Shimizu, N. (1999): Young geochemical features in cratonic peridotites from southern Africa and Siberia; *in* Mantle Petrology: Field Observations and High-Pressure Experimentation: A Tribute to Francis R. (Joe) Boyd; Y. Rei, C. Bertka and B.O. Mysen (ed.), Geochemical Society, Special Publication 6, p. 47–55.

Shimizu, N., Pokhilenko, N.P., Boyd, F.R. and Pearson, D.G. (1997): Geochemical characteristics of mantle xenoliths from the Udachnaya kimberlite pipe; Russian Geology and Geophysics, v. 38, p. 205–217.

Skelton, D., Clements, B., McCandless, T.E., Hood, C., Aulbach, S., Davies, R. and Boyer, L.P. (2003): The Buffalo Head Hills kimberlite province, Alberta; *in* Slave Province and Northern Alberta Field Trip Guidebook, B.A. Kjarsgaard (ed.), Eighth International Kimberlite Conference, Geological Survey of Canada, Miscellaneous Publication G-293. p. 14–16.

Skupinski, A. and Langenberg, C.W. (2001): Petrography of the Mountain Lake pipe, Grande Prairie area, Alberta, Canada; Alberta Energy and Utilities Board, EUB/AGS Special Report 15, 38 p.

Sobolev, N.V., Lavrent'ev, Y.G., Pokhilenko, N.P. and Usova, L.V. (1973): Chrome-rich garnets from the kimberlites of Yakutia and their paragenesis; Contributions to Mineralogy and Petrology, v. 40. p. 39–52.

Stachel, R., Brey, G.P. and Harris, J.W. (2000): Kankan diamonds (Guinea) I: from the lithosphere down to the transition zone; Contributions to Mineralogy and Petrology, v. 140, p. 1–15.

Stachel, T. Viljoen, F., Brey, G.P. and Harris, J.W. (1998): Metasomatic processes in lherzolitic and harzburgitic domains of diamondiferous lithospheric mantle: REE in garnets from xenoliths and inclusions in diamonds; Earth and Planetary Science Letters, v. 159, p. 1–12.

Thériault, R.J. and Ross, G.M. (1991): Nd isotopic evidence for crustal recycling in the ca. 2.0 Ga subsurface of Western Canada; Canadian Journal of Earth Sciences, v. 28, p. 1140–1147.

Türkoğlu, E., Unsworth, M.J. and Pană, D.I. (2007): Deep electrical structure of Buffalo Head Hills, northern Alberta: implications for diamond exploration; Alberta Energy and Utilities Board, EUB/AGS Special Report 88, 34 p.

Yaxley, G.M., Green, D.H. and Kamenetsky, V. (1998): Carbonatite metasomatism in the southeastern Australian lithosphere; Journal of Petrology, v. 39, p. 1917–1930.

Appendix 1. Electron microprobe data from selected garnet xenocrysts from the northern Alberta kimberlite province. Data values in weight per cent. LA-ICP-MC trace element Ti values are included for comparison and validity of data.

Mountain Lake ultramafic cluster														
Grain ID	Probe ID	Spot	TiO2	Na2O	K2O	SiO2	FeO	CaO	MgO	Al2O3	Cr2O3	MnO	Total	Ti (ppm)
RE03-ML1-0.5-1a	13	Core	0.25	0.02	0.00	39.71	6.73	6.23	20.49	6.70	7.74	0.35	88.29	1510
RE03-ML1-0.5-1b	14	Rim	0.25	0.03	0.00	40.90	6.70	6.50	19.79	17.78	7.74	0.33	100.09	1498
RE03-ML1-0.5-2a	15	Core	0.13	0.03	0.00	40.76	5.99	6.73	20.23	18.20	7.66	0.29	100.12	797
RE03-ML1-0.5-2b	16	Rim	0.11	0.03	0.00	41.03	5.92	6.67	20.37	17.90	7.68	0.32	100.12	647
RE03-ML1-0.25-3a	21	Core	0.10	0.00	0.00	40.72	5.94	6.64	20.31	17.98	7.65	0.28	99.70	623
RE03-ML1-0.25-3b	22	Rim	0.10	0.01	0.00	40.21	5.98	6.60	20.22	18.21	7.56	0.30	99.27	605
RE03-ML1-0.25-4a	23	Core	0.58	0.16	0.01	39.76	6.49	5.99	20.35	18.59	6.49	0.32	98.83	3476
RE03-ML1-0.25-4b	24	Rim	0.58	0.05	0.00	39.84	6.48	5.83	20.67	18.50	6.31	0.35	98.68	3476
RE03-ML1-0.25-5a	25	Core	0.10	0.01	0.00	40.55	5.95	6.64	20.20	18.05	7.61	0.30	99.50	605
RE03-ML1-0.25-5b	26	Rim	0.11	0.01	0.00	40.50	5.95	6.64	20.22	17.99	7.56	0.29	99.34	653
RE03-ML1-0.25-6a	27	Core	0.81	0.05	0.00	40.02	6.41	6.77	19.78	16.03	9.11	0.36	99.42	4825
RE03-ML1-0.25-6b	28	Rim	0.79	0.06	0.00	39.75	6.49	6.73	19.54	16.21	9.16	0.34	99.14	4717
RE03-ML1-0.25-7a	29	Core	0.56	0.04	0.00	39.71	6.65	6.65	19.60	16.39	9.18	0.34	99.21	3356
RE03-ML1-0.25-7b	30	Rim	0.58	0.05	0.00	40.04	6.53	6.71	19.68	16.39	9.27	0.36	99.71	3464
RE03-ML2-0.5-1a	33	Core	0.58	0.04	0.00	40.26	6.20	6.77	19.80	15.82	9.81	0.34	99.76	3446
RE03-ML2-0.5-1b	34	Rim	0.55	0.03	0.00	40.42	6.24	6.79	19.72	16.21	9.63	0.30	99.99	3308
RE03-ML2-0.25-1a	39	Core	0.05	0.02	0.00	41.16	6.05	6.63	20.24	18.09	7.68	0.30	100.28	276
RE03-ML2-0.25-1b	40	Rim	0.05	0.05	0.00	41.21	6.01	6.57	20.27	18.05	7.64	0.29	100.21	288
RE03-ML2-0.25-2a	41	Core	0.11	0.02	0.00	40.88	6.89	6.40	19.72	17.03	8.69	0.35	100.19	683
RE03-ML2-0.25-2b	42	Rim	0.14	0.02	0.00	40.29	6.86	6.43	19.47	16.99	8.84	0.34	99.46	839
RE03-ML2-0.25-3a	43	Core	0.13	0.04	0.00	40.33	6.84	6.39	19.59	16.86	8.86	0.36	99.47	773
RE03-ML2-0.25-3b	44	Rim	0.12	0.03	0.00	40.59	6.88	6.45	19.54	17.01	8.86	0.35	99.90	713
RE03-ML2-0.25-6a	49	Core	0.14	0.03	0.00	41.33	6.22	5.91	20.41	19.24	6.47	0.30	100.13	851
RE03-ML2-0.25-6b	50	Rim	0.17	0.03	0.00	41.32	6.22	5.93	20.83	18.97	6.44	0.34	100.30	1001
RE03-ML2-0.25-8a	51	Rim	0.13	0.04	0.00	40.76	6.87	6.48	19.55	17.19	8.74	0.34	100.19	791
RE03-ML2-0.25-8b	52	Rim	0.13	0.04	0.00	40.43	6.84	6.42	19.45	16.98	8.86	0.34	99.57	749
RE03-ML2-0.25-8c	53	Core	0.57	0.05	0.00	39.94	6.23	6.84	19.44	16.21	9.66	0.33	99.37	3410
RE03-ML2-0.25-8d	54	Core	0.59	0.05	0.00	40.23	6.25	6.79	19.77	16.16	9.59	0.31	99.84	3536
RE03-ML2-0.25-8e	55	Rim	0.11	0.06	0.00	40.60	6.88	5.59	19.95	19.06	6.75	0.41	99.51	629
RE03-ML2-0.25-8f	56	Rim	0.10	0.04	0.00	40.72	6.89	5.59	20.15	19.24	6.70	0.43	99.96	617
Buffalo Head Hills kimberlite field - K2														
Grain ID	Probe ID	Spot	TiO2	Na2O	K2O	SiO2	FeO	CaO	MgO	Al2O3	Cr2O3	MnO	Total	Ti (ppm)
AB-K2-Gt01	375	Core	0.00	0.00	0.01	41.93	9.47	5.64	18.85	21.31	2.95	0.51	100.67	0
AB-K2-Gt01	376	Rim	0.00	0.01	0.00	42.07	9.45	5.41	18.72	21.52	2.92	0.53	100.63	0
AB-K2-Gt02	377	Core	0.41	0.03	0.00	42.08	7.26	5.22	20.67	20.55	3.56	0.33	100.10	2457
AB-K2-Gt02	378	Rim	0.42	0.06	0.00	42.19	7.19	5.30	20.70	20.84	3.55	0.30	100.55	2487
AB-K2-Gt03	379	Core	0.41	0.05	0.00	41.95	7.30	5.11	20.88	20.80	3.55	0.34	100.39	2433
AB-K2-Gt03	380	Rim	0.34	0.03	0.01	42.11	7.25	5.10	20.55	20.80	3.54	0.32	100.06	2020
AB-K2-Gt05	383	Core	0.00	0.03	0.00	41.91	7.68	5.31	19.73	20.04	5.20	0.44	100.34	0
AB-K2-Gt05	384	Rim	0.00	0.05	0.00	41.76	7.49	5.27	19.78	19.97	5.29	0.50	100.11	0
AB-K2-Gt06	385	Core	0.58	0.11	0.00	42.12	7.78	4.85	20.72	21.33	2.70	0.40	100.58	3464
AB-K2-Gt06	386	Rim	0.54	0.08	0.00	42.17	7.75	4.89	20.67	21.03	2.91	0.31	100.34	3212
AB-K2-Gt07	387	Core	0.03	0.02	0.00	41.75	9.36	5.93	18.78	21.65	2.80	0.62	100.94	180
AB-K2-Gt07	388	Rim	0.00	0.00	0.00	41.78	9.17	5.77	18.58	21.56	2.91	0.62	100.39	0
AB-K2-Gt08	389	Core	0.16	0.00	0.00	42.55	7.62	4.66	21.08	21.56	2.75	0.32	100.70	929
AB-K2-Gt08	390	Rim	0.17	0.01	0.00	42.23	7.46	4.65	20.91	21.46	2.66	0.37	99.93	1043
AB-K2-Gt09	391	Core	0.01	0.01	0.00	41.58	7.52	5.92	19.47	19.24	6.21	0.42	100.38	78
AB-K2-Gt09	392	Rim	0.06	0.04	0.00	41.68	7.64	5.80	19.35	19.09	6.20	0.49	100.34	372
AB-K2-Gt10	393	Core	0.02	0.02	0.00	41.88	9.37	5.97	18.31	21.29	3.02	0.62	100.50	114
AB-K2-Gt10	394	Rim	0.06	0.02	0.01	41.76	9.31	5.92	18.52	21.40	2.95	0.61	100.55	336
AB-K2-Gt11	395	Core	0.01	0.01	0.00	41.86	9.36	5.68	18.50	21.50	2.87	0.58	100.38	72
AB-K2-Gt11	396	Rim	0.06	0.01	0.00	41.93	9.28	5.54	18.60	21.70	2.74	0.59	100.46	366
AB-K2-Gt13	399	Core	0.75	0.04	0.00	42.21	7.72	5.11	20.32	20.14	3.63	0.28	100.20	4507
AB-K2-Gt13	400	Rim	0.70	0.07	0.00	41.93	7.74	5.16	20.45	20.13	3.57	0.29	100.03	4207
AB-K2-Gt14	401	Core	0.81	0.08	0.00	41.64	7.40	5.65	19.86	18.09	5.82	0.32	99.67	4861
AB-K2-Gt14	402	Rim	0.76	0.09	0.00	41.73	7.53	5.93	19.77	18.03	6.02	0.29	100.15	4579
AB-K2-Gt15	403	Core	0.04	0.00	0.00	42.24	8.98	5.40	19.00	21.81	2.63	0.59	100.69	228
AB-K2-Gt15	404	Rim	0.00	0.02	0.00	41.92	8.90	5.49	18.94	21.72	2.58	0.56	100.14	0
AB-K2-Gt18	409	Core	0.28	0.04	0.00	42.03	7.16	5.51	20.49	20.58	3.89	0.35	100.33	1702
AB-K2-Gt18	410	Rim	0.29	0.04	0.00	42.00	7.33	5.54	20.16	20.54	3.89	0.33	100.12	1720
AB-K2-Gt20	413	Core	0.77	0.08	0.00	41.76	8.62	5.09	20.00	20.93	2.40	0.28	99.93	4609
AB-K2-Gt20	414	Rim	0.76	0.09	0.00	41.66	8.69	5.22	20.19	20.92	2.38	0.32	100.22	4537
AB-K2-Gt21	415	Core	0.01	0.01	0.01	41.92	9.29	5.68	18.70	21.73	2.94	0.61	100.90	84
AB-K2-Gt21	416	Rim	0.03	0.04	0.01	41.95	9.07	5.65	18.89	21.79	2.72	0.59	100.74	186
AB-K2-Gt22	417	Core	0.03	0.02	0.01	41.81	8.94	5.60	18.92	21.86	2.69	0.53	100.41	204

Grain ID	Probe ID	Spot	TiO2	Na2O	K2O	SiO2	FeO	CaO	MgO	Al2O3	Cr2O3	MnO	Total	Ti (ppm)
AB-K2-Gt22	418	Rim	0.01	0.03	0.00	41.57	8.96	5.63	18.63	21.69	2.71	0.56	99.80	84
AB-K2-Gt23	419	Core	0.02	0.03	0.00	42.07	7.70	5.15	19.97	22.44	2.26	0.42	100.06	126
AB-K2-Gt23	420	Rim	0.03	0.05	0.00	42.09	7.81	5.06	20.09	22.33	2.18	0.38	100.02	198
AB-K2-Gt24	421	Core	0.75	0.05	0.00	41.62	8.49	5.30	20.07	20.22	3.33	0.25	100.08	4477
AB-K2-Gt24	422	Rim	0.79	0.06	0.00	41.92	8.33	5.34	20.09	20.32	3.28	0.30	100.44	4729
AB-K2-Gt25	423	Core	0.16	0.03	0.01	42.33	7.49	4.50	20.95	21.62	2.68	0.33	100.10	971
AB-K2-Gt25	424	Rim	0.14	0.03	0.00	42.36	7.39	4.45	21.29	21.59	2.73	0.37	100.35	851
Buffalo Head Hills kimberlite field - K6														
Grain ID	Probe ID	Spot	TiO2	Na2O	K2O	SiO2	FeO	CaO	MgO	Al2O3	Cr2O3	MnO	Total	Ti (ppm)
AB-K6-Gt02	579	Core	0.59	0.06	0.01	41.87	8.08	4.56	20.45	19.99	3.03	0.32	98.97	3542
AB-K6-Gt02	580	Rim	0.46	0.08	0.00	41.68	7.82	4.61	20.69	20.30	3.10	0.36	99.10	2781
AB-K6-Gt03	581	Core	0.87	0.08	0.01	41.15	8.83	5.17	19.51	17.93	5.04	0.30	98.89	5238
AB-K6-Gt03	582	Rim	0.90	0.10	0.00	41.32	8.84	5.18	19.51	18.16	4.76	0.29	99.06	5370
AB-K6-Gt04	583	Core	0.40	0.08	0.00	41.59	7.59	4.85	20.12	18.72	5.23	0.30	98.88	2367
AB-K6-Gt04	584	Rim	0.39	0.07	0.00	41.54	7.62	4.91	20.31	18.89	5.08	0.34	99.15	2325
AB-K6-Gt05	585	Core	0.40	0.04	0.00	40.66	7.30	6.47	18.60	14.67	10.13	0.36	98.63	2397
AB-K6-Gt05	586	Rim	0.42	0.04	0.00	40.43	7.35	6.47	18.58	14.73	10.02	0.34	98.37	2499
AB-K6-Gt06	587	Core	0.71	0.11	0.00	41.61	8.38	4.52	20.54	20.38	2.21	0.31	98.78	4279
AB-K6-Gt06	588	Rim	0.69	0.09	0.00	41.65	8.32	4.51	20.51	20.54	2.12	0.27	98.70	4129
AB-K6-Gt07	589	Core	0.49	0.09	0.00	41.60	7.13	4.93	20.93	18.81	4.56	0.33	98.87	2931
AB-K6-Gt07	590	Rim	0.54	0.08	0.00	41.72	6.97	4.85	20.79	18.90	4.48	0.26	98.59	3236
Buffalo Head Hills kimberlite field - K11														
Grain ID	Probe ID	Spot	TiO2	Na2O	K2O	SiO2	FeO	CaO	MgO	Al2O3	Cr2O3	MnO	Total	Ti (ppm)
AB-K11-Gt01	537	Core	0.70	0.05	0.01	41.62	7.67	5.04	20.14	19.10	4.23	0.28	98.84	4177
AB-K11-Gt01	538	Rim	0.66	0.03	0.01	41.56	7.60	4.94	20.29	18.97	4.20	0.33	98.59	3932
AB-K11-Gt02	539	Core	0.26	0.03	0.00	41.75	8.00	4.69	20.25	19.42	4.42	0.36	99.18	1540
AB-K11-Gt02	540	Rim	0.29	0.06	0.00	41.69	7.95	4.68	20.18	19.46	4.39	0.37	99.07	1762
AB-K11-Gt03	541	Core	0.88	0.08	0.01	41.48	8.81	5.11	19.69	19.47	3.15	0.35	99.02	5268
AB-K11-Gt03	542	Rim	0.81	0.09	0.00	41.21	8.89	5.08	19.62	19.34	3.12	0.36	98.52	4855
AB-K11-Gt04	543	Core	0.12	0.03	0.00	40.69	7.85	5.65	18.77	17.80	7.35	0.40	98.66	707
AB-K11-Gt04	544	Rim	0.12	0.05	0.01	40.76	8.00	5.71	19.00	17.66	7.53	0.45	99.29	713
AB-K11-Gt05	545	Core	0.13	0.04	0.00	41.20	7.68	4.87	20.11	19.89	4.66	0.46	99.04	803
AB-K11-Gt05	546	Rim	0.16	0.03	0.00	41.38	7.74	4.90	19.89	19.64	4.58	0.37	98.70	971
AB-K11-Gt06	547	Core	0.31	0.07	0.00	41.62	7.20	4.42	20.81	20.40	3.45	0.36	98.64	1858
AB-K11-Gt06	548	Rim	0.26	0.07	0.00	41.72	7.28	4.50	20.85	20.71	3.41	0.37	99.17	1558
AB-K11-Gt07	549	Core	0.35	0.04	0.00	41.03	7.43	5.38	19.80	18.16	6.41	0.31	98.91	2116
AB-K11-Gt07	550	Rim	0.45	0.07	0.00	41.23	7.44	5.34	19.60	18.23	6.44	0.34	99.14	2703
AB-K11-Gt08	551	Core	0.55	0.02	0.00	40.70	7.49	6.30	18.79	16.89	7.13	0.42	98.28	3272
AB-K11-Gt08	552	Rim	0.52	0.04	0.00	40.83	7.51	6.41	19.01	16.94	7.23	0.35	98.84	3093
AB-K11-Gt13	561	Core	0.21	0.05	0.01	41.31	7.61	4.83	19.87	19.50	4.69	0.39	98.47	1253
AB-K11-Gt13	562	Rim	0.16	0.02	0.00	41.35	7.65	4.94	20.10	19.69	4.71	0.40	99.02	959
AB-K11-Gt14	563	Core	0.40	0.04	0.00	41.62	7.13	5.07	20.34	20.50	3.52	0.35	98.97	2403
AB-K11-Gt14	564	Rim	0.33	0.03	0.00	41.61	7.19	5.10	20.46	20.63	3.45	0.33	99.14	1990
AB-K11-Gt15	565	Core	0.11	0.03	0.01	41.08	7.32	5.44	19.60	18.28	6.59	0.40	98.86	629
AB-K11-Gt15	566	Rim	0.08	0.02	0.00	41.00	7.09	5.41	19.49	18.21	6.58	0.39	98.27	503
AB-K11-Gt16	567	Core	0.11	0.05	0.01	41.51	8.04	5.00	19.57	20.03	4.33	0.42	99.06	629
AB-K11-Gt16	568	Rim	0.10	0.01	0.00	41.19	8.08	5.11	19.56	20.15	4.36	0.45	99.01	587
AB-K11-Gt20	575	Core	0.80	0.06	0.00	41.23	7.93	5.82	19.48	17.17	6.34	0.35	99.19	4813
AB-K11-Gt20	576	Rim	0.76	0.10	0.00	41.13	7.88	5.79	19.40	17.22	6.23	0.35	98.85	4525
Buffalo Head Hills kimberlite field - K14														
Grain ID	Probe ID	Spot	TiO2	Na2O	K2O	SiO2	FeO	CaO	MgO	Al2O3	Cr2O3	MnO	Total	Ti (ppm)
AB-K14-Gt01	469	Core	0.22	0.06	0.00	42.40	8.08	4.45	20.64	21.40	2.89	0.42	100.55	1295
AB-K14-Gt01	470	Rim	0.23	0.03	0.00	42.21	8.16	4.45	20.62	21.55	2.81	0.36	100.43	1396
AB-K14-Gt02	471	Core	0.43	0.09	0.00	41.84	7.71	4.77	20.63	19.18	4.80	0.34	99.79	2601
AB-K14-Gt02	472	Rim	0.50	0.08	0.00	41.86	7.87	4.76	20.56	19.17	4.77	0.33	99.89	2985
AB-K14-Gt03	473	Core	0.72	0.05	0.00	42.27	8.59	4.57	20.65	20.38	2.73	0.34	100.30	4321
AB-K14-Gt03	474	Rim	0.76	0.08	0.00	42.34	8.59	4.53	20.65	20.17	2.72	0.31	100.14	4537
AB-K14-Gt05	477	Core	0.16	0.06	0.00	41.40	7.68	6.07	18.83	17.49	7.70	0.46	99.85	971
AB-K14-Gt05	478	Rim	0.14	0.04	0.00	41.17	7.74	5.98	19.12	17.72	7.57	0.43	99.91	851
AB-K14-Gt06	479	Core	0.46	0.09	0.00	41.93	7.38	4.86	21.00	19.29	4.41	0.28	99.70	2745
AB-K14-Gt06	480	Rim	0.41	0.06	0.00	42.09	7.44	4.93	20.89	19.30	4.42	0.32	99.86	2475
AB-K14-Gt09	485	Core	0.18	0.05	0.00	41.44	8.09	6.11	18.58	18.35	6.65	0.46	99.91	1103
AB-K14-Gt09	486	Rim	0.15	0.02	0.00	41.58	8.14	6.18	18.75	18.58	6.51	0.45	100.36	905
AB-K14-Gt11	489	Core	0.12	0.02	0.00	41.42	9.95	5.82	17.87	21.80	2.57	0.57	100.14	707
AB-K14-Gt11	490	Rim	0.10	0.00	0.01	41.53	10.04	5.73	17.93	21.73	2.71	0.65	100.42	581
AB-K14-Gt12	491	Core	0.74	0.08	0.00	42.30	8.58	4.50	20.48	20.31	2.60	0.30	99.89	4453
AB-K14-Gt12	492	Rim	0.69	0.06	0.01	41.85	8.63	4.59	20.50	20.27	2.70	0.31	99.61	4147
AB-K14-Gt13	493	Core	0.68	0.08	0.00	41.95	8.68	4.32	20.48	20.68	2.16	0.27	99.31	4094

Grain ID	Probe ID	Spot	TiO2	Na2O	K2O	SiO2	FeO	CaO	MgO	Al2O3	Cr2O3	MnO	Total	Ti (ppm)
AB-K14-Gt13	494	Rim	0.70	0.07	0.00	42.09	8.55	4.17	20.63	20.70	2.19	0.32	99.42	4177
AB-K14-Gt14	495	Core	0.29	0.04	0.00	41.99	7.82	4.55	20.51	20.42	3.92	0.32	99.85	1726
AB-K14-Gt14	496	Rim	0.26	0.07	0.01	41.81	7.51	4.57	20.36	20.18	3.91	0.34	99.01	1552
AB-K14-Gt16	499	Core	0.38	0.00	0.01	41.69	7.44	5.72	19.58	18.81	5.40	0.33	99.35	2254
AB-K14-Gt16	500	Rim	0.40	0.02	0.00	41.55	7.53	5.71	19.46	18.88	5.34	0.34	99.23	2415
AB-K14-Gt18	503	Core	0.08	0.04	0.01	41.53	9.82	5.75	18.07	21.65	2.53	0.56	100.04	479
AB-K14-Gt18	504	Rim	0.11	0.03	0.01	41.23	9.90	5.63	18.10	21.54	2.66	0.52	99.72	635
AB-K14-Gt20	507	Core	0.09	0.01	0.00	41.95	9.05	5.67	18.49	21.53	2.48	0.54	99.81	527
AB-K14-Gt20	508	Rim	0.05	0.03	0.01	41.58	9.18	5.61	18.39	21.55	2.40	0.52	99.31	282
AB-K14-Gt21	509	Core	0.12	0.02	0.00	41.76	9.04	5.64	18.65	21.86	2.11	0.53	99.73	737
AB-K14-Gt21	510	Rim	0.13	0.03	0.01	41.71	8.87	5.66	18.51	21.78	2.36	0.51	99.57	773
AB-K14-Gt22	511	Core	0.68	0.09	0.00	42.15	8.48	4.44	20.18	20.16	2.64	0.27	99.08	4058
AB-K14-Gt22	512	Rim	0.71	0.08	0.00	41.71	8.37	4.43	20.33	20.02	2.57	0.27	98.49	4243
AB-K14-Gt23	513	Core	0.09	0.02	0.01	41.53	9.10	5.51	18.22	21.66	2.36	0.53	99.03	515
AB-K14-Gt23	514	Rim	0.12	0.01	0.00	41.43	9.23	5.50	18.37	21.67	2.40	0.51	99.24	689
AB-K14-Gt30	527	Core	0.69	0.07	0.00	41.90	8.45	4.51	20.44	20.21	2.58	0.28	99.13	4159
AB-K14-Gt30	528	Rim	0.68	0.07	0.00	41.67	8.45	4.40	20.32	20.14	2.64	0.28	98.65	4100
AB-K14-Gt31	529	Core	0.58	0.05	0.00	41.40	7.40	4.92	20.32	19.20	4.43	0.38	98.69	3500
AB-K14-Gt31	530	Rim	0.65	0.06	0.00	41.48	7.49	4.83	20.42	19.24	4.54	0.32	99.03	3890
AB-K14-Gt32	531	Core	0.06	0.04	0.00	40.16	7.76	5.95	18.30	15.77	10.09	0.42	98.55	342
AB-K14-Gt32	532	Rim	0.05	0.03	0.00	40.40	7.78	5.93	18.23	16.01	9.92	0.48	98.83	318
AB-K14-Gt33	533	Core	0.31	0.05	0.00	41.93	7.78	4.51	20.33	20.00	3.48	0.29	98.67	1828
AB-K14-Gt33	534	Rim	0.29	0.03	0.01	41.65	7.69	4.41	20.40	20.16	3.47	0.35	98.46	1750
AB-K14-Gt34	535	Core	0.28	0.06	0.00	41.88	7.80	4.53	20.40	20.35	3.58	0.36	99.23	1672
AB-K14-Gt34	536	Rim	0.26	0.06	0.00	41.69	7.76	4.47	20.61	20.24	3.49	0.32	98.90	1576
Birch Mountains field - Kendu														
Grain ID	Probe ID	Spot	TiO2	Na2O	K2O	SiO2	FeO	CaO	MgO	Al2O3	Cr2O3	MnO	Total	Ti (ppm)
RE02-KD-01-03	47	Core	0.07	na	na	40.00	7.65	6.97	19.31	17.56	7.09	0.56	99.21	396
RE02-KD-01-04	48	Core	0.10	na	na	39.30	8.03	7.26	18.86	17.16	7.08	0.54	98.36	581
RE02-KD-01-05	49	Core	0.10	na	na	39.38	8.15	8.08	18.14	16.59	8.06	0.56	99.09	599
RE02-KD-01-13	57	Core	0.14	na	na	39.53	8.24	7.78	18.13	16.55	8.03	0.60	99.02	833
RE02-KD-02-02	66	Core	0.01	na	na	40.62	8.00	6.42	19.66	19.60	4.64	0.58	99.54	78
RE02-KD-02-03	67	Core	0.00	na	na	40.75	7.38	5.37	21.19	20.70	3.11	0.53	99.04	0
RE02-KD-02-04a	68	Rim	0.31	na	na	40.33	8.18	5.68	20.28	18.41	5.88	0.55	99.65	1834
RE02-KD-02-04b	69	Core	0.00	na	na	41.32	7.49	5.12	21.29	21.40	2.85	0.54	100.02	0
RE02-KD-02-04c	70	Rim	0.05	na	na	40.77	8.10	5.93	20.28	20.81	2.98	0.46	99.38	288
RE02-KD-02-05	71	Core	0.01	na	na	40.49	8.05	6.10	19.89	19.24	5.23	0.57	99.59	60
RE02-KD-02-16	82	Core	0.02	na	na	40.88	7.45	5.19	21.17	20.86	2.97	0.57	99.11	126
RE02-KD-02-17	83	Core	0.00	na	na	40.45	8.11	7.32	18.96	18.52	5.97	0.58	99.93	0
RE02-KD-02-18	84	Core	0.00	na	na	39.97	8.16	7.37	18.75	18.00	6.01	0.60	98.86	0
RE02-KD-02-19	85	Core	0.35	na	na	40.07	10.15	5.12	20.08	19.98	2.44	0.39	98.66	2122
RE02-KD-02-20	86	Core	0.35	na	na	40.14	10.17	5.13	20.11	20.26	2.47	0.41	99.10	2074
Birch Mountains field - Legend														
Grain ID	Probe ID	Spot	TiO2	Na2O	K2O	SiO2	FeO	CaO	MgO	Al2O3	Cr2O3	MnO	Total	Ti (ppm)
VR88467A	1	Core	0.67	na	na	41.61	6.37	6.35	19.63	17.57	7.48	0.25	99.93	4016
VR88467A	5	Core	0.73	na	na	41.43	6.21	5.99	19.78	18.08	7.26	0.26	99.74	4375
VR88467A	6	Core	0.69	na	na	41.53	6.48	6.29	19.74	17.77	7.61	0.38	100.49	4135
VR88467A	9	Core	0.56	na	na	41.73	6.26	6.49	19.63	17.01	8.58	0.25	100.51	3356
VR88467A	13	Core	0.90	na	na	40.86	6.40	7.09	18.86	15.51	9.79	0.25	99.66	5394
VR88467A	17	Core	0.78	na	na	41.35	6.42	6.25	19.92	17.21	7.49	0.30	99.72	4675
VR88467A	23	Core	0.98	na	na	41.10	6.78	6.79	19.40	16.73	8.06	0.28	100.12	5874
VR88467A	26	Core	0.66	na	na	41.43	6.08	6.31	19.87	17.47	7.92	0.35	100.09	3956
VR88467A	28	Core	0.77	na	na	41.39	6.00	6.23	19.91	17.30	8.29	0.27	100.16	4615
VR88467A	33	Core	0.72	na	na	41.77	6.29	5.95	19.84	18.11	7.38	0.31	100.37	4315
VR88467A	35	Core	0.26	na	na	41.35	6.48	7.12	18.52	15.76	10.54	0.27	100.30	1558
VR88467A	36	Core	0.08	na	na	41.32	6.34	7.07	18.69	16.07	10.41	0.27	100.25	479
VR88467A	39	Core	0.39	na	na	40.91	6.52	7.34	18.89	15.37	10.53	0.27	100.22	2337
VR88478A	2	Core	0.11	na	na	41.32	5.65	6.20	19.80	18.94	7.55	0.25	99.82	659
VR88478A	3	Core	0.36	na	na	40.66	6.33	6.56	19.49	16.72	9.32	0.25	99.69	2158
VR88478A	4	Core	0.50	na	na	40.49	6.60	6.46	19.13	17.54	8.61	0.33	99.66	2997
Birch Mountains field - Xena														
Grain ID	Probe ID	Spot	TiO2	Na2O	K2O	SiO2	FeO	CaO	MgO	Al2O3	Cr2O3	MnO	Total	Ti (ppm)
VR87896A	1	Core	0.91	na	na	41.09	6.53	6.21	19.75	17.26	8.00	0.23	99.98	5454
VR87896A	2	Core	0.95	na	na	41.23	6.50	5.98	19.98	17.09	7.99	0.15	99.87	5694
VR87896A	3	Core	0.89	na	na	41.14	6.36	5.95	20.12	17.77	7.51	0.31	100.05	5334
VR87896A	4	Core	0.87	na	na	41.44	6.63	5.95	19.69	17.20	7.69	0.22	99.69	5214
VR87896A	6	Core	0.33	na	na	42.00	6.47	5.38	20.24	19.47	5.65	0.31	99.85	1978

Appendix 2. LA-ICP-MC trace element data from selected garnet xenocrysts from the northern Alberta kimberlite province. Data values in parts per million. TNi calculated using the calibration of Canil (1999).

Mountain Lake ultramafic cluster																																				
	Probe	TNi																																		
Grain ID	spot	(° C)	Mg	Sc	Ti	V	Cr	Mn	Ni	Ga	Rb	Sr	Y	Zr	Nb	Cs	Ba	La	Ce	Pr	Nd	Sm	Eu	Gd	Tb	Dy	Ho	Er	Tm	Yb	Lu	Hf	Ta	Pb	Th	U
RE03-ML1-0.25-3a	Core	1168	141486.58	140.14	2641.04	167.55	15609.46	1679.69	82.85	6.09	<0.029	0.49	14.87	34.25	0.37	<0.030	0.04	0.08	0.47	0.19	1.59	0.92	0.33	1.51	0.31	2.47	0.54	1.75	0.23	1.89	0.30	0.83	0.04	<0.065	1.03	0.01
RE03-ML1-0.25-3b	Rim	1174	133289.56	215.62	758.84	237.94	32109.66	1544.02	84.73	4.88	<0.042	0.33	8.06	4.24	1.13	<0.031	0.02	0.11	0.99	0.26	1.39	<0.51	0.15	0.70	0.13	1.19	0.32	0.93	0.19	1.37	0.25	<0.145	<0.064	<0.077	0.63	0.03
RE03-ML1-0.25-4a	Core	1170	130118.15	208.39	651.98	241.90	31536.33	1564.26	83.52	4.70	0.03	0.37	7.81	3.47	0.79	<0.028	<0.0111	0.16	1.02	0.22	1.79	0.56	0.10	0.68	0.17	1.17	0.34	0.77	0.18	1.25	0.27	<0.106	<0.056	<0.068	0.06	0.03
RE03-ML1-0.25-4b	Rim	1147	136210.84	170.19	3364.66	230.56	27324.22	1834.38	75.68	6.02	<0.037	0.55	9.35	35.98	0.66	<0.028	<0.0160	0.05	0.71	0.25	2.19	1.23	0.44	1.56	0.33	1.86	0.34	0.98	0.17	1.19	0.23	0.83	0.08	0.07	3.13	0.03
RE03-ML1-0.25-5a	Core	1161	128990.63	161.40	3226.42	229.42	26774.71	1781.69	80.43	6.73	0.10	2.29	9.49	36.63	0.81	<0.027	5.95	0.17	0.85	0.24	2.37	1.19	0.49	1.75	0.29	1.70	0.41	1.11	0.16	1.32	0.22	0.89	0.07	0.27	0.69	0.02
RE03-ML1-0.25-5b	Rim	1180	128264.46	214.63	630.95	237.01	32135.35	1563.17	87.10	4.61	<0.040	0.27	8.23	3.46	0.81	<0.031	0.04	0.13	0.91	0.23	1.34	0.72	0.14	0.60	0.16	1.06	0.34	0.84	0.18	1.21	0.30	<0.160	0.05	<0.083	3.39	0.03
RE03-ML1-0.25-6a	Core	1186	129472.89	214.38	611.23	244.83	32770.53	1588.33	89.00	4.60	<0.036	0.30	8.04	2.94	0.90	<0.032	<0.0187	0.14	1.00	0.26	1.34	<0.61	0.13	0.66	0.17	1.16	0.29	0.91	0.16	1.36	0.27	<0.116	<0.063	<0.073	2.60	0.03
RE03-ML1-0.25-6b	Rim	1177	121941.81	146.71	4313.06	198.87	38407.49	1787.54	85.75	10.48	<0.030	1.00	26.24	97.53	0.69	<0.028	<0.0180	0.15	1.19	0.38	3.36	2.42	1.05	4.46	0.80	5.53	0.86	2.39	0.39	2.15	0.35	2.29	<0.051	<0.060	0.06	0.02
RE03-ML1-0.25-7	Core	1198	122827.69	148.81	4349.01	205.05	39729.22	1830.49	93.69	10.96	<0.024	1.13	26.90	95.19	0.68	<0.025	0.04	0.17	1.16	0.37	3.31	2.24	1.01	4.26	0.80	5.39	1.20	2.85	0.28	2.17	0.33	2.61	0.07	<0.071	0.32	0.01
RE03-ML1-0.5-2-2	Core	1160	140661.81	181.66	1495.22	252.00	30871.61	1780.67	79.81	7.69	<0.031	0.24	17.00	4.10	0.95	<0.027	<0.0108	0.05	0.23	0.07	0.40	<0.54	0.17	0.79	0.22	2.46	0.68	1.92	0.31	2.62	0.39	0.18	0.07	<0.071	0.91	0.01
RE03-ML1-0.5-2a	Core	1164	133841.53	179.65	1491.13	260.69	31319.71	1744.89	81.17	7.99	<0.031	0.24	16.33	3.78	1.00	<0.0246	0.03	0.06	0.24	0.07	0.34	<0.45	0.13	0.84	0.24	2.54	0.64	2.01	0.35	2.95	0.39	<0.126	0.12	<0.069	1.16	0.03
RE03-ML1-0.5-2b	Core	1176	138867.58	212.63	710.55	244.86	32518.97	1583.76	85.48	4.90	<0.030	0.30	7.67	2.49	0.94	<0.027	<0.0137	0.11	0.99	0.25	1.45	0.50	0.09	0.37	0.11	1.15	0.20	0.94	0.12	1.16	0.25	<0.129	<0.055	<0.069	0.26	<0.0171
RE03-ML2-0.25-1	Core	1178	121127.94	212.47	279.24	300.31	33792.97	1648.21	86.09	4.02	<0.037	0.41	7.25	6.37	2.11	<0.035	<0.0181	0.20	1.29	0.30	1.69	0.63	0.14	0.43	0.11	1.09	0.32	1.07	0.20	1.40	0.28	0.17	0.20	<0.083	0.17	0.07
RE03-ML2-0.25-10a	Core	1184	107104.63	179.33	2649.03	258.48	42397.34	1744.78	88.38	5.33	<0.038	0.97	14.55	69.65	0.89	<0.031	<0.0130	0.16	1.40	0.44	4.12	1.57	0.84	3.17	0.45	2.97	0.52	1.55	0.20	1.29	0.19	1.56	<0.059	<0.072	2.18	0.03
RE03-ML2-0.25-2a	Core	1183	119534.06	215.46	286.58	310.88	33811.61	1653.76	88.17	4.76	<0.054	0.46	7.15	6.06	2.14	<0.035	<0.0149	0.24	1.24	0.27	1.62	<0.57	0.16	0.33	0.09	0.99	0.29	0.82	0.20	1.36	0.26	0.25	0.13	0.11	0.64	0.08
RE03-ML2-0.25-2b	Rim	1143	114643.27	128.64	607.65	242.40	38597.54	1861.51	74.22	6.79	<0.037	0.58	10.21	4.25	1.07	<0.035	<0.0103	0.15	0.70	0.09	0.81	0.78	0.23	0.71	0.14	1.55	0.42	1.24	0.21	1.59	0.25	<0.144	0.06	<0.085	0.21	0.03
RE03-ML2-0.25-3	Core	1150	110877.72	125.23	620.52	249.36	38702.61	1893.21	76.40	7.58	<0.036	0.69	10.52	5.03	1.02	<0.028	<0.0089	0.15	0.85	0.18	0.97	<0.63	0.19	0.93	0.22	1.59	0.45	1.13	0.25	1.67	0.26	0.18	0.13	<0.075	0.13	0.03
RE03-ML2-0.25-6a	Core	1132	111734.56	124.28	605.11	240.50	37989.63	1817.26	70.84	7.00	<0.03	0.51	10.10	4.47	1.01	<0.033	<0.0090	0.11	0.70	0.11	0.63	<0.49	0.17	0.86	0.22	1.68	0.46	1.33	0.20	1.38	0.29	0.22	0.06	<0.076	0.41	0.02
RE03-ML2-0.25-6b	Rim	1169	120896.19	161.76	698.19	232.86	29352.93	1697.30	83.06	4.65	<0.051	0.75	9.96	18.48	1.00	<0.039	<0.0187	0.10	0.76	0.26	1.54	0.84	0.21	1.15	0.23	1.36	0.40	1.36	0.23	1.64	0.25	0.59	0.11	0.08	0.34	0.05
RE03-ML2-0.25-8a	Core	1164	114495.33	160.91	674.84	233.34	28458.46	1655.33	81.37	4.08	<0.036	0.82	9.57	17.44	1.05	<0.030	0.04	0.11	0.84	0.21	1.50	1.39	0.33	0.82	0.19	1.60	0.40	1.16	0.22	1.56	0.31	0.54	0.09	0.08	0.42	0.03
RE03-ML2-0.25-8b	Rim	1152	111350.72	127.40	594.91	243.53	38877.48	1882.07	77.37	6.99	<0.050	0.64	10.66	4.90	0.96	<0.033	<0.0258	0.17	0.89	0.17	1.12	<0.66	0.21	1.19	0.17	1.65	0.38	1.13	0.27	1.45	0.24	0.20	0.08	<0.096	8.69	0.03
RE03-ML2-0.25-9a	Core	1147	107204.56	126.45	574.18	244.82	38483.59	1859.57	75.51	7.43	<0.034	0.56	10.47	4.42	1.05	<0.034	<0.0160	0.14	0.82	0.18	0.96	0.64	0.21	0.57	0.14	1.49	0.44	1.12	0.23	1.77	0.29	0.27	0.06	<0.081	2.09	0.04
RE03-ML2-0.25-9b	Rim	1172	106714.76	180.81	2672.01	253.48	42583.11	1741.81	84.07	5.22	<0.045	1.02	13.95	67.02	0.80	<0.030	0.02	0.18	1.40	0.41	3.72	2.53	0.79	2.84	0.38	2.63	0.56	1.23	0.19	1.16	0.27	1.39	<0.051	<0.080	0.05	0.04
RE03-ML2-0.5-1a	Core	1139	126231.20	144.19	2436.21	260.78	32354.36	2097.92	72.96	7.55	0.03	0.84	10.06	54.79	0.73	<0.031	<0.0162	0.10	0.86	0.34	2.96	1.91	0.57	2.70	0.33	1.91	0.37	1.14	0.18	1.60	0.20	0.89	0.07	<0.083	8.61	0.02
RE03-ML2-0.5-1b	Rim	1169	118507.76	177.17	3045.93	243.85	39791.18	1679.84	82.97	5.06	<0.033	0.94	14.27	64.38	0.84	<0.0248	0.02	0.18	1.36	0.40	3.51	2.47	0.72	2.97	0.53	2.99	0.49	1.60	0.19	1.36	0.17	1.60	0.07	<0.058	0.61	0.03
RE03-ML2-0.5-2	Core	1160	112635.17	172.16	2943.91	244.09	40654.71	1637.58	79.87	5.07	<0.027	0.95	12.31	62.33	0.87	<0.0194	0.02	0.19	1.26	0.40	3.56	2.26	0.76	2.73	0.41	2.52	0.46	1.18	0.14	0.98	0.24	1.49	0.07	<0.063	1.76	0.02

Buffalo Head Hills kimberlite field - K2																																				
	Probe	TNi																																		
Grain ID	spot	(° C)	Mg	Sc	Ti	V	Cr	Mn	Ni	Ga	Rb	Sr	Y	Zr	Nb	Cs	Ba	La	Ce	Pr	Nd	Sm	Eu	Gd	Tb	Dy	Ho	Er	Tm	Yb	Lu	Hf	Ta	Pb	Th	U
AB-K2-Gt01a	Rim	833	114945.20	141.11	52.70	98.88	12339.84	3055.55	13.06	2.78	<0.094	0.19	5.70	13.11	0.28	<0.030	<0.137	<0.034	0.39	0.25	2.43	1.15	0.40	1.43	0.15	1.44	0.23	0.68	0.10	0.77	0.17	0.18	<0.048	0.07	0.68	0.09
AB-K2-Gt01b	Core	842	111670.07	133.92	45.71	107.10	13398.31	3164.09	13.90	2.39	<0.073	0.14	6.21	16.25	0.23	0.03	<0.131	<0.025	0.35	0.20	2.50	1.16	0.59	1.55	0.19	1.10	0.19	0.73	0.14	0.95	0.20	<0.143	<0.050	<0.064	3.71	0.10
AB-K2-Gt01c	Core	885	115053.16	137.39	53.60	132.79	17317.19	3778.25	18.73	3.69	<0.065	0.17	5.92	14.09	0.28	<0.0213	<0.13	0.03	0.41	0.28	2.64	1.23	0.48	1.36	0.17	1.31	0.20	0.69	0.12	1.09	0.17	0.12	<0.055	<0.064	2.09	0.16
AB-K2-Gt01d	Rim	841	109922.30	137.44	47.35	119.86	14943.55	3177.37	13.86	2.96	<0.060	0.17	5.99	14.66	0.23	<0.0222	<0.128	<0.022	0.41	0.25	2.62	1.67	0.53	1.34	0.20	0.97	0.20	0.62	0.14	1.10	0.20	<0.104	<0.051	<0.063	0.65	0.13
AB-K2-Gt02a	Core	1046	129943.66	113.13	2478.26	202.80	18183.64	2017.01	47.05	6.03	<0.056	0.20	15.42	34.36	0.43	<0.025	0.14	<0.027	0.20	0.10	1.08	1.31	0.36	1.51	0.33	2.62	0.61	1.84	0.30	1.61	0.28	0.71	0.18	0.07	5.11	0.02
AB-K2-Gt03a	Rim	1048	126242.50	106.19	2332.55	191.05	17482.81	1939.59	44.92	8.85	<0.075	0.29	14.92	34.65	0.30	<0.025	<0.151	<0.024	0.28	0.09	0.53	0.64	0.41	0.94	0.26	1.48	0.49	1.43	0.14	1.42	0.30	0.84	<0.061	<0.074	25.14	<0.01
AB-K2-Gt02b	Core	1037	123517.33	113.87	2478.53	210.19	18111.04	1977.47	47.60	6.25	<0.065	0.20	16.09	36.59	0.37	<0.033	<0.167	0.03	0.15	0.08	1.03	0.95	0.38	1.45	0.36	2.51	0.57	1.94	0.25	1.94	0.32	0.74	<0.050	<0.069	6.49	<0.0163
AB-K2-Gt03b	Rim	1045	117177.26	109.62	2387.78	202.55	16913.94	1876.92	46.77	5.91	<0.058	0.18	14.72	35.00	0.32	<0.0240	<0.105	<0.033	0.13	0.07	1.11	0.52	0.34	1.80	0.29	2.09	0.53	1.72	0.26	1.58	0.28	0.75	0.04	<0.056	1.45	0.02
AB-K2-Gt05	Core	924	116769.57	156.35	78.41	134.87	25229.08	2447.06	23.91	2.67	<0.074	0.17	2.98	53.40	0.64	<0.028	<0.151	0.05	0.37	0.11	1.91	2.75	0.98	3.42	0.46	1.52	0.14	0.31	0.07	0.60	0.18	0.80	<0.059	<0.070	0.38	0.03
AB-K2-Gt06	Core	1046	126308.40	106.72	3429.41	191.52	14003.13	1972.58	47.18	8.37	<0.070	0.18	19.76	54.54	0.19	<0.036	<0.145	<0.027	0.13	0.06	0.64	1.36	0.40	2.12	0.41	3.52	0.67	2.49	0.38	2.67	0.40	1.25	<0.057	<0.077	1.97	<0.0149
AB-K2-Gt07	Core	809	114870.70	180.49	156.02	81.62	14957.69	3419.36	10.93	2.70	<0.076	0.17	31.11	15.01	0.13	0.06	<0.146	0.04	0.39	0.18	1.95	2.14	0.72	3.50	0.70	5.07	1.05	2.83	0.45	3.16	0.45	0.19	<0.042	<0.087	0.54	0.15
AB-K2-Gt08	Core	1060	128044.97	112.50	1050.71	166.01	13833.60	1842.78	50.39	6.62	<0.068	0.15	14.96	10.02	0.28	<0.025	<0.178	0.02	0.13	0.04	0.47	<0.43	0.20	1.11	0.21	2.26	0.57	1.83	0.23	2.33	0.41	0.26	0.05	<0.057	1.16	<0.0155
AB-K2-Gt09	Core	908	116763.98	159.56	185.66	151.89	30264.09	2622.84	21.64	2.23	<0.071	0.32	8.41	42.50	0.50	<0.032	<0.140	0.15	0.92	0.23	2.18	1.48	0.76	2.34	0.39	2.10	0.42	0.68	0.08	0.87	0.10	0.59	<0.063	<0.093	0.45	0.12
AB-K2-Gt10	Core	816	111179.47	181.43	127.20	75.53	14880.64	3441.91	11.52	2.05	<0.073	0.14	35.65	15.63	0.20	<0.033	<0.198	0.04	0.26	0.11	1.56	1.33	0.75	3.31	0.75	5.97	1.24	3.56	0.62	3.34	0.60	<0.140	<0.063	<0.085	0.78	0.10
AB-K2-Gt11	Core	801	111547.13	164.61	152.96	81.27	13528.78	3223.11	10.30	4.47	<0.064	0.18	27.52	15.67	0.22	<0.022	<0.170	0.03	0.38	0.14	1.99	1.43	0.76	2.79	0.65	4.90	1.01	2.72	0.41	2.94	0.46	<0.148	<0.051	<0.063	1.25	0.19
AB-K2-Gt13	Core	1157	128044.88	109.04	4187.38	197.77	17827.02	1748.63	79.01	8.06	<0.062	0.44	24.57	64.65	0.33	<0.023	<0.140	0.04	0.37	0.10	1.45	1.16	0.48	2.83	0.58	4.51	0.92	2.51	0.40	2.90	0.35	1.88	<0.052	<0.081	0.04	<0.0173
AB-K2-Gt14	Core	1179	127043.43	125.38	4812.47	232.82	31074.68	1786.66	86.45	6.32	<0.061	0.73	16.79	75.31	0.52	<0.025	0.22	0.05	0.57	0.23	2.12	1.31	0.68	2.82	0.41	3.08	0.53	1.31	0.19	1.32	0.28	1.77	<0.053	<0.050	5.77	0.01
AB-K2-Gt15	Core	838	118503.30	164.05	22.25	94.70	13381.30	3236.21	13.57	2.09	<0.073	0.16	3.43	8.51	0.37	<0.030	<0.097	<0.029	0.41	0.25	2.52	0.66	0.46	0.83	0.08	0.62	0.10	0.37	0.06	0.76	0.15	<0.144	<0.048	<0.065	0.23	0.07
AB-K2-Gt18	Core	1016	124365.83	128.12	1731.69	222.41	20035.04	1948.00	40.30	5.63	<0.061	0.23	10.67	32.60	0.30	<0.026	<0.159	<0.031	0.15	0.08	0.64	<0.50	0.31	1.16	0.25	2.03	0.37	1.41	0.21	1.63	0.20	0.83	<0.054	<0.073	0.06	0.02
AB-K2-Gt20	Core	1100	121872.24	105.76	4467.50	211.36	12423.34	1842.69	61.13	8.87	0.05	0.42	25.20	69.24	0.24	<0.022	<0.096	0.04	0.35	0.11	1.15	0.88	0.54	2.75	0.53	4.02	1.07	2.87	0.41	3.64	0.49	1.58	0.05	<0.078	0.64	<0.01
AB-K2-Gt21a	Rim	804	112787.74	165.17	148.59	83.84	14424.27	3244.23	10.58	2.77	<0.074	0.13	27.68	14.64	0.21	<0.033	<0.199	0.03	0.35	0.17	1.90	1.70	0.86	3.20	0.62	4.92	0.96	2.87	0.39	3.20	0.50	<0.147	<0.054	<0.097	0.93	0.14
AB-K2-Gt21b	Core	808	110965.65	158.51	155.49	83.32	14305.95	3165.07	10.90	2.34	<0.070	0.15	29.01	15.64	0.19	<0.025	<0.187	<0.026	0.40	0.16	1.89	1.89	0.74	3.11	0.65	4.67	0.87	2.60	0.42	3.13	0.49	0.24	<0.044	<0.079	0.76	0.13
AB-K2-Gt21c	Core	828	114930.82	162.63	156.03	95.00	15607.80	3494.19	12.66	3.26	<0.065	0.20	26.35	14.98	0.23	<0.033	<0.129	0.02	0.38	0.18	2.00	1.22	0.56	2.41	0.57	4.14	1.00	2.98	0.40	2.94	0.45	0.31	<0.041	<0.08	2.49	0.20

Grain ID	spot	(° C)	Mg	Sc	Ti	V	Cr	Mn	Ni	Ga	Rb	Sr	Y	Zr	Nb	Cs	Ba	La	Ce	Pr	Nd	Sm	Eu	Gd	Tb	Dy	Ho	Er	Tm	Yb	Lu	Hf	Ta	Pb	Th	U
AB-K2-Gt21d	Rim	831	110277.98	168.67	153.30	89.40	15681.51	3437.55	12.87	2.99	<0.051	0.15	28.47	13.72	0.22	<0.0228	0.19	<0.0181	0.44	0.16	1.74	1.28	0.70	3.01	0.57	5.20	0.96	2.93	0.44	3.11	0.48	0.19	<0.058	<0.046	0.55	0.17
AB-K2-Gt22	Core	805	114496.05	151.60	140.69	77.48	13739.36	3161.59	10.65	2.03	<0.062	0.18	29.05	15.42	0.20	<0.033	<0.207	<0.043	0.28	0.11	1.90	1.43	0.79	3.06	0.74	5.48	1.05	3.30	0.41	3.00	0.37	0.19	<0.068	<0.072	2.37	0.11
AB-K2-Gt23	Core	836	124586.04	141.55	76.24	119.94	11543.51	2463.48	13.40	1.98	<0.076	0.21	2.92	18.19	0.16	<0.029	<0.171	<0.029	0.43	0.21	3.10	2.11	0.74	1.81	0.19	0.55	0.15	0.26	0.06	0.45	0.06	0.25	0.02	<0.09	6.53	0.03
AB-K2-Gt24	Core	1152	128924.70	107.57	4622.16	207.21	18775.53	1943.13	77.37	9.89	0.07	0.46	26.94	69.96	0.28	<0.028	<0.148	0.04	0.38	0.15	1.57	1.38	0.53	2.21	0.59	4.21	1.06	3.26	0.47	3.35	0.51	2.04	<0.046	<0.075	2.37	<0.0153
AB-K2-Gt25	Core	1071	129509.13	112.32	1047.01	165.43	14447.96	1897.20	53.40	6.44	<0.062	0.12	13.83	7.14	0.31	<0.036	<0.145	<0.027	0.13	<0.0220	0.49	<0.44	0.17	0.64	0.20	1.66	0.54	1.86	0.27	2.42	0.31	<0.161	<0.067	<0.093	0.42	<0.0147

Buffalo Head Hills kimberlite field - K6

	Probe	TNi																																	
Grain ID	spot	(° C)	Mg	Sc	Ti	V	Cr	Mn	Ni	Ga	Rb	Sr	Y	Zr	Nb	Cs	Ba	La	Ce	Pr	Nd	Sm	Eu	Gd	Tb	Dy	Ho	Er	Tm	Yb	Lu	Hf	Ta	Pb	Th	U
AB-K6-Gt02	Core	1230	146762.70	111.90	3144.08	235.71	24878.71	2483.11	106.28	10.80	<0.076	0.42	11.15	21.69	0.40	<0.039	<0.14	0.06	0.27	0.09	0.80	0.59	0.22	0.87	0.22	2.02	0.38	1.59	0.19	1.96	0.34	0.37	<0.045	<0.097	0.40	<0.0213
AB-K6-Gt03	Core	1209	136878.42	99.35	4901.44	279.57	40242.56	2445.43	97.91	15.16	<0.076	0.47	17.86	54.77	0.59	<0.036	<0.118	0.05	0.50	0.18	1.64	0.99	0.47	2.17	0.43	3.45	0.65	2.11	0.37	1.96	0.30	1.35	<0.053	<0.066	2.09	0.02
AB-K6-Gt04	Core	1192	141088.88	122.23	2299.10	262.71	41767.88	2531.49	91.36	10.24	<0.060	0.31	11.79	24.76	0.50	<0.035	<0.137	<0.022	0.30	0.09	1.11	0.61	0.35	1.30	0.26	2.08	0.43	1.27	0.19	1.38	0.21	0.49	<0.061	<0.106	3.62	0.02
AB-K6-Gt05	Core	1184	124489.81	174.77	2062.28	377.92	78948.27	2644.74	88.55	7.89	<0.078	0.88	6.24	32.67	0.89	<0.027	<0.159	0.11	0.85	0.30	2.83	1.89	0.49	1.47	0.27	1.47	0.24	0.62	0.07	0.54	0.10	0.62	0.12	<0.079	35.95	0.03
AB-K6-Gt06	Core	1255	150056.31	91.77	4111.04	250.08	17632.58	2375.87	117.09	15.18	<0.071	0.58	15.71	51.14	0.34	<0.027	<0.145	0.05	0.32	0.10	1.31	0.50	0.37	1.93	0.38	2.42	0.55	2.01	0.25	1.81	0.33	1.41	0.05	0.08	23.00	<0.0194
AB-K6-Gt07	Core	1269	151600.72	114.22	3063.72	295.05	38257.10	2372.78	123.00	12.62	<0.075	0.62	12.50	47.52	0.75	<0.034	<0.091	0.05	0.69	0.20	1.48	0.71	0.41	0.98	0.28	2.46	0.49	1.38	0.20	1.20	0.33	1.12	0.10	0.09	166.18	0.02

Buffalo Head Hills kimberlite field - K11

	Probe	TNi																																	
Grain ID	spot	(° C)	Mg	Sc	Ti	V	Cr	Mn	Ni	Ga	Rb	Sr	Y	Zr	Nb	Cs	Ba	La	Ce	Pr	Nd	Sm	Eu	Gd	Tb	Dy	Ho	Er	Tm	Yb	Lu	Hf	Ta	Pb	Th	U
AB-K11-Gt01	Core	1229	131759.98	100.23	3985.26	233.34	25829.09	1946.76	105.69	11.53	<0.038	0.76	17.00	86.72	0.52	<0.0206	<0.101	0.10	0.79	0.25	2.31	1.05	0.58	2.07	0.38	3.15	0.64	2.15	0.30	2.11	0.33	2.34	0.06	<0.041	0.04	0.03
AB-K11-Gt02a	Core	1148	137575.86	122.12	1742.56	269.36	29496.84	2217.74	75.84	10.76	<0.072	0.32	8.96	7.72	0.29	<0.034	<0.119	0.04	0.20	0.05	0.57	<0.54	0.19	0.88	0.18	1.35	0.32	0.92	0.19	1.31	0.20	0.23	<0.059	<0.099	0.35	<0.0177
AB-K11-Gt02b	Rim	1125	129671.37	120.07	1726.87	273.67	28406.69	2165.62	68.48	10.95	<0.054	0.27	8.56	7.63	0.43	<0.034	<0.171	0.05	0.22	0.06	0.35	0.74	0.13	0.75	0.16	1.10	0.34	1.11	0.14	1.26	0.17	0.24	0.04	<0.075	0.14	<0.0198
AB-K11-Gt03a	Core	1167	132844.48	114.41	4680.44	313.82	22514.91	2397.40	82.39	12.62	<0.066	0.67	17.37	115.00	0.55	<0.025	<0.137	0.15	1.08	0.31	2.57	1.44	0.51	2.23	0.43	3.41	0.62	1.97	0.22	2.05	0.32	2.94	0.05	0.06	0.33	0.04
AB-K11-Gt03b	Rim	1183	122821.65	114.10	4795.52	308.67	21297.44	2300.79	87.89	12.04	<0.053	0.63	17.56	121.28	0.55	<0.034	<0.144	0.11	0.99	0.29	2.51	1.17	0.58	1.83	0.42	2.80	0.69	2.07	0.28	2.07	0.36	2.97	0.11	<0.071	0.61	0.05
AB-K11-Gt04	Core	1028	121100.64	146.99	609.93	304.91	50718.71	3022.03	42.95	6.84	<0.070	0.16	2.32	8.09	0.58	<0.038	<0.158	0.15	0.37	0.07	1.02	0.70	0.24	0.66	0.08	0.57	0.09	<0.137	0.05	0.39	0.10	0.22	<0.061	<0.110	0.31	0.05
AB-K11-Gt05	Core	1012	129195.66	130.99	1081.56	234.57	32929.87	2717.05	39.41	7.19	<0.074	0.35	10.81	13.82	0.43	<0.034	<0.115	<0.031	0.28	0.15	1.14	0.97	0.25	0.94	0.16	1.50	0.38	1.29	0.23	1.89	0.31	0.30	0.05	0.06	0.67	<0.024
AB-K11-Gt06	Core	1103	135490.16	107.18	1575.56	213.27	24200.13	2485.90	61.89	8.89	<0.069	0.33	14.48	19.31	0.45	<0.043	0.10	0.05	0.27	0.10	0.68	0.59	0.26	1.25	0.25	2.54	0.49	1.68	0.26	1.85	0.36	0.47	<0.054	<0.112	234.06	<0.0204
AB-K11-Gt07	Core	1104	129040.84	132.09	2277.78	318.51	45065.81	2630.34	62.17	10.88	<0.082	0.43	7.99	23.03	0.61	<0.038	<0.170	0.05	0.33	0.11	1.36	<0.47	0.27	1.07	0.26	1.42	0.27	0.67	0.12	0.88	0.11	0.48	0.08	<0.091	11.55	0.02
AB-K11-Gt08	Core	1149	122818.21	188.43	2877.58	442.53	49957.49	2751.46	76.38	7.85	<0.065	0.37	17.45	63.66	0.89	<0.033	<0.133	0.13	1.08	0.33	2.82	2.22	0.90	3.93	0.64	3.16	0.64	1.65	0.24	1.61	0.22	1.83	0.05	<0.092	1.37	0.07
AB-K11-Gt13	Core	1095	134879.72	122.61	1073.28	248.47	35332.79	2742.62	59.83	9.41	<0.077	0.23	8.99	7.18	0.35	<0.035	<0.153	<0.027	0.28	0.09	0.48	<0.42	0.11	0.79	0.19	1.28	0.32	1.09	0.21	1.28	0.22	0.26	<0.041	<0.078	0.12	0.05
AB-K11-Gt14	Core	1123	134717.53	113.26	2092.69	257.14	26424.81	2366.22	68.02	8.85	<0.076	0.21	13.67	34.84	0.28	<0.032	<0.096	0.03	0.22	0.07	1.37	1.44	0.34	1.85	0.28	2.46	0.48	1.42	0.25	1.95	0.28	0.88	<0.065	<0.081	0.18	<0.0157
AB-K11-Gt15	Core	1093	128777.72	142.06	640.02	305.81	47741.40	2636.74	59.16	5.97	<0.076	0.43	2.34	12.73	0.72	<0.036	<0.167	0.03	0.41	0.19	1.79	1.08	0.30	0.99	0.10	0.47	0.07	0.19	<0.037	0.48	0.11	0.28	<0.062	<0.068	157.44	0.02
AB-K11-Gt16	Core	1030	133308.59	121.20	618.70	272.41	33393.20	3030.65	43.38	10.27	<0.079	0.05	8.37	5.14	0.78	<0.031	<0.186	0.03	0.11	0.04	<0.149	<0.45	0.11	0.67	0.16	1.41	0.28	1.00	0.17	1.20	0.24	<0.162	<0.040	<0.079	13.76	<0.0187
AB-K11-Gt20	Core	1206	133561.59	129.02	4458.04	313.27	48886.62	2417.98	96.59	12.35	<0.065	0.95	17.78	101.38	0.61	<0.036	<0.118	0.10	0.79	0.27	2.25	1.25	0.61	2.18	0.47	3.30	0.67	2.05	0.28	2.54	0.37	2.63	0.05	<0.069	6.26	0.03

Buffalo Head Hills kimberlite field - K14

	Probe	TNi																																	
Grain ID	spot	(° C)	Mg	Sc	Ti	V	Cr	Mn	Ni	Ga	Rb	Sr	Y	Zr	Nb	Cs	Ba	La	Ce	Pr	Nd	Sm	Eu	Gd	Tb	Dy	Ho	Er	Tm	Yb	Lu	Hf	Ta	Pb	Th	U
AB-K14-Gt01	Core	1018	136026.66	111.34	1272.90	181.66	15496.48	2344.12	40.68	8.24	<0.064	0.13	14.21	11.88	0.51	<0.034	<0.196	<0.027	0.17	0.06	0.62	<0.47	0.16	1.31	0.20	1.69	0.44	1.60	0.29	2.25	0.32	0.52	<0.054	<0.064	0.67	0.22
AB-K14-Gt02	Core	1119	131731.55	115.60	2926.02	236.37	25910.36	2008.42	66.74	9.44	<0.059	0.45	14.86	24.40	0.44	<0.029	<0.100	<0.024	0.33	0.12	1.26	0.79	0.37	1.46	0.32	2.40	0.56	1.60	0.25	1.87	0.30	0.89	<0.051	<0.062	1.46	0.03
AB-K14-Gt03	Core	1160	133397.03	93.51	4239.42	205.54	15028.74	1856.16	79.88	9.94	<0.068	0.46	13.04	48.01	0.38	<0.027	<0.132	0.04	0.32	0.11	1.27	0.57	0.46	1.77	0.30	2.07	0.47	1.41	0.30	1.95	0.32	1.16	0.09	<0.07	0.03	<0.0165
AB-K14-Gt05	Core	1005	122350.72	155.04	926.39	299.46	41835.21	2529.63	38.01	6.59	<0.079	0.37	6.58	13.73	1.44	0.03	<0.137	0.24	1.28	0.29	2.30	0.96	0.31	0.97	0.17	1.26	0.24	0.74	0.11	0.65	0.08	0.37	0.12	0.08	1.50	0.13
AB-K14-Gt06	Core	1160	136648.91	111.98	2745.63	235.93	25052.71	1881.02	79.90	7.60	<0.080	0.55	10.31	20.86	0.50	<0.030	<0.153	0.05	0.45	0.18	1.66	0.56	0.32	1.15	0.27	1.80	0.33	1.12	0.22	1.42	0.22	0.58	<0.064	<0.077	6.01	<0.0207
AB-K14-Gt09	Core	1003	120876.16	171.27	1014.24	376.81	36932.14	2886.70	37.57	8.92	<0.070	0.28	3.12	13.13	0.65	<0.036	<0.120	0.10	0.65	0.20	1.36	<0.49	0.14	0.74	0.09	0.71	0.13	0.36	0.06	0.59	0.14	0.38	<0.057	<0.075	5.69	0.05
AB-K14-Gt11	Core	766	115929.64	176.23	666.61	130.31	15153.52	3683.77	7.83	3.79	<0.075	0.07	19.90	17.15	0.23	<0.036	<0.127	<0.025	0.07	<0.029	0.39	<0.47	0.27	1.02	0.29	2.69	0.70	2.27	0.43	3.28	0.59	0.69	<0.064	<0.105	1.77	<0.0168
AB-K14-Gt12	Core	1174	135360.91	92.06	4181.16	213.35	16030.78	1957.65	84.70	11.02	<0.062	0.49	12.99	45.91	0.33	<0.032	<0.115	0.03	0.32	0.14	1.02	0.52	0.39	1.26	0.28	2.21	0.51	1.65	0.19	1.60	0.27	0.96	0.08	<0.078	0.65	0.02
AB-K14-Gt13	Core	1175	134697.20	92.03	4167.42	210.93	12616.64	1875.86	85.02	11.36	<0.080	0.48	15.00	43.38	0.31	<0.031	<0.142	0.06	0.34	0.10	1.23	0.76	0.36	1.48	0.32	2.37	0.60	1.77	0.28	1.96	0.34	1.08	0.05	<0.072	0.42	<0.0145
AB-K14-Gt14	Core	1086	131021.03	115.16	1651.71	225.36	23120.97	2152.10	57.25	8.60	<0.075	0.26	9.64	16.56	0.33	<0.031	<0.217	0.03	0.20	0.08	0.58	<0.39	0.21	0.62	0.22	1.56	0.34	1.19	0.19	1.35	0.19	0.34	<0.052	0.07	8.28	<0.0175
AB-K14-Gt16	Core	1079	127917.15	147.28	2101.45	365.52	31441.89	2211.82	55.32	10.63	<0.067	0.17	15.02	19.04	0.32	0.04	0.11	<0.028	0.19	0.07	0.48	<0.47	0.29	1.38	0.36	2.08	0.57	1.73	0.20	1.64	0.33	0.61	<0.048	<0.064	0.29	<0.0209
AB-K14-Gt18	Core	815	120246.28	170.28	676.29	135.93	16402.31	3443.45	11.50	3.58	<0.072	0.06	19.59	17.86	0.16	0.05	<0.177	0.02	0.08	0.02	0.60	<0.53	0.23	1.18	0.32	2.62	0.71	2.29	0.43	3.47	0.54	0.47	<0.074	<0.067	19.01	0.02
AB-K14-Gt20	Core	825	125712.13	163.46	448.45	121.36	15852.75	3314.53	12.33	3.46	<0.062	0.05	16.15	9.43	0.18	<0.033	<0.226	<0.022	0.04	0.02	0.25	0.55	0.26	1.33	0.31	2.33	0.64	1.90	0.27	2.24	0.35	0.22	<0.062	<0.091	0.58	<0.0245
AB-K14-Gt21	Core	855	128760.97	181.82	559.89	130.34	16209.34	3273.04	15.25	3.61	<0.082	<0.038	22.36	21.69	0.14	<0.035	<0.162	<0.024	0.08	0.02	0.60	<0.49	0.31	1.96	0.41	3.41	0.80	2.90	0.40	3.73	0.76	0.41	0.06	<0.071	2.10	<0.0185
AB-K14-Gt22	Core	1182	134372.72	91.90	4027.09	205.27	16528.95	2001.04	87.76	11.64	<0.064	0.51	13.13	46.31	0.34	<0.035	<0.140	0.04	0.32	0.15	1.24	0.59	0.41	1.21	0.23	2.29	0.45	1.55	0.21	1.39	0.30	1.14	<0.061	<0.069	0.97	<0.0212
AB-K14-Gt23	Core	816	123224.05	167.98	504.09	115.54	13457.38	3386.84	11.52	12.97	<0.084	0.11	18.75	20.78	0.25	<0.045	<0.217	<0.036	0.04	0.03	0.46	0.88	0.28	1.83	0.31	2.80	0.67	2.61	0.40	2.99	0.45	0.49	<0.062	<0.096	0.13	<0.023
AB-K14-Gt30	Core	1230	138777.36	92.95	3940.86	238.59	19609.51	2176.54	106.26	12.78	<0.071	0.45	12.36	43.51	0.44	<0.030	<0.108	0.03	0.35	0.10	0.94	0.67	0.38	1.51	0.29	1.92	0.43	1.57	0.24	1.55	0.26	0.93	<0.038	<0.056	2.55	<0.0144
AB-K14-Gt31	Core	1154	137884.14	113.00	3419.37	256.55	29385.20	2358.09	77.90	9.82	<0.075	0.43	12.69	40.79	0.47	<0.041	<0.150	<0.033	0.36	0.12	1.35	0.86	0.40	1.53	0.30	2.45	0.45	1.51	0.20	1.42	0.21	0.95	0.05	<0.080	6.52	0.02
AB-K14-Gt32	Core	1001	122289.84	173.24	304.25	318.81	64403.65	3186.58	37.32	6.47	<0.075	0.81	2.77	36.06	1.28	<0.031	<0.151	0.13	1.09	0.33	2.01	0.64	0.23	0.44	0.11	0.63	0.06	0.24	<0.034	0.32	0.09	0.86	0.08	<0.078	3.57	0.06
AB-K14-Gt33	Core	1136	138461.25	103.91	1703.69	232.57	24061.51	2350.48	71.91	11.10	<0.059	0.22	13.16	19.47	0.51	<0.034	<0.200	<0.027	0.22	0.08	0.66	0.75	0.28	0.99	0.23	2.07	0.45	1.55	0.24	1.86	0.34	0.56	<0.058	<0.080	0.77	<0.0154
AB-K14-Gt34	Core	1130	137819.92	105.29	1610.77	228.62	23871.53	2279.06	70.02	9.44	<0.082	0.24	12.21	16.98	0.42	<0.030	<0.194	0.04	0.22	0.09	0.68	<0.46	0.18	1.20	0.28	1.77	0.45	1.48	0.26	1.93	0.25	0.38	<0.059	<0.082	0.04	0.02

Grain ID	spot	(° C)	Mg	Sc	Ti	V	Cr	Mn	Ni	Ga	Rb	Sr	Y	Zr	Nb	Cs	Ba	La	Ce	Pr	Nd	Sm	Eu	Gd	Tb	Dy	Ho	Er	Tm	Yb	Lu	Hf	Ta	Pb	Th	U
Birch Mountains field - Kendu																																				
	Probe	TNi																																		
Grain ID	spot	(° C)	Mg	Sc	Ti	V	Cr	Mn	Ni	Ga	Rb	Sr	Y	Zr	Nb	Cs	Ba	La	Ce	Pr	Nd	Sm	Eu	Gd	Tb	Dy	Ho	Er	Tm	Yb	Lu	Hf	Ta	Pb	Th	U
RE02-KD-01-03a	Core	852	111347.70	191.84	895.85	257.68	37009.48	3277.46	14.97	3.73	0.07	0.19	2.30	9.45	0.50	<0.033	<0.151	0.07	0.55	0.14	1.34	1.17	0.27	0.94	0.09	0.73	0.06	0.36	0.03	0.56	0.11	<0.140	<0.051	<0.071	0.39	0.14
RE02-KD-01-03b	Rim	841	107863.30	192.24	896.28	259.74	36911.74	3169.58	13.80	3.76	<0.060	0.18	2.17	10.73	0.44	<0.0234	<0.132	0.10	0.51	0.15	1.59	<0.47	0.23	0.48	0.12	0.48	0.06	0.22	0.05	0.74	0.11	0.21	<0.039	<0.063	25.16	0.13
RE02-KD-01-04a	Rim	833	125003.58	156.17	287.03	215.12	26377.42	3095.84	13.07	2.81	<0.046	0.04	3.09	10.39	0.27	<0.0181	<0.089	0.07	0.21	0.05	0.45	<0.41	0.07	0.39	0.07	0.48	0.14	0.41	0.11	0.55	0.09	0.34	<0.046	<0.043	1.25	0.04
RE02-KD-01-04b	Core	831	123114.23	155.66	294.05	218.05	26316.51	2995.29	12.89	2.82	<0.064	2.80	3.39	10.43	0.50	<0.0245	1.89	0.57	1.12	0.14	0.62	0.53	0.10	0.33	0.09	0.67	0.12	0.25	0.06	0.56	0.10	0.27	0.03	<0.050	0.19	0.06
RE02-KD-01-04c	Core	843	122031.27	158.77	308.76	223.35	27615.56	3093.94	14.06	2.71	<0.063	0.13	3.20	10.20	0.29	<0.029	<0.159	<0.029	0.20	0.04	0.33	<0.47	0.11	0.46	0.07	0.54	0.20	0.36	0.07	0.83	0.14	0.47	<0.048	<0.068	0.15	0.05
RE02-KD-01-04d	Rim	870	124658.34	157.40	311.07	237.45	28477.57	3250.05	16.87	3.47	<0.062	0.28	3.45	12.72	0.31	<0.0223	<0.158	0.13	0.30	0.04	0.38	<0.51	0.13	0.30	0.11	0.75	0.19	0.47	0.06	0.86	0.17	0.39	<0.050	<0.071	0.21	0.03
RE02-KD-01-05	Core	836	134046.03	198.15	128.92	68.09	15953.61	3259.74	13.32	2.32	<0.075	0.05	2.52	2.91	0.14	<0.027	<0.185	0.02	0.11	0.04	0.29	<0.48	0.09	0.35	0.08	0.30	0.13	0.35	0.07	0.58	0.08	0.14	<0.042	<0.056	0.43	0.04
RE02-KD-01-13	Core	961	213700.84	168.15	3400.17	276.04	3858.53	4435.38	29.76	21.56	0.09	0.38	32.13	110.52	0.66	<0.034	0.31	0.06	0.21	0.07	1.00	0.89	0.56	2.62	0.51	4.78	1.16	3.96	0.55	4.85	0.60	2.07	<0.070	<0.090	48.12	0.01
RE02-KD-02-02	Core	856	128855.70	204.08	323.35	116.82	14839.86	2645.28	15.41	1.90	<0.10	<0.049	13.19	3.06	1.98	<0.046	<0.173	0.06	0.10	0.03	<0.170	<0.68	<0.048	0.36	0.10	0.95	0.49	2.10	0.39	3.44	0.62	<0.179	0.09	<0.084	268.04	<0.0165
RE02-KD-02-03	Core	852	138409.16	255.99	293.54	100.23	15063.44	3354.98	15.00	1.65	0.08	0.15	1.66	6.30	1.74	<0.036	<0.188	0.11	0.43	0.15	1.29	1.04	0.28	0.53	0.07	0.29	<0.037	0.21	0.08	0.93	0.23	<0.137	<0.049	0.12	29.31	0.05
RE02-KD-02-04	Core	852	121317.26	214.13	66.14	206.07	30011.60	3418.27	14.99	2.56	<0.086	0.11	0.65	3.45	0.32	<0.03	<0.095	0.09	0.64	0.17	1.26	<0.53	0.05	<0.31	0.06	0.20	0.06	<0.133	0.04	0.40	0.11	<0.127	<0.053	<0.092	0.12	0.08
RE02-KD-02-05a	Rim	955	129496.47	107.97	2603.29	186.53	13378.06	2455.32	28.80	9.40	<0.090	5.39	30.85	113.10	1.04	<0.029	4.12	1.41	2.44	0.28	1.87	1.74	0.64	2.88	0.70	5.46	1.25	4.02	0.54	3.82	0.55	2.21	<0.055	<0.079	0.20	0.04
RE02-KD-02-05b	Core	1000	141533.61	105.62	2645.36	207.05	14537.62	2763.66	37.04	10.73	0.09	7.18	30.59	118.99	1.34	<0.0192	3.88	0.92	2.11	0.26	1.77	1.02	0.64	3.18	0.73	5.35	1.24	3.97	0.61	3.59	0.57	2.31	0.07	0.09	0.26	0.04
RE02-KD-02-05c	Rim	988	139478.23	102.30	2674.37	201.62	14554.95	2716.04	34.65	9.77	0.05	1.70	29.17	115.31	0.61	<0.0168	1.12	0.38	0.82	0.14	1.43	1.14	0.56	3.04	0.65	5.30	1.16	3.50	0.55	3.73	0.51	2.39	0.03	0.06	0.12	0.02
RE02-KD-02-16	Core	877	135423.95	222.76	34.56	179.15	22882.51	3518.75	17.69	2.53	<0.116	0.11	1.32	3.52	0.26	<0.045	<0.235	0.09	0.44	0.09	0.71	<0.80	0.10	<0.32	0.06	0.28	<0.062	0.33	0.05	0.44	0.11	<0.156	0.09	<0.086	0.93	0.07
RE02-KD-02-17	Core	844	140097.06	262.59	79.48	103.31	15598.32	3371.26	14.14	1.46	<0.054	0.12	2.34	5.89	0.19	<0.0227	<0.118	0.05	0.37	0.16	1.74	0.91	0.41	0.84	0.12	0.39	0.09	0.46	0.08	0.96	0.17	0.11	<0.035	<0.077	1.29	0.05
RE02-KD-02-18	Core	969	127446.84	207.53	1407.48	117.37	27397.18	3249.00	31.26	4.15	0.38	11.70	29.11	88.90	1.27	<0.031	24.05	0.51	1.09	0.32	3.10	2.88	1.07	4.30	0.89	5.69	1.10	2.50	0.38	2.74	0.31	0.93	<0.048	0.18	2.12	0.05
RE02-KD-02-19	Core	832	130775.01	252.81	71.40	88.50	13862.62	3051.82	12.99	1.10	<0.079	0.12	2.02	5.49	0.17	<0.039	0.23	0.04	0.32	0.15	1.56	0.71	0.30	0.47	<0.045	0.21	0.07	0.24	0.07	0.62	0.20	<0.146	<0.045	<0.086	1.60	0.06
RE02-KD-02-20	Core	942	196646.56	345.92	79.55	116.74	21587.01	4745.27	26.60	1.82	<0.099	0.13	2.24	6.11	0.31	0.04	<0.141	0.05	0.31	0.12	1.31	0.80	0.27	1.28	0.08	0.45	0.06	0.28	0.07	0.78	0.19	<0.190	<0.070	<0.075	1.80	0.05
Birch Mountains field - Legend																																				
	Probe	TNi																																		
Grain ID	spot	(° C)	Mg	Sc	Ti	V	Cr	Mn	Ni	Ga	Rb	Sr	Y	Zr	Nb	Cs	Ba	La	Ce	Pr	Nd	Sm	Eu	Gd	Tb	Dy	Ho	Er	Tm	Yb	Lu	Hf	Ta	Pb	Th	U
VR88467A-01	Core	1151.516	161344.91	125.37	4836.65	256.66	38701.81	1745.66	77.06	5.25	<0.098	0.90	13.80	113.20	1.10	<0.0160	<0.113	0.09	0.93	0.38	3.68	2.52	0.86	1.83	0.59	3.16	0.61	1.27	0.19	0.95	0.19	2.59	0.06	0.30	0.79	0.04
VR88467A-05	Core	1136.855	146698.73	121.53	4573.12	238.15	36128.64	1705.72	72.28	4.29	<0.042	0.91	11.57	94.16	0.97	0.21	<0.104	0.16	0.89	0.30	2.75	2.02	0.80	1.83	0.46	2.58	0.41	0.86	0.12	0.93	0.12	2.12	<0.059	<0.058	0.24	0.02
VR88467A-06	Core	1165.489	150044.45	125.53	4682.59	259.60	38973.29	1813.34	81.81	4.85	0.10	0.88	13.44	99.24	1.28	<0.0186	0.12	0.11	0.96	0.35	3.08	1.39	0.76	1.86	0.49	3.11	0.46	1.23	0.18	1.03	0.17	2.62	0.07	0.12	2.02	0.04
VR88467A-09	Core	1154.356	140470.22	150.67	4226.52	263.74	44640.32	1824.10	78.01	3.87	0.07	0.98	8.00	110.43	1.34	<0.0156	<0.137	0.13	1.11	0.44	4.01	2.06	0.99	1.90	0.45	2.20	0.28	0.64	0.08	0.46	0.15	2.68	0.10	<0.062	1.98	0.04
VR88467A-13	Core	1197.832	158064.36	152.76	4522.94	283.73	46839.47	2047.79	93.55	4.99	0.08	1.03	5.43	97.75	1.43	<0.0193	<0.139	0.12	0.98	0.37	3.58	2.24	0.82	1.70	0.38	1.62	0.17	0.47	0.07	0.58	0.15	1.89	0.05	0.13	0.35	0.03
VR88467A-17	Core	1169.531	139057.98	129.26	4802.28	264.90	39626.04	1833.17	83.22	5.25	0.31	1.17	13.44	107.28	1.27	<0.0190	0.67	0.14	1.01	0.35	3.19	1.85	0.77	2.38	0.54	3.22	0.50	1.15	0.16	1.11	0.18	2.82	0.08	<0.066	0.42	0.05
VR88467A-23	Core	1178.260	141306.23	134.97	6578.58	298.95	46628.94	2013.32	86.32	7.41	<0.042	0.96	27.12	141.83	1.22	<0.0167	<0.089	0.09	1.13	0.42	3.58	3.07	1.06	2.57	0.77	5.40	1.05	2.75	0.38	2.33	0.30	3.59	0.05	0.08	0.34	<0.024
VR88467A-26	Core	1197.331	140590.44	146.83	4601.39	245.88	45838.33	1908.80	93.36	4.20	<0.040	1.05	8.60	79.55	1.42	<0.0202	<0.144	0.13	1.14	0.42	3.31	2.04	0.68	1.89	0.36	2.21	0.26	0.65	0.08	0.58	0.15	1.64	0.12	<0.088	4.65	0.03
VR88467A-28	Core	1196.909	134509.25	142.62	4802.94	244.11	44050.36	1813.93	93.20	4.51	<0.042	0.99	10.59	86.62	1.21	<0.0222	<0.120	0.11	1.14	0.45	3.51	1.92	0.78	1.91	0.40	2.38	0.35	0.69	0.13	0.80	0.18	1.91	0.09	0.30	0.26	<0.0191
VR88467A-33	Core	1157.084	129415.84	127.43	5154.63	267.41	37038.23	1749.36	78.93	5.04	<0.042	0.94	17.53	107.61	1.13	<0.0217	<0.135	0.16	1.12	0.30	3.28	2.16	0.81	2.38	0.58	3.77	0.63	1.60	0.17	1.38	0.21	2.79	0.09	0.10	36.20	0.03
VR88467A-35	Core	1136.666	123620.45	169.18	2018.64	331.25	55030.66	1794.91	72.22	4.55	<0.033	1.06	5.48	96.71	1.76	<0.0132	<0.143	0.23	1.89	0.66	5.81	2.64	0.96	2.25	0.39	1.81	0.27	0.54	0.06	0.50	0.13	2.46	0.17	0.06	4.16	0.06
VR88467A-36	Core	1120.697	122153.61	212.42	934.97	328.23	53378.09	1875.58	67.25	3.51	<0.047	1.06	3.97	72.30	1.82	<0.0187	<0.113	0.23	1.84	0.66	6.66	2.41	0.85	1.49	0.21	1.16	0.19	0.41	0.07	0.67	0.13	1.65	0.13	<0.068	15.54	0.07
VR88467A-39	Core	1162.942	140412.28	201.05	3400.34	306.99	63430.41	2054.87	80.93	4.18	<0.061	1.13	4.75	130.28	1.66	<0.034	<0.148	0.21	1.66	0.64	5.58	3.77	1.09	1.90	0.31	1.24	0.20	0.29	<0.036	0.70	0.13	2.78	0.07	<0.097	0.53	0.05
VR88478A-02	Core	1206.071	141791.03	193.06	2132.11	320.39	46428.89	1756.26	96.71	3.74	0.08	0.95	4.05	79.23	1.18	<0.023	<0.144	0.14	1.44	0.44	3.97	1.42	0.65	1.98	0.25	1.11	0.20	0.36	<0.041	0.31	0.09	1.52	0.09	<0.058	0.44	0.06
VR88478A-03a	Core	1174.175	140002.80	200.97	3236.93	256.09	44980.57	2050.66	84.86	4.66	<0.073	0.95	7.70	107.90	0.92	<0.030	<0.180	0.15	1.18	0.36	3.65	2.26	0.90	2.35	0.41	1.90	0.27	0.72	0.07	0.55	0.07	2.44	0.07	<0.076	1.34	0.04
VR88478A-03b	Rim	1161.253	134659.31	199.81	3325.50	249.52	44558.70	2015.84	80.35	4.34	<0.079	0.83	7.38	105.83	0.90	<0.028	<0.133	0.14	1.05	0.36	3.81	1.93	0.89	3.21	0.36	1.85	0.31	0.58	0.09	0.55	0.13	2.30	0.08	<0.059	5.20	0.02
VR88478A-04	Core	1135.755	120751.44	205.35	1559.70	319.44	47519.27	1838.48	71.93	3.49	<0.072	0.75	4.32	87.64	1.23	<0.031	0.42	0.14	1.32	0.43	4.03	2.43	0.72	2.03	0.27	0.86	0.17	0.48	0.07	0.38	0.08	1.87	0.11	0.28	4.16	0.04
Birch Mountains field - Xena																																				
	Probe	TNi																																		
Grain ID	spot	(° C)	Mg	Sc	Ti	V	Cr	Mn	Ni	Ga	Rb	Sr	Y	Zr	Nb	Cs	Ba	La	Ce	Pr	Nd	Sm	Eu	Gd	Tb	Dy	Ho	Er	Tm	Yb	Lu	Hf	Ta	Pb	Th	U
VR87896A-01a	Core	1201	0.89	17.01	9.32	2.62	9.50	0.55	0.01	0.33	0.02	0.22	9.46	17.26	2.48	0.13	0.10	0.44	1.11	2.72	3.95	8.89	13.18	10.04	11.79	11.01	11.76	9.11	10.31	8.93	7.94	13.42	27.98	0.10	84.25	1.39
VR87896A-01b	Rim	1191	0.85	17.84	8.96	2.65	9.50	0.53	0.01	0.30	0.00	0.10	7.34	16.53	1.76	0.00	0.00	0.35	0.99	2.43	4.70	9.75	11.86	9.99	10.26	9.00	8.24	6.77	8.59	5.28	7.88	13.25	0.00	0.00	204.20	0.00
VR87896A-02a	Core	1243	0.90	16.32	8.79	2.88	9.36	0.58	0.01	0.38	0.01	0.08	9.05	16.17	2.06	0.00	0.00	0.36	0.89	2.33	5.16	9.29	10.86	9.12	10.24	11.19	11.56	10.37	8.44	8.39	11.61	12.94	3.03	0.00	578.70	2.44
VR87896A-02b	Rim	1220	0.88	15.82	9.52	2.78	9.50	0.56	0.01	0.41	0.00	0.10	9.78	16.64	1.83	0.00	0.00	0.39	1.06	2.22	4.12	9.81	11.14	11.48	12.41	12.00	10.94	9.14	8.83	7.98	7.23	12.66	0.00	0.02	191.02	1.16
VR87896A-03	Core	1194	0.89	16.47	8.77	2.57	8.71	0.53	0.01	0.33	0.00	0.11	8.93	16.06	1.81	0.00	0.00	0.19	0.91	2.02	4.63	7.45	10.46	9.23	9.58	11.54	8.57	8.42	7.17	7.90	7.80	12.36	4.60	0.00	84.37	1.52
VR87896A-04a	Core	1215	0.86	15.20	9.26	2.60	9.47	0.53	0.01	0.37	0.01	0.27	9.84	16.62	2.02	0.00	0.19	0.38	1.14	2.49	4.72	11.88	11.78	12.66	11.11	13.17	9.48	8.58	7.43	7.23	6.29	11.86	7.90	0.00	109.84	2.18
VR87896A-04b	Rim	1253	0.90	15.68	9.35	2.92	9.86	0.58	0.01	0.50	0.00	0.08	9.65	16.05	1.83	0.00	0.00	0.20	0.84	2.35	4.09	9.48	10.22	11.34	10.93	12.07	10.35	9.17	6.97	8.40	7.87	10.88	0.00	0.00	36.71	3.02
VR87896A-06	Core	1183	0.89	14.18	3.20	3.16	8.06	0.62	0.01	0.55	0.00	0.04	4.77	9.06	2.29	0.00	0.00	0.25	0.80	1.91	3.02	3.97	5.06	4.70	6.11	5.35	5.03	4.73	4.50	5.33	5.98	6.43	1.74	0.00	5.48	3.93